



**RENEWABLE ENERGY MICROGRID FOR IRON-ORE RAIL FREIGHT
SHUNTING YARDS**

By

BABALO DEKEDA

Thesis submitted in fulfilment of the requirements for the degree

Master of Engineering: Electrical Engineering

In the Faculty of Engineering and the Built Environment

CAPE PENINSULA UNIVERSITY OF TECHNOLOGY

Supervisor: Dr Marco Adonis

Bellville

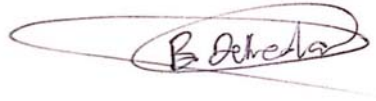
2021

CPUT copyright information

The thesis/dissertation may not be published either in part (in scholarly, scientific or technical journals), or as a whole (as a monograph), unless permission has been obtained from the University

DECLARATION

I, **Babalo Dekeda**, declare that the contents of this thesis/dissertation represent my own unaided work, and that the thesis/dissertation has not previously been submitted for academic examination towards any qualification. Furthermore, it represents my own opinions and not necessarily those of the Cape Peninsula University of Technology.

A handwritten signature in black ink, appearing to read 'B. Dekeda', enclosed within a large, loopy oval scribble.

Signed

06/10/2021

Date

Contents

DECLARATION	i
ABSTRACT	vi
ACKNOWLEDGEMENTS	viii
LIST OF FIGURES.....	ix
LIST OF TABLES	xii
ABBREVIATIONS AND ACRONYMS	xiii
GLOSSARY OF TERMS	xvi
CHAPTER 1: Introduction.....	1
1.1 Background	1
1.2 Problem Statement	4
1.3 Aim and Objectives.....	4
1.3.1 Aim.....	4
1.3.2 Research Objectives	4
1.4 Project Scope.....	5
1.5 Thesis Outline	5
CHAPTER 2: Literature Review.....	7
2.1 Overview	7
2.3 Freight Rail Yard Infrastructure	9
2.4 Microgrid System with Renewable Energy Technologies	10
2.5 Literature Summary	17
CHAPTER 3: Feasibility Study of Microgrid System	18
3.1 Overview	18
3.2 Data Collection.....	18
3.2.1 Load.....	18
3.2.2 Sources of Energy	20
3.2.2.1 Solar resource.....	21
3.2.3 Wind Energy	21

3.3 MG Design Specifications	22
3.3.1 Case Studies	22
3.3.2 HOMER Simulation Software	24
3.3.2.1 Simulation Settings	25
3.3.3 MG Hybrid System Components	25
3.3.3.1 PV Solar	25
3.3.3.2 Wind Turbine	26
3.4 Chapter Summary.....	27
CHAPTER 4: Technical Specification Modelling and Results.....	28
4.1 Overview	28
4.2 MATLAB/Simulink software	28
4.3 MG Components Modelling Methodology	28
4.3.1 PV Solar module	30
4.3.1.1 Modelling Design and Results	30
4.3.1.2 PV solar plant description	34
4.3.2 Wind Turbine	35
4.3.2.1 Wind turbine plant and Technical description	35
4.3.2.1.1 Major Components.....	36
4.3.2.1.2 Wind Turbine Specifications.....	38
4.3.4 Energy Storage System (ESS).....	39
4.4 Chapter Summary.....	45
CHAPTER 5: Modelling Hybrid Energy Management System.....	46
5.1 Introduction	46
5.2 Model Development.....	47
5.3 Fuzzy Logic Controller Design.....	48
5.4 Chapter Summary.....	53
CHAPTER 6: Real-Time Modelling.....	54
6.1 Real-time Modelling and Simulation Overview	54

6.1.1 Introduction	54
6.1.2 Real-Time Simulation Concepts	54
6.1.2.1 ARTEMis Modelling Tool	55
6.1.3 Timing Mechanism	56
6.1.4 OPAL-RT Architecture	57
6.1.5 Architecture of RT-LAB Simulator and Configuration Errors	59
6.1.6 RT-LAB Model Compilation Errors and Solutions	61
6.2 Chapter Summary	64
CHAPTER 7: Operated Modes and Scenarios in Real-Time Simulation	66
7.1 Introduction	66
7.2 The Developed System Configuration and Operating Mode Algorithms	66
7.2.1 Microgrid Connection	66
7.2.2 Designed Operating Modes of the Developed Microgrid System.....	67
7.3 Chapter Summary	70
Chapter 8: Results and Discussion	72
8.1 Overview	72
8.2 Homer Energy Modelling Results.....	72
8.3 Modelling design and Results of PV solar array and Wind turbine on MATLAB/Simulink	73
8.3.1 PV Array Modelling and Results	73
8.3.2 Wind Turbine Modelling and Results	77
8.4 Simulation Results of the Implemented Case Scenarios using MATLAB/Simulink.....	80
8.4.1 Implemented Cases Scenarios	81
8.4.2 Simulation Results of the microgrid system with changing load profile and RE system as input variables of FLC	82
8.4.3 Simulation Results of the SOC as required by the EMS of the microgrid system	84
8.4.4 Simulation Results of the microgrid system for the output variables of FLC as per the case scenarios	85
8.4.4.1 Case 1: Simulation Results of the MG system with WT providing an acceptable output power and with PV and BESS unable to provide an acceptable output power	85

8.4.4.2 Case 2: Simulation Results of the MG system with WT and BESS unable to provide an acceptable output power.....	86
8.4.4.3 Case 3: Simulation Results of the MG system when RES power reached maximum limits	87
8.4.4.4 Case 4: Simulation Results of the MG system with RES unable to provide an acceptable output power	88
8.5 Real-Time Modelling with Implemented Case Studies and Results	89
8.5.1 Case Study 1.....	89
8.5.2 Case Study 2.....	92
8.5.3 Case Study 3.....	94
8.5.4 Summary of Results and their Impact on Railway Yard.....	97
8.5.4.1 Case Study 1 Summary	99
8.5.4.2 Case Study 2 Summary	99
8.5.4.3 Case Study 3 Summary	100
Chapter 9: Conclusion and Future work	102
9.1 Conclusion.....	102
9.2 Future Work	104
BIBLIOGRAPHY	105

ABSTRACT

Global warming and climate change has purposely encouraged the use of environmentally friendly energy so as to reduce greenhouse gas emissions generated from the use of fossil fuels. As such, coal as it is a widely used non-renewable energy source is studied recently in-order to find ways of mitigating its causes in greenhouse effect. Coal is still one amongst the highest providers of electricity generated in South Africa, although it is a major cause of global warming and climate change with the accompanying CO₂ emissions and high-water usage depending on cooling technology. It is of public knowledge to note that, in South Africa, the state's power utility is experiencing many challenges on their power production and distribution network due to insufficient supply of coal, the significant growth in geographical distribution as well as the load changes. The growth in economic requirements and transformation in technology as well as environmental policy are constantly advancing in the market. However, the industries, organizations and society at large should take drastic actions in changing this situation. The engineers are focused in a mission of improving the technology and environment; and renewable energy-based microgrid (MG) applications is developing interest, globally because of its reliability and efficiency in supplying power for both grid-tied and off-grid modes. Although renewable energy (RE) microgrids are an increasingly adopted method used in supplying power to the residences, industries, hospitals etc., this system has not yet found its ground in railway industry, to assist in supplying the vast of railway equipment and railway facilities. Moreover, as new and advanced technologies are introduced into the railway environment, more energy costs saving technology should be a priority in order to reduce energy expenses. Thus, Transnet Freight Rail (TFR) as freight rail operator in South Africa should be irresistible on that initiative.

In this research, the development of an economically and environmentally viable real-time hardware-in-the-loop (HIL) model of MG for a railway-shunting yard is studied. The developed microgrid system consist of a PV solar system of 1.5MW and wind turbine of 3MW that act as distributed energy resources as well as 1MWh of lithium-ion batteries for energy storage system (ESS). The distributed energy resources (DER's) will be used in supplying power to the railway yard equipment and facilities, efficiently. The use of renewable energy sources must continue in-order to drive the global energy transformation, so that society can benefit from a clean environment and collective future. The developed microgrid system as designed in this research acts as a back-up system that works in both off-grid and grid-tied modes. Nonetheless, the design and development of the energy management system (EMS) for the developed renewable energy-based microgrid is incorporated in order to effectively maintain the supply of 5MVA load. Additionally, the main purpose of the suggested EMS working together with Li-ion batteries for the developed microgrid system was to improve the use of energy efficiency and manage the peak load demand by scheduling the generation according to the availability of wind and solar energy. Thus, the EMS was designed using fuzzy logic controller (FLC) which is the control method attainable on MATLAB/Simulink. Consequently, MATLAB/Simulink model was also used to design and develop the developed microgrid system with its

energy management system and therefore, the OPAL-RT simulation model simulates, control and analyse the model in real-time. Furthermore, the simulated results in both MATLAB/Simulink model and OPAL-RT simulation show that, the amount of power demanded by the load will always be equal to the power generated by the developed system when operating in both modes.

Keywords: Microgrids, Renewable Energy, EMS, Grid-tied, Off-grid, railway yard, ESS

ACKNOWLEDGEMENTS

I wish to thank:

- My supervisor Dr Marco Adonis for his guidance and support throughout the course of this research
- Transnet's employees for their effort and support.
- My parents and family, for believing in me and supporting me during difficult times.
- My best friend Nathi Mathiya, who encouraged and supported me to pursue M.Eng.
- All the other people who are not mentioned here, but who contributed in my research indirectly.

The financial assistance of National Research Foundation (NRF) towards this research is acknowledged. Opinions expressed in this thesis and the conclusions arrived at, are those of the author, and are not necessarily to be attributed to the National Research Foundation.

LIST OF FIGURES

Figure 1-1: A microgrid envisioned for a small town	3
Figure 2-1: Sentrarrand freight rail and Port Elizabeth Shunting yards	9
Figure 2-2: Energy storage options	17
Figure 3-1: Seasonal load profile for typical Salkor rail yard	19
Figure 3-2: Average Daily Electricity Usage from January 2012 - January 2013	20
for Stamford Rail Yard.....	20
Figure 3-3: Annual DNI average for South Africa.....	20
Figure 3-4: Daily radiation and Clearness Index for Saldanha Bay from July 2017 to June 2018	21
Figure 3-5: Monthly Average wind speed for Saldanha Bay from July 2017 to June 2018	22
Figure 3-6: Microgrid system schematic diagram designed in HOMER.....	24
Figure 3-7: Architecture of HOMER software.....	25
Figure 3-8: Power Curves for GE1.5xl and GE 1.5sle wind turbines	26
Figure 4-1: Architectural Design of the developed Microgrid System	29
Figure 4-2: Ideal PV Model characteristic.....	30
Figure 4-3: MPPT Controller designed on MATLAB/Simulink.....	33
Figure 4-5: PV Solar Array modelled designed on MATLAB/Simulink.....	35
Figure 4-6: Wind Turbine General Schematic	36
Figure 4-7: Schematic of GE 1.5MWsle Wind Turbine.....	36
Figure 4-8: Major Components of Doubly-Fed Wind Turbine	38
Figure 4-9: Equivalent Circuit Model of Battery Model in SimScape.....	39
Figure 4-11: Ideal BESS Configuration	42
Figure 4-12: Battery Discharge Characteristics (Voltage vs Time) generated on MATLAB/Simulink	43
Figure 5-1: Basic Fuzzy Inference System Diagram.....	47
Figure 5-2: $P_{Equilibrium}$ Membership Function generated on MATLAB/Simulink.....	49
Figure 5-3: SOC Membership Function generated on MATLAB/Simulink.....	49
Figure 5-5: Fuzzy Rules surface diagram generated on MATLAB/Simulink.....	53
Figure 6-1: OPAL-RT OP4510 Simulator.....	54
Figure 6-2(a): Real-Time Simulation Setup using OPAL RT Simulator	56
Figure 6-3: Time-step timing mechanism in RT-LAB.....	57
Figure 6-4: Real-Time Simulation Setup PCs	58
Figure 6-5: Architecture of Target PC (OP 4510 Machine) Connected to Host PC	59

Figure 6-6: License Manager Error for MATLAB vR2017a	60
Figure 6-8: Improper Parameter Setting Error	62
Figure 6-9: Simulink C-Code Generation Error	63
Figure 6-10: Error on Location of the Workspace in RT-LAB.....	63
Figure 7-1: RT-LAB Microgrid System with DC Bus Connection modelled using OPAL-RT ...	67
Figure 7-3: Load Demand Less than Power Generated by DER's.....	69
Figure 7-4: Load Demand Greater than Power Generated by DER's	70
Figure 8-1: -V characteristic for a PV array at a constant temperature of 25°C simulated on MATLAB/Simulink.....	73
Figure 8-2: P-V characteristic for a PV array at a constant temperature of 25°C simulated on MATLAB/Simulink	77
Figure 8-3: I-V characteristic for a PV array at a constant irradiance of 1000W/m ² simulated on MATLAB/Simulink	77
Figure 8-4: P-V characteristic for a PV array at a constant irradiance of 1000W/m ² simulated on MATLAB/Simulink	77
Figure 8-5: Pmean, Vmean and Duty cycle PV scopes simulated on MATLAB/Simulink.....	77
Figure 8-6: Wind Turbine plant modelled.....	77
Figure 8-12: Varying power produced by RES simulated using MATLAB/Simulink	83
Figure 8-13: Varying power required by load demand simulated using MATLAB/Simulink	83
Figure 8-14: Power Balance ($P_{\text{Equilibrium}}$) from load demand and RES simulated using MATLAB/Simulink	84
Figure 8-15: SOC of Battery Energy Storage System simulated using MATLAB/Simulink.....	85
Figure 8-16: PV solar and BESS unable to provide enough Output power simulated using MATLAB/Simulink	86
Figure 8-17: WT and BESS unable to provide enough Output power simulated using MATLAB/Simulink	87
Figure 8-18: P_{BESS} and P_{Grid} graphs at RES output power of 4MW maximum levels simulated using MATLAB/Simulink.....	88
Figure 8-19: P_{BESS} and P_{Grid} graphs when RES unable to provide enough output power simulated using MATLAB/Simulink.....	89
Figure 8-20: Load Demand and RES Power for Case Study 1 simulated using OPAL-RT simulator	90
Figure 8-21: SOC and Power of Battery Energy Storage System (P_{BESS}) for Case Study 1 simulated using OPAL-RT simulator	92

Figure 8-22: Load Demand and RES Power for Case Study 2 simulated using OPAL-RT simulator	92
Figure 8-23: Main Grid Power needed and Battery Energy Storage System Battery needed for Case Study 2 simulated using OPAL-RT simulator	93
Figure 8-24: Battery SOC and Power of Battery Energy Storage System (P_{BESS}).....	94
For Case Study 2 simulated using OPAL-RT simulator	94
Figure 8-26: Battery SOC and Power of Battery Energy Storage System (P_{BESS}) for Case Study 3 simulated using OPAL-RT simulator	96
Figure 8-27: Main Grid Power needed and Battery Energy Storage System Battery needed for Case Study 3 simulated using OPAL-RT simulator	97
Figure 8-28: RES Energy and Needed Main Grid Energy Graphs for Case Study 2.....	98
Figure 8-29: RES Energy and Needed Main Grid Energy Graphs for Case Study 3.....	98
Figure 8-30: Power (W) Comparison Graph vs Time for Case Study 1	99
Figure 8-31: Power (W) Comparison Graph vs Time for Case Study 2	100
Figure 8-32: Power (W) Comparison Graph vs Time for Case Study 3	101

LIST OF TABLES

Table 4-1: Standard Test Condition (STC) of SunPower SPR-320E-WHT-D PV module @ 1000W/m ² Irradiation and 25°C temperature.	32
Table 4-2: 1.5MW Wind Turbine Specification.....	38
Table 4-3: Battery Discharge Values.....	42
Table 4-4: Lithium-ion battery Simulation Results.....	44
Table 5-1: Fuzzy Logic Controller Rules for BEMS	52
Table 6-1: Software and Hardware equipment used	58
Table 8-1: HOMER Cost Effectiveness Simulation Results (Dekeda and Adonis, 2019).....	73
Table 8-2: Summary of results taken at 95% level of SOC	81
Table 8-3: Summary of the Three Case Studies Modelled.....	97

ABBREVIATIONS AND ACRONYMS

AC	Alternating Current
ARTEMis	Advanced Real time electro Mechanical Simulator
BES	Battery Energy Storage
BESS	Battery Energy Storage System
BMS	Battery Management System
BREEAM	Building Research Establishment Environmental Method
CAES	Compressed Air storage systems
CDPES	Centre for Distributed Power and Electronic System
CERTS	Consortium for Electric Reliability Technology Solutions
CO ₂	Carbon dioxide
COE	Cost of Energy
CPU	Central Processing Unit
CPUT	Cape Peninsula University of Technology
CSP	Concentrating Solar Power
CTC	Centralized Traffic Control
DC	Direct Current
DER	Distributed Energy Resources
DFIG	Doubly-Fed Induction Generator
DGs	Distributed Generation
DHI	Diffuse Horizontal Irradiation
DNI	Direct Normal Irradiation
EBIDTA	Earnings, Before Interest, Taxes, Depreciation, and Amortization
EMS	Energy Management System
ESS	Energy Storage System
FGD	Flue Gas Desulphurization
FIS	Fuzzy Inference System
FLC	Fuzzy Logic Controller

FTP	File Transfer Protocol
GHI	Global Horizontal Irradiation
GUI	Graphical User Interface
HIL	Hardware-In the-Loop
HOMER	Hybrid Optimization Model for Electric Renewables
HVAC	High Voltage Alternating Current
Hz	Hertz
IEEE	Institute of Electrical and Electronics Engineers
IRP	Integrated Resource Plan
kVA	Kilo Volt-Amperes
kW	Kilo Watts
LV	Low Voltage
MF	Membership Function
MGs	Microgrids
MPPT	Maximum Power Point Tracking
MVA	Mega Volt-Amperes
MW	Mega Watts
NASA	National Aeronautics and Space Administration
NPC	Net Present Cost
NPS	Negative Phase Sequence
NREL	National Renewable Energy Laboratory
O&M	Operation and Maintenance
OCGTS	Open Cycle Gas Turbines
PCC	Point of Common Coupling
PCS	Power Control System
POL	Petroleum, Oils, and Lubricants
PPS	Positive Phase Sequence
PQR	Power Quality and Reliability

PV	Photo Voltaic
RE	Renewable Energy
REIPPP	Renewable Energy Independent Power Producer Procurement Program
RES	Renewable Energy Source
RMS	Root Mean Square
ROH	Routine Overhaul
RT	Real-Time
SMES	Superconducting Magnetic Energy Storage
SoC	State of Charge
SPS	Sim Power System
SSN	Several State-Space
TFR	Transnet Freight Rail
THD	Total Harmonic Distortion
TPS	Traction Power Supply
TPSS	Traction Power Substation
UPS	Uninterrupted Power Supply
UV	Ultra Violet
VA	Volt-Amperes
VSC	Voltage Source Converter
VSC	Voltage Source Converter
VSI	Voltage Source Inverter
WT	Wind Turbine

GLOSSARY OF TERMS

Distributed energy resources	Sources of electric power that are not directly connected with a bulk power transmission system; these include Both generation and energy storage technologies
Generator	An electric machine that converts mechanical energy to electrical energy
IEC 61850	An international standard for communication in substations, also extensible to the rest of the power system
Inverter	A device or system that converts direct current to alternative current
Megawatts	A unit of power (rate of energy consumption) 1 megawatt is equal to 1 000 000 Watts
MATLAB	A multi-paradigm mathematical processing environment and fourth generation programming language
Model	A depiction of real world systems in a software Environment such as Simulink for improved understanding.
Simulink	An environment for block diagrams where multi-domain simulations and Model-Based Designs are carried out.
Distributed generation	The process of generating electricity using renewable energy resources – these resources generating the electricity are usually distributed over an area, like a photovoltaic farm. Electricity obtained by distributed generation is usually fed into a microgrid
Distribution network	A system of cables that deliver power to consumers at usage voltage levels
Electric power system	An assemblage of equipment and circuits for generating, transmitting and distributing electrical energy

Fossil Fuel	Fuel produced by remains of living organisms that built Up underground over geological periods; it mainly consists of carbon and hydrogen
Greenhouse	Emissions Gas emitted into the atmosphere that absorbs infrared radiation, thus contributing to the greenhouse effect xx
Load	A device that consumes electrical power
Microgrid	A micro power system that comprises a cluster of loads, storage and multiple DG sources. A microgrid can usually function in autonomous mode, or it can be linked to the national electricity grid
Real-time digital simulator modular	A fully digital power system simulator that performs detailed hard real-time electromagnetic transient simulations of the power system's behaviour and response
Renewable energy resource	Natural sources of energy such as sunlight, wind, rain, tides and geothermal heat, which are naturally refilled
Smartgrid	The term given to the modernized electric grid that uses ICT and computational intelligence to improve the efficiency, reliability, economics and sustainability of electricity supply
Voltage profile	A plot of voltage differences of a given supply network over a period of time
Fossil fuel	Fuel produced by remains of living organisms that built up underground over geological periods; it mainly consists of carbon and hydrogen

CHAPTER 1: Introduction

1.1 Background

The economy of any country is improved by efficient and reliable rail network, in which the movement of goods and commodities are transported. In South Africa, Transnet Freight Rail (TFR) is the largest national railway-freight logistics operator and a division of Transnet SOC Ltd that transports and delivers a broad range of bulk general freight commodities and containerized freight in the Southern African region (Transnet Integrated Report, 2016). This freight division manages long heavy haul exporting lines such as iron-ore line and coal line, thus, providing railway links between production hubs and ports, with operating shunting yards and depots in-between (Environment, 2016). Zwolski (2011) defined the railway yard as a series of railway tracks that form a complex network for sorting, storing, loading and unloading the wagons and locomotives.

TFR's rail network consists of a mix of electrification methods of 3kV_{DC} (4 935km), the preferred 25kV_{AC} (2 309km), and the only 50kV_{AC} (861km) which is on the iron-ore line (Africa, 2014). Nonetheless, the local municipalities supply electricity to most of the shunting yards and depots. For example, the local municipalities in Saldanha Bay and Sishen, supply 11kV_{AC} voltage to the Salkor and Erts freight-rail shunting yards, respectively. The railway shunting yards are used to service the locomotives and wagons. This service includes the bleeding of the brakes on every wagon and locomotive, visual inspection on the railway vehicles as well as connecting the railway vehicles back together by lacing their brake lines on their way out of the railway yard. In addition, the office work is basically performed in depots on these railway yards, because they share the same electricity network supply with the shunting yards.

With increased competition from the trucking companies, the freight rail industry is facing a growing need to make their operations faster and cheaper (Li et al., 2016). This is normally done by using the most reliable, efficient and environmentally friendly technologies. Notably, Transnet Freight Rail (TFR) is no exception to the difficulties experienced with the introduction of advancing technologies both in their operating railway shunting yards and mainlines. Furthermore, in the past years, TFR has installed technologies and developed infrastructure as a focus of standardizing their technologies to improve operational efficiency, safety and business performance. .

The major facilities and electrical equipment on the railway yard locations include the following:

- i. Administration and operations tower building for employees,
- ii. Diesel locomotive workshop, utilities rooms and ablutions,
- iii. Security office,

- iv. Fuel Storage and Dispensing Facility,
- v. Tippler building, including subsurface structure,
- vi. Conveyor transfer towers,
- vii. Signals and Telecommunication Equipment,
- viii. Train control and operations offices,
- ix. Petroleum, Oils,
- x. Train Wash Facility,
- xi. Maintenance-of-Way Storage Tracks and
- xii. Control Tower

The global drive of improving technology and environment protection has led to the evolution of renewable energy (RE) and microgrids (MGs) into an increasingly adopted method of supplying power (Akinyele, Belikov and Levron, 2018). Electricity is a central element next to heat and fuels for understanding the global energy challenges. It is in fact the controlling energy carrier used around the world residentially, commercially and in industrial processes. The growing importance of energy sustainability imposes the need to monitor and control the optimal usage of energy assets in South Africa. At the same time, the various utility grids and some hybrid microgrid (MG) systems are scaling up the penetration of renewable energy resources. Also, due to an intermittence nature of wind and solar energy, the growth in renewable sources increase the challenges these systems will meet (Crabtree et al., 2010).

Notably, the renewable energy in many parts of the world, is beginning to be earmarked as a major part of the future energy mix as seen on Figure 1.1, where it can offer a way to increase electrification and decrease the share of fossil fuels in the generation mix (Ustun, 2017a). Currently, 91% of South Africa's electricity is derived from large coal mines in the North East prior to being sent via high voltage transmission lines to the rest of the country (Bugaje, 2006). Furthermore, South Africa is currently the fifth largest producer of coal in the world and is the sixth largest consumer (Slann, 2013). This in turn has resulted in South Africa being an extremely energy-intensive country and the twelfth highest carbon dioxide emitter in the world (Slann, 2013). Remarkably, the electricity tariffs increase along with diminishing natural resources and increased consumer energy demand is slowly making renewable energy more desirable and financially viable in South Africa (Cameron and Rossouw, 2012).

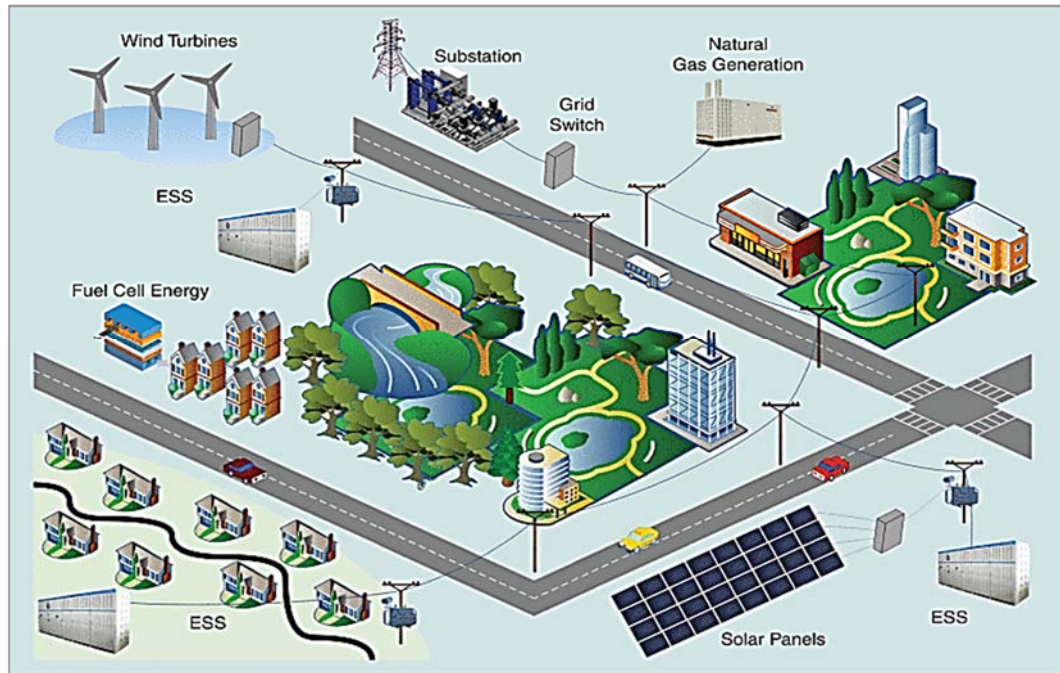


Figure 1-1: A microgrid envisioned for a small town (Q. Fu et al, 2013)

In today's cost-competitive and market-driven economy, engineers are seeking technologies or methods of reducing energy expenses and environmental impact (Osuri, Ngoma and Chowdhury, 2005). South Africa alone produces more than half of the electricity generated in the entire African continent Osuri et al. (2005), thus, energy is very important in every aspect of the economic and Social development of any country. Using renewable energy sources (RES) for electricity generation in South Africa would have tangible environmental benefits, given that 91% of electricity generation is currently based on coal (Winkler, 2005). This research project came into existence after productive discussions on managing the future energy demands in which a more flexible, informative, configurable and physical energy system in the voltage distribution power networks of freight rail shunting yards, is required.

This research project is constituted to the initiative made by Transnet Freight Rail (TFR) in 2012, to improve the energy efficiency, contributing to reduce carbon emissions and assist with the country's generation capacity constraints. However, Transnet Freight Rail (TFR) required a detailed energy management strategy to optimize its electrical energy demand in railway operations. The following were specific aspects of focus in that initiative:

- i. Best methods for improving railway electrification infrastructure offered by new technologies.
- ii. The correction of electrical power factor
- iii. Improving energy-efficiency of rail traction, workshops and railway buildings.

A decision was taken to work on MGs, which are emerging and becoming more attractive structures with integration of renewable based distributed generation (DG) units and energy storage systems (ESS).

1.2 Problem Statement

In order to ensure the smooth operations at a rail yard, a reliable power supply is paramount. Traditionally, reliance was on grid-supplied power, but in recent years, the single national electricity utility has experienced generation constraints and has begun countrywide load shedding. The generation constraints begun in 2008 and has persisted to the present day causing the current grid intermittency. This consequently affects rail yard operations. These rolling blackouts play havoc on industrial processes and operations. Moreover, the fact that there are no renewable energy-based backup power-systems put in place for shunting yards' operation at Transnet Freight Rail (TFR) other than uninterrupted power supplies (UPS) with batteries that last for 2 hours is a major problem addressed in this research. These current electric power supplies affect the entire business during power failure or power outages by the local utility grid.

The secondary issue that will be addressed is the electricity (energy) expenditure by this freight rail organization for its day to day operations that is bought from the utility grid; as in 2016/2017 financial year, energy expenses increased by 6.1% and that affected their Earnings Before Interest, Taxes, Depreciation, and Amortization (EBITDA) performance (Transnet SOC Ltd, 2016). South Africa has an increasing rate of energy demand, global warming, environmental challenges, as well as the dramatic change in the consumption behaviour of user on conventional energy. Furthermore, the energy consumption by natural gases in South Africa accounts for 4% and coal still provides the bulk of electricity generated in South Africa, with the accompanying CO₂ emissions and high-water usage (Li et al, 2016).

1.3 Aim and Objectives

1.3.1 Aim

The aim of this research project was to design a real-time model of a microgrid (MG) which could be used in supplying power to the railway yard equipment and facilities, efficiently using renewable energy sources (PV solar and wind turbine) as distributed energy resources DERs.

1.3.2 Research Objectives

- i. Perform a feasibility study and cost-analysis of the renewable energy microgrid using Homer Energy.
- ii. Select, design and model a distribution feeder in real-time using Simulink and RT- Lab.
- iii. Model and simulate Hybrid AC/DC MG consisting solar PV, wind turbine and battery energy storage system (BESS) using MATLAB/Simulink
- iv. Link and simulate in real-time the feeder distribution with distributed energy resources (DERs) and ESS models using Simulink in OPAL-RT.
- v. Implement, simulate and analyse the energy management system (EMS) of the renewable energy microgrid in real-time using OPAL-RT.

1.4 Project Scope

This research project is for the development and innovation of photovoltaic solar renewable and wind energy-based microgrid (MG) that can supply power to freight rail yard. The design of this particular power supply system will act as a back-up or emergency supply in case of power outages and also with the planned power-saving schedules, it will be connected to the main grid; whereas, at places with high levels of solar radiation and wind speed, it will act as the first method used to supply the yard. The microgrid (MG) was built using photovoltaic (PV) solar panels and wind turbines, which acts as a distributed energy generation and lithium-ion batteries acts as an energy storage system (ESS). This type of microgrid (MG) system has an ability to operate in both modes i.e. islanded and grid-connected modes. In the yards' substation, there will be a 1600 kVA transformer, which steps down the incoming voltage from 6.6kV_{AC} or 11kV_{AC} to 400V_{AC} for low voltage (LV) equipment and 500kVA transformers that step down 400V_{AC} to 220V_{AC} or 110V_{DC} for control and instrumentation. A maximum (peak) of 5MVA was required to run the rail yard.

This is anticipated to lower operational energy expenses for freight rail companies, assist the yards in case of power outages and minimize costs of maintenance; thus, reduces greenhouse gas emissions as mentioned earlier. The new simulation equipment called OPAL-RT simulator was used to model and simulates all the relevant data in real time situations. Whereas, the Homer Energy software was initially used to effectively assess the costs and reliability of the microgrid system and the main grid. Additionally, the MATLAB/Simulink simulation software was used to simulate power components involved in the design. The department of infrastructure electrical services at Transnet Freight Rail (TFR) together with the Centre for Distributed Power and Electronic System (CDPES) at Cape Peninsula University of Technology (CPUT) assisted in the development and design of this research.

1.5 Thesis Outline

- Chapter 1: The background on railway yards and research problem statement are presented in this chapter. Moreover, the chapter also highlights the objectives together with the scope of methodology of this thesis.
- Chapter 2: This chapter sets out the literature on railway yards with the discussion on the performance and various microgrid control components that were used by different writers. It also covers the different methods of interfacing the microgrid system in order to meet the requirements topologies.
- Chapter 3: The discussion regarding the feasibility of the developed system and the financial effects coursed by the implementation of the developed microgrid system designed are covered on this chapter. Thus, the different cases of the developed system are investigated on this chapter and present all the simulations that were performed on HOMER Energy.
- Chapter 4: Chapter 4 covers all the technical specifications of the different components used on the developed microgrid system. It also entails all the simulated results of the performance of the components used on the designed microgrid using MATLAB/Simulink.

- Chapter 5: This chapter discusses the results and the outcomes of the Energy Management System developed on this research thesis. It also presents all the simulation results that are found using the MATLAB / SIMULINK platform.
- Chapter 6: This section of the thesis outlines the overview and configuration of the OPAL-RT simulator with RT-LAB software.
- Chapter 7: Operated modes and scenarios in real-time simulation are discussed in this chapter.
- Chapter 8: This section of the thesis discusses the results of the simulated model using MATLAB/Simulink and in real-time using OPAL-RT simulator.
- Chapter 9: Outlines the conclusion and presents the suggestions as well as recommendations for future work.

CHAPTER 2: Literature Review

2.1 Overview

This chapter briefly reviews the background on operational processes and infrastructural improvements in rail freight yards. Almost upon the start of transporting freight via rail, the rail freight yards in railway industry (also classified as shunting yards or marshalling yards) are used as a base where the separation and re-assembling of trains are operated. Even though rail freight transportation is viewed as one of the best transport system considering environmental friendliness and containing rail yards, which play a very crucial role in railway freight operations, most freight transportation is still being done by road because of timesaving (Ustun, 2017). Freight services are affected deeply by the use of shunting yards as a result starting from 1950s; publishers have made much research about the maintenance and efficiency in operations, technology as-well as infrastructure in rail freight yards (Arefifar et al, 2016).

The transportation of freight via rail is a movement of goods between two different connection points within a railway network; however, with the exception of some routes that are inter-modal, it is unusual that these movements of goods from their origin to their destination travel on a point-to-point link. Furthermore, in rail freight yards, the load itself is not shifted from one train to another, and that act as one of its main characteristics (Ustun, 2017). Therefore, in order to allow the movement of a small number of freight cars and make the economies of scale useable, the process called shunting is needed. Thus, the decoupling of the freight vehicles from inbound trains and the formation of new outbound trains that are heading to the final destination or other shunting yards occurs (Zwolski, 2011.).

A railway yard that consists of a set of tracks for parking and sorting railway vehicles, performing further processing operations, as-well as performing maintenance and checks is called a shunting yard. In shunting yards, railway vehicles of inbound trains are separated and administered in a classified rail track to form a newly arranged train that will be ready for departure. Additionally, in rail freight transportation, rail freight shunting yards act as important components of infrastructure, and hence the financial savings are hugely increased by any small improvements in infrastructure or operations that results from a decrease of train boarding times in a shunting yard. Upon being defined on this thesis, the railway yard is made up of system of tracks laid usually on a level ground for receiving, storing, sorting, making up trains and dispatching railway vehicles. Nonetheless, sorting, reception and train departure are the most important functions of rail freight shunting yards. Shunting yards are used for freight transportation and passenger transportation, which are two different sectors of railway transportation; however, the functions of a shunting yard in both sectors are similar, although the numbers of wagons of freight trains are higher than those of passenger trains. Another aspect is that single units of passenger trains can be able to self-propelled. However, passenger rail operations will not be considered in this chapter and the entire thesis, because the focus is on rail freight operations (Ustun, 2017).

2.2 Rail freight shunting yards

Rail freight shunting yards can be found anywhere in the world, where there is a rail network, for example Bugaje (2006) in North America, Bailey shunting yard is the largest rail freight yard, globally. Union Pacific Railroad that is the second largest freight rail company in United State manages this yard. The area of 11.5km² for this shunting yard consists of 200 tracks that lie separately with 17 and 16 rail lines for receiving and departing, respectively. It is approximated that 14 000 of wagons pass through the shunting yard every day and 3 000 coaches are sorted daily. Fuelling and servicing centre for locomotives operates more than 8 500 locomotives, while wagon repair centre operates more than 1 500 wagons both in one month. (Slann, 2013).

Bayhead in Durban is a main and large shunting yard in the province of Kwa-Zulu Natal (KZN) that has north and south sections; and divided into five sub-units. The north section is served by a hump, which reduces the shunting requirements and consists of over 45 railroads. North-east and south-west of this yard, the Umbilo shed which is adjacent to the yard and a large former PX shed are located, respectively. Trains with containers use the Kings Rest yard for access. Whereas, the trains in Free-State main line and Glencoe-Vryheid line are served on the Danskraal shunting yard which is one of the eight freight rail shunting yards in KZN. Moreover, this rail-yard act as a train crew changeover point and comprise of a running shed for locomotives and depot maintenance for infrastructure.

Mugha Isarai yard is the largest shunting yard in India and the longest in Asia. This yard covers a huge expanse of length 12.5km and consists of 7 sub-yards and an electric and diesel locomotive sheds that holds 147 locomotives and 53 locomotives, respectively; as well as a wagon routine overhaul (ROH) shed. In daily operations, Mugha Isarai rail shunting yard operates 1 500, as well as 5 000 wagons during its peak time. The traffic in this yard is substantially reduced due to the termination of piecemeal loading. (Slann, 2013). Salkor freight-rail shunting yard in Saldanha Bay facilitates 342-wagon train compilation, which transport iron-ore from Northern Cape to the port of Saldanha Bay and other commodities such as manganese. It consists of facilities assisting for heavy maintenance for rail vehicles and provides the provisioning of locomotives and driver exchange point. Additionally, train inspections, break-ups of train compilation, air-breaks and tests are performed on this yard. Trains for dispatching on the main line are prepared on this yard, because it functions as a consolidation facility. In addition, in the future, this yard will be expanded towards north in-order to reduce the running time of the section.

Ronaldsvlei is an AC/DC exchange rail yard that facilitates locomotive exchange from 25kV_{AC} to 3kV_{DC} or vice versa which provides all the shunting duties for Coega railway yard. Currently, Coega railway yard services the automotive and container industries via the bulk terminal, but in the future it will facilitate

manganese also that is currently offloaded and shipped in Port Elizabeth harbour. The rail facilities at Coega will be expanded to include an arrival and departure yards capable of processing 200-wagon trains, two bulk-tiplers for offloading, as well as heavy maintenance facilities for rolling stock.

2.3 Freight Rail Yard Infrastructure

The energy efficiency of railway vehicles (i.e. locomotives and wagons) or rail-transport is already at a very high level today, nevertheless, railways have a great potential for increasing that energy efficiency even further and one which directly correlates to reduce emissions Li et al. (2016) not only in railway vehicles. Furthermore, freight rail shunting yards provide great opportunity for improving the rail freight sector to green technology. The energy consumption of railways is extremely low as compared to other systems of transportation such as road, aviation transportation etc. Therefore, many publications regard that as a tremendous advantage of rail transport over other systems of transportation. Consequently, in comparisons for passenger and freight transportation, the railways have proven their excellent position in CO₂ emission per ton km and therefore, these specific emissions are nearly directly coupled to renewable plants in energy generation.



Figure 2-1 (a): Sentrarrand freight rail shunting yard at night



Figure 2-1 (b): Yard control equipment installed at Foreshore, Port Elizabeth

For efficient working of a shunting yard, the electricity must be available at all times for lighting as seen on Figure 2.1(a) and Figure 2.1(b) and supplying the infrastructure buildings as-well as equipment used to perform operations (Transnet, 2016). Consolidating freight is an important component when greening the freight sector, more especially with a goal of reducing trucks on the road. Additionally, it is fundamental to efficiently undertake the enhancement in the capacity of railway yards in-order to increase support for green freight programs, thus freight rail yards must be designed and be strategically positioned to support consolidation of freight and also functions as a centre for distribution of goods (Transnet, 2016). The development of automation in a railway-shunting yard is another important aspect; hence, the researchers try to improve the rail yard equipment for the highest possible degree of automation. Thus, the efficiency in the shunting yards rises when the operations and processes are automated and certainly, with the assistance

of automation developers or manufacturers, personnel can be hugely optimized when supervising the automation machinery (Ustun, 2017).

Improvements in infrastructure, energy distribution technology and operational processes in rail freight shunting yards can lead to a better competitiveness of rail transport, which is the purpose of many political actions aiming at CO₂ reductions and rail yard efficiency (Zwolski, 2011). Currently, sustainability and renewable energies are the two main objectives the railway engineers are focusing on; furthermore, with the implementation of Building Research Establishment Environmental Assessment Method (BREEAM), the conditions of these two objectives can be achieved. The implementation of BREEAM standard provides a concise framework for identifying and implementing practical and measurable green building design, construction and maintenance solutions that reinforce the efficiency (Ustun, 2017). Therefore, the possible improvements regarding energy consumption and green technology in railway industry, precisely on freight rail shunting yards is manifested on this research project (Li et al., 2016).

2.4 Microgrid System with Renewable Energy Technologies

Concepts, case studies, and research approaches that have been used by researchers in the past to develop, model, and design the MGs integrated with RE technologies in the railway industry, are summarized in this chapter. This section mainly establishes:

- i. The effect of global warming and climate change,
- ii. Use of RE technologies community residences, hospitals, and military base,
- iii. Current power electrification used in rail shunting yards,
- iv. Effectiveness of implementing the MGs on the railway shunting yards,
- v. Usage of renewable energy systems in the railway industry and energy storage systems.

Moreover, there are case studies of potential MG projects that were examined also on this section that focuses on the electricity supply of railway yards, stations, and the use of RE microgrids around the world. Notably, these case studies look into the economics of installing a MG system, different types of storage systems, the impacts on environment, as well as potential barriers to implementation. The issue of global warming and climate change caused by the greenhouse effect has purposely encouraged the use of environmentally friendly energy to reduce greenhouse gas emissions generated from the use of fossil fuels (Pravitasari and Nisworo, 2017). Bahrami and Abbaszadeh (2013a) argued that, the studies have proven the energy consumption has increased by two folds in the last 40 years where the global energy consumption rate in 2012 was 10 Gtoe/year and that is predicted to rise to 14 Gtoe/year by 2020, thus indicating a constant rise in years to come.

Haigh (2013) added that, coal is the most polluting energy source on the planet, and the main cause of the world's CO₂ emissions which needs proper engagements, especially in South Africa. In 2014, the first unit

of Kusile power station started to be operational. This is a power station that was approved by South African government which will generate an estimated 37 million tons of CO₂ equivalent emissions annually and increase the country's total contribution to climate change by 10% (Haigh, 2013). However, the recent studies made by Kamboj and Chanana (2017) has shown that, the growth in level of environment emissions and growing energy demand have develop serious concerns which made renewable energy sources more appealing Kamboj and Chanana (2017), especially in supplying communities, hospitals, military bases and universities.

There has been little progress with deploying renewables in South Africa, more especially in railway yards and stations as compared to other European and Asian countries (African Development Bank, 2015). Rail yards represent critical points in the rail network, thus technologies that are cost-effective, less maintained, and environmentally friendly, should be in place for day-to-day operations and in cases of unforeseen circumstances. For example, along the Western Cape via West Coast to Northern Cape and around the world, many organizations, industries, and small communities are piloting the use of renewable energy to satisfy their energy demand.

Kathu solar park which has over 340 000 solar PV modules installed and Redstone solar thermal power project in Northern Cape, South Africa for instance has incorporated a 100MW centralized solar PV plant along with other sustainable living practices in order to satisfy the majority of its energy demand. This is therefore a part of the government's Renewable Energy Independent Power Producer Procurement Program (REIPPPP) (Zikalala and Chowdhury, 2015). However, there are many renewable energy plants that are fully operational in the Northern Cape, like Sishen Solar Energy Facility which has a nominal peak capacity of 74MW and this technology rather than coal-fired generation, it avoids 208 000 metric tons of CO₂ emissions by conventional coal-fired power stations into the atmosphere (Fluri et al., 2009).

Furthermore, on the Northern side of Western Cape i.e. West Coast, Vredenburg and Vredendal, there is an on-shore wind plant with the capacity of 90.8MW and a Solar Photovoltaic plant with the capacity of 8.8MW, respectively, that are operational. There are also many impressive examples of renewable energy driven MGs being used to power military bases especially in the United States of America (U.S.A) (Slann, 2013). One of those projects is, the Joint Base Pearl Harbour – Hickam military base in Hawaii has 146 kW solar energy systems and 50kW of wind power that is added to the existing renewable energy systems already on site (Feldman and Settle, 2013). The Fort Bragg military base in North Carolina, U.S.A. is another example of a military base with a renewable energy driven MG. The base has a management centre where monitoring of various generation systems and electricity distribution network occurs (Slann, 2013). The project studies, clearly shows that renewable energy technologies in railway industry, especially in rail yards has not found its ground, as they still use the conventional energy for electrical supply of the rail yards to power yard equipment, workshops and buildings during emergency and normal operation situations. In

2006, Nikouee and Ledbetter (2006) who was an electrical maintenance engineer in metropolitan Atlanta, designed and developed a DC traction power supply (TPS) and distribution system for Marta's Armour yard rail services and facility.

The yard is supplied by a local central stand-alone traction power substation (TPSS) which converts 19.8kV_{AC}, 3-phase, 60Hz voltage to 750V_{DC} that is distributed throughout the yard and maintenance shop. Moreover, the main objective of the Armour yard design and construction was for a maximum reliability and flexibility of operation, to serve as a proving ground for the new and emerging technology in DC power distribution system. This DC system used 60-cell round cell, lead-acid battery bank and a charger to control power for all the critical circuits, which has 8 hours of operation for back up, and power emergencies. Eskom (2015) reported on the construction project of the Medupi rail yard. This yard will assist Medupi power station in delivering the limestone via existing rail network. The Medupi power station will retrofit the flue gas desulphurization plant (FGD), which reduces sulphur dioxide emissions by at least 90% by reacting it with a limestone sorbent. The current plan to supply the rail yard, is to use the 6.6kV_{AC} limestone substation, which form part of the FGD plant. The main sub-station will distribute power into the yard lighting mini sub-station.

The yard's sub-station will have a transformer that will step down the three-phase, 6.6kV_{AC} voltage to 400V_{AC} voltage for light voltage (LV) equipment and 220V_{AC} or 110V_{DC} for control and instrumentation. The DC voltage will be generated by means of a UPS with a battery backup and the required DC voltage will be tapped off from the UPS. The electrical system will provide all equipment within the rail yard boundaries with electrical power (Eskom, 2015). Correspondingly, on the thesis written by Lin and Cheng (2009), concluded that, railways are environmentally friendly and most fuel-efficient methods of freight transportation. Additionally, the quality of air can be improved by trains, reduce the greenhouse gas emissions, and use of fuels and pollution (Lin and Cheng, 2009). However, that has not yet been critically applied on the technologies used to supply power for freight-rail yards and facilities around. Since the energy demand is rising and reserves of the natural sources are restricted, that makes a faster expansion of renewable sources a key factor in earning revenue and is the most important component of economic development (Vasant and Pawar, 2017, Kamboj and Chanana, 2017, Pravitasari and Nisworo, 2017).

Renewable energy is an unlimited source, which is free and sustainable unlike fossil fuels (Jawaid et al., 2012). Furthermore, Crabtree et al. (2010) judges that renewable energy sources provide clean energy because they are non-pollutant and non-contributor to greenhouse effects, global warming and produces little or no waste products such as CO₂ or other chemical pollutants. Therefore, they have a minimal impact on the environment, and thus they are used to add energy reserves to the system (Pravitasari and Nisworo, 2017). In the class of renewable energy technologies such as, wind turbines, geothermal, biofuels, hydropower etc., the PV solar is a most renewable energy technology used in a railway industry, primarily

for signalling sites (Smee et al., 2015). It is mostly used in the grid connected and the generator backed-solar power supplies (Smee et al., 2015). Although, PV solar is the most adopted renewable energy technology in the railway industry, it is incapable of acting as a main method of power supply to railway yard equipment and facilities (e.g. relay rooms, offices, workshops), instead it is used to back-up main power supply and charging batteries. In consideration of the foregoing, the slow application of renewable energy and MGs in railway industry must change positively and gain significant share of South African energy mix in the coming years to enable the country to continue developing.

It is easy to recognize the environmental and economic advantages of utilizing the alternative and renewable forms of energy; nevertheless, the disadvantages must be taken into consideration too. Notably, one amongst the other drawbacks of renewable energy technologies is that, it is difficult to generate the quantities of electricity that are as large as those produced by traditional fossil fuel generators (Crabtree et al., 2010). For that purpose, the power generation from all renewable energy resources, up to the satisfactory level, is very costly as compared to the conventional energy systems (Pravitasari and Nisworo, 2017). Renewable energy often relies on the weather for its source of power and this can impact the reliability of a consistent energy supply. When these resources are unavailable, so is the capacity to make energy from them and that can be unpredictable and inconsistent, Crabtree et al. (2010), argued.

However, Rajesh et al. (2017) mentioned that, the use of MGs together with RE technologies as developed by Consortium for Electric Reliability Technology Solutions (CERTS) can improve a consumer confidence and power quality. Rajesh et al. (2017) defined MG as a localized power system that is managed as a single unit for the exchange of power with the utility grid via a coupling point, and made up of loads, distributed generation, and energy storage. Moreover, Asmus (2010) and Schulz et al. (2012) defined MG in a broader manner than Rajesh et al. (2017), by stating that, it is a micro power system where different types of components such as DG units, controlled and un-controlled loads and storage devices are connected together in such a manner that the controlled power electronics devices and protective devices are operating together. Nonetheless, both Rajesh et al. (2017) and Justo et al. (2013a) identified important and identical factors that are involved in the definition of a MG which are DG and Storage devices.

Moreover, MG concept heavily depends on the reduction of production costs of renewable energy generation, storage technologies, reliability and flexibility of electric power system, and energy management systems, hence able to operate with and without utility grid connection. MGs with distributed generation sources and renewable energy sources can help reduce the present energy crisis and also help modernize the traditional grid Singh et al. (2017), more especially in railway industry. Therefore, there is no doubt that, MG is a system that is capable of working in isolation or in connection to the mains grid (Planas et al., 2015a); thus, becoming a way of integrating renewable energies, lowering costs and providing better grid quality all around the world (Rajesh et al., 2017). Consequently, it can be disconnected from the

traditional grid and operate autonomously as physical and/or economic conditions dictate (Zamor and Srivastava, 2010).

MGs can be operated based on the principles of the AC power systems i.e. AC MGs, or DC power systems i.e. DC MGs (Justo et al., 2013b) or both principles can be applied in one MG which that system is called Hybrid. Although distribution in DC is essentially more efficient than AC, because in DC there is no reactive power (Starke et al., 2008), the AC MG is more focused nowadays due to its ability to operate in conjunction with main grid, simple structure and cost effectiveness (Rajesh et al., 2017). Recent studies have shown that DC MG interface can result in significantly simpler control structure, more energy efficient distribution and higher current carrying capacity for the same line ratings (Dragicevic et al., 2016). Yet Justo et al. (2013b) argues that, according to the history perspective, AC power network has been standard choice for both commercial and industrial sectors since the late 19th century; thus, AC is easy to transform voltage into different levels and capable of transmitting power over a long distance, which makes it a main choice of power networks.

The growth and evolution of the future electricity grids is expected to come with the perfect basic MG structure (Wang et al., 2017). However, it is important nowadays to accept flexible MGs that operate in both modes i.e. in grid-tied mode and “off-grid” mode. In “grid-tied” mode, the MGs are allowed to import power from the electricity grid, whereas in “off-grid” mode, they are isolated from the upstream power grid and utilize their local generators as the source of power supply when needed (Wang et al., 2017). Typically, an "off-grid" MG is built in areas that are far distant from any transmission and distribution infrastructure and, therefore, have no connection to the utility grid (Dada, 2014a).

Hybrid power systems face far more challenges when operating in islanding mode than they do in grid connected mode. During islanding mode, Ma et al., (2017) declared that, the AC side will no longer be viewed as an infinite bus, which results in load variations adversely affecting the frequency and voltage of the system. If the system has a high penetration of renewable power, the situation can be even worse. However, the power flow should be balanced between the AC and DC sides to maintain stability on both sides of the grid and that should happen at any time (Ma et al., 2017). In recent years the number of technological developments on the design prototypes for energy electricity by using unconventional sources or renewable sources have been studied (Vasant and Pawar, 2017). Now more than ever, due to the increase in global warming, economic issues and challenges outlined above; renewable energy technologies such as wind and solar are developed to become key players in improving accessibility to energy not only on commercial and residential purpose, but also in railway industry around the world (Pillay, 2016).

In, 2013, the BNSF Railway which is a largest freight rail company in North America started to operate its own solar array located in Stockton. This solar array has 800-kilowatt (kW) ground-mounted solar system

that includes more than 3,330 PV solar panels covering approximately 3 acres. The annual energy usage in this freight rail company is 1.8 million kilowatt-hours (kWh), with 75% of this energy used at night. The estimated energy generated from the solar array is at 1.3 million kWh annually. Net metering and variable pricing optimize the financial returns of the BNSF. Therefore, the surplus energy generated by the solar array during the day is sold at premium rates, and the energy from the grid is purchased at lower costs during the night (Smith and Taylor, 2008).

In 2017, the NJ Transit railway company in United States selected Jacobs Engineering Group to provide the general engineering services and design of the NJ Transit MG, a project that will cost approximately over R7 billion (\$577 million). This MG system will be capable of providing reliable power for critical transit infrastructure that supports the rail systems operated by NJ Transit and other operators of the Northeast Corridor (NEC). Therefore, the highly resilient power will be supplied during critical times when the main electric grid on the region is compromised due to storms or other events. This new MG design will consist of a central, natural gas-fired power plant and associated substations, transmission/distribution lines to substations that electrify the tracks and operating controls for critical portions of the NJ Transit and the NEC systems, as well as connections to the Pennsylvania, Jersey, Maryland (PJM) commercial grid (Santoro and Daleo, 2015).

It is very important to improve power stability in the railway systems in order to increase energy efficiency, thus the idea of using energy storage system is much vital in the railway industry. The energy storage idea in the railway industry is not new, especially in DC powered systems. In 1970, JNR tested a lead-acid battery system that was expected to reduce line voltage fluctuations for its rural railway line to be used as a storage system in place. Later, in 1980, the Japanese railway company called Keihin Kyūkō Electric Railways introduced a flywheel system that was used in their substations. However, both these attempts were not necessarily successful, because regular maintenance was required for the flywheel system, and very short battery life was observed for the lead-acid battery based system due to frequent charge-discharge cycles. Additionally, the charge discharge rate was not high, because the introduction costs implicated that wider application was impossible (Takagi, 2009).

In 2016, Efficacity which is an institute that specializes in the research development of the energy efficiency in urban areas, led a project about the use of braking energy in order to manage and optimize the energy consumption in railway stations and yards. This institute used MG to perform an investigation on concepts of energy where the storage of braking energy of trains with a stationary electrical saving system was used. The idea was to store energy in hybrid storage system and restate it judiciously at different moments of the day, i.e. during peak or low energy consumption hours, to various kinds of station and yard loads. On the investigations, the methods to generate the braking energy were found, such as with a reversible AC/DC the energy can be balanced to the medium voltage grid, and electrical storage (Galaï-Dol et al., 2016a). When

the supply demand is low, the energy generated can be stored at a large scale, because it is widely agreed that, when using renewable energy systems to supply any kind of load, will never reach its full potential (Slann, 2013). Therefore, large-scale storage options that include pumped storage and compressed air storage systems (CAES) such as the following, can be utilized (Crabtree et al., 2010), although many sites lack the necessary geography, or the available capital required to install such systems:

- i. Thermal storage that balances fluctuations and allows the after- hours of peak sunshine to produce electricity,
- ii. The effective use of flywheels for frequency regulation, and
- iii. The use of Superconducting magnetic energy storage (SMES) for regulating power quality.

Furthermore, Crabtree et al.(2010) concluded that batteries offer another means of grid-level energy storage when electrical supply exceeds demand and they are feasible for any location, unlike pumped hydro and CAES. Therefore, batteries are the most commonly used method of storing energy at this moment in time especially for smaller-scale projects (Slann, 2013). Due to the potential of the battery market for applications such as the renewable energy and electric vehicle industries, more innovative and efficient battery technologies are constantly being developed and released onto the global market. G. Crabtree et al. (2010) suggested that, the use of energy storage system can be divided into three categories of utility applications which are:

- i. For management of power in base load,
- ii. Supporting the grid in the form of distributed load or storage or
- iii. Quality and peak of storage power as-well as in the application of uninterruptable power supply.

However, each of these categories represents different timescales from seconds to hours. Figure 2.2 details a number of energy storage options, including a few different battery chemistries.

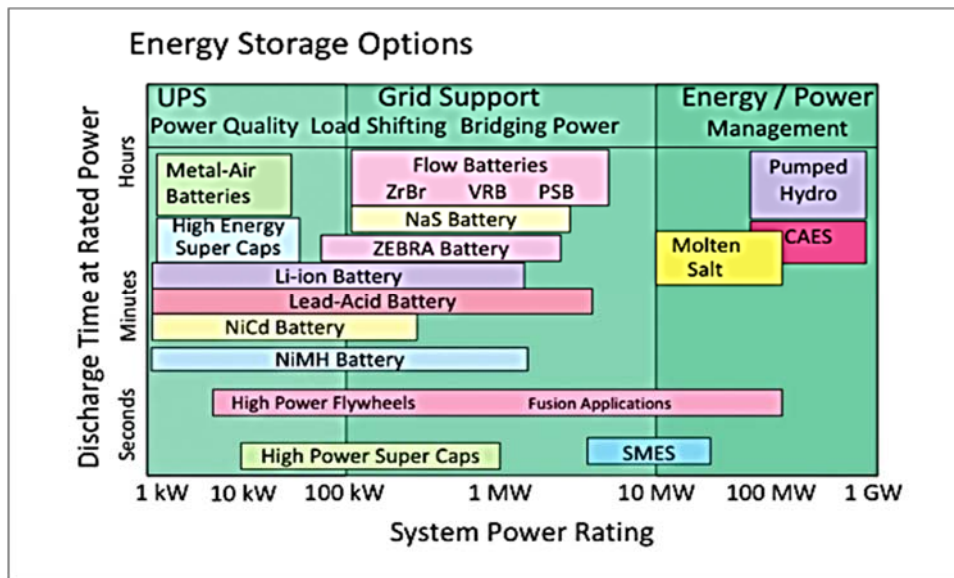


Figure 2-2: Energy storage options, (Crabtree et al., 2010)

2.5 Literature Summary

The reviewed literature demonstrated that designers and researchers before, but mostly for supplying the hospitals, military bases and for residential purposes, have used the methods and models intended to be used in this project. From the reviewed literature, it can be established that there has been little number of railway companies that has used MGs with PV solar and wind turbines as DERs this developed method of system in order to supply the freight rail shunting yards. In addition, it is clear that, there is little research done around the understanding of renewable energy technologies in the railway industry about the use of RE as main source of power supply in the rail yards of South Africa.

Moreover, the most of the rail yards are still using the conventional energy to supply power to the rail yards and charge the UPS batteries. Another gap identified is the use of lead-acid battery storage systems which JNR believed that the line fluctuations will be reduced when this type of batteries are used. A storage system with a mix of super capacitors and batteries allows the using of the residual braking energy at a choosing daily time. Therefore, it would be difficult to change all the already existing equipment but it can be interesting to forecast it for new rail yard concepts. Therefore, it is very important to consider the storage and timescale in order to determine the energy storage for a particular MG project.

CHAPTER 3: Feasibility Study of Microgrid System

3.1 Overview

This chapter outlines the modelling and simulation of the electricity generation, consumption of the typical freight-rail yard and the costs involved for the MG system; thus, providing analysis of the economic and technical aspects of the system. HOMER as a free software application was used to perform all the technical, financial designs and evaluation modelling of the microgrid system. This software application as explained on the sub-section, allowed the consideration of different technology options to account for energy resource availability and other variables during design phase.

Hence, the region of focus on this research study is Saldanha Bay in Western Cape Province; the background research was done to gather the various information and data about varying Saldanha Bay weather forecast, solar radiation as well as the load of the rail freight yard in this area of focus. With respect to the proposal of this research, essentially the renewable energy resources that were analysed and considered for their suitability for this MG design were solar and wind. Additionally, all other renewable energy technology options that are available in South Africa were not considered and are not explained in this research design.

Secondly, after covering the above-mentioned step, the feasibility study of the possible technologies involved in renewable energy systems, energy storage system for the generated electricity, network of the electricity locally (i.e. Salkor freight rail yard and municipality) and the components of the microgrid were all effectively performed. It is of importance to note that the technologies that were researched for this project report were those available in the market recently and available in HOMER libraries, although it is known that technologies changes with time. In this chapter, the details and all the reasons behind the choices of the technologies considered for this research will be thoroughly explained as well as the technical designs of the microgrid system.

3.2 Data Collection

3.2.1 Load

Proposing a realistic model of load (e.g. electrical, thermal, and deferrable) is the first step in MG system design. Therefore, in this research, the prototypical Salkor rail yard facilities-load requirements were used to perform simulations and are presented. The most critical electrical usage in Salkor rail freight yard's facilities are principally a centralized traffic control (CTC) building, yard automation (i.e. signalling and telecommunication equipment), machinery and tools, lighting (yard lights and inside the building), rectifiers and tools, as well as HVAC. Additionally, the maximum load peak of 5MVA with the power factor of 90% for the whole rail yard was assumed and the power outages were averaged to be one to three days per year. Power is supplied by local municipalities in most of the rail freight shunting yards in South Africa and the electricity tariffs from those municipalities differs from Eskom's tariffs which is the national electricity transmission state owned company. As a result, the average electricity tariffs used in this research was as high as R1.49/kWh in South Africa. The seasonal load profile is illustrated on Figure 3.1 for a typical rail freight shunting yard.

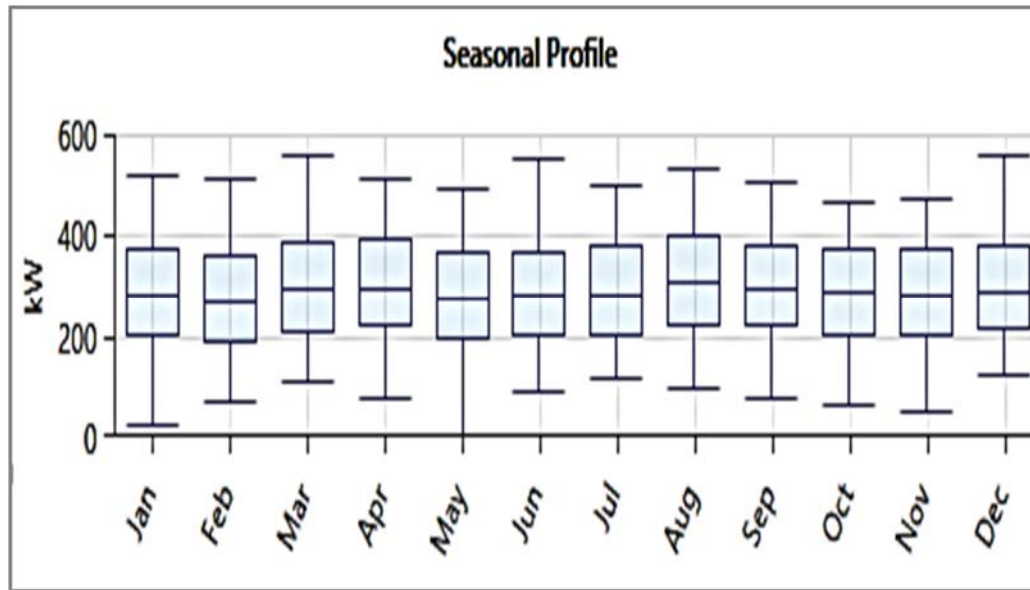


Figure 3- 1: Seasonal load profile for typical Salkor rail yard

In-order for the load-data to be more practically aligned, the random-variability inputs were set to 20% day-to-day and 15% of time-step-to-step to allow the industrial load to have a degree of variability at different times of the year. Due to the non-availability of the data that proves the on-peak and off-peak hours and also to the fact that the yard’s operations and working shifts run for 24 hours in 7 days, the load was set to be on its maximum peak for the whole 24 hours a day. However, it is of importance to note that only few buildings that are not utilized on weekends and between 23:59 to 06:00 as well as 17:00 to 23:59 during weekdays. Table 3.1 depicts the estimated cost and calculated consumption of electricity data for 25 June 2014 to 24 July 2014 period of Salkor Rail Yard according to the billing invoice from Eskom (Eb, 2014).

Table 3-1: Estimated cost and calculated consumption of electricity data for Salkor Rail Yard

Figure 3.2 shows the average daily usage for the period of January 2012 – January 2013 for Stamford

Month/Year	Price per kWh (off and on peak)	Calculated kWh	Monthly Cost	Estimated yearly cost
July 2014	R1.49	190 375 kWh	R283 655	R3 403 860

railway yard. Stamford’s consumption in summer is having a slightly higher demand than winter, thus proving the similar case for Salkor railway yard electricity usage for the year.

Therefore, the data depicted in Figure 3.2 was used as the daily electricity usage to perform the technical and economic aspects of the microgrid system in HOMER Energy software.

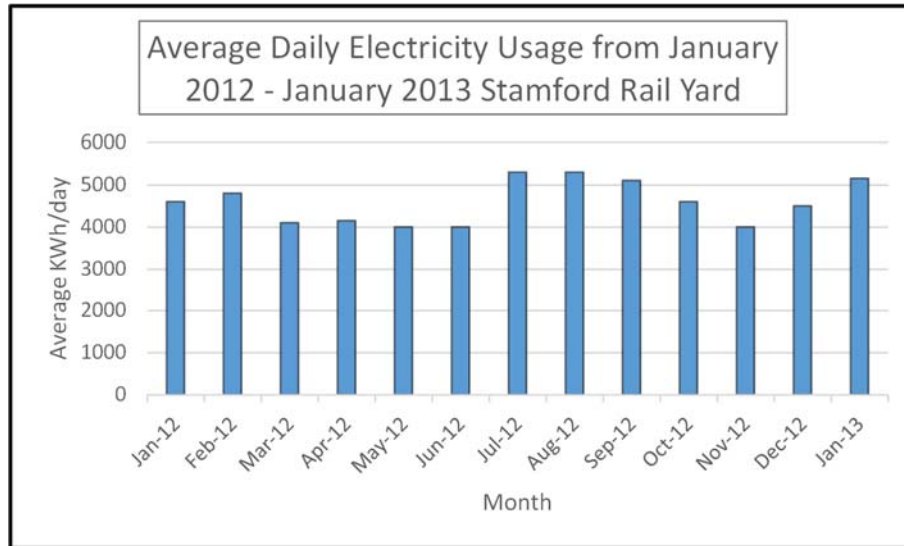


Figure 3-2: Average Daily Electricity Usage from January 2012 - January 2013 for Stamford Rail Yard (Necci et al., 2014)

3.2.2 Sources of Energy

With respect to Figure 3.3, it is clear that most parts of South Africa inherit more than 2000kWh/m² per year of GHI and some parts of the Northern Cape receives more than 2600kWh/m² per year of GHI (Slann, 2013).

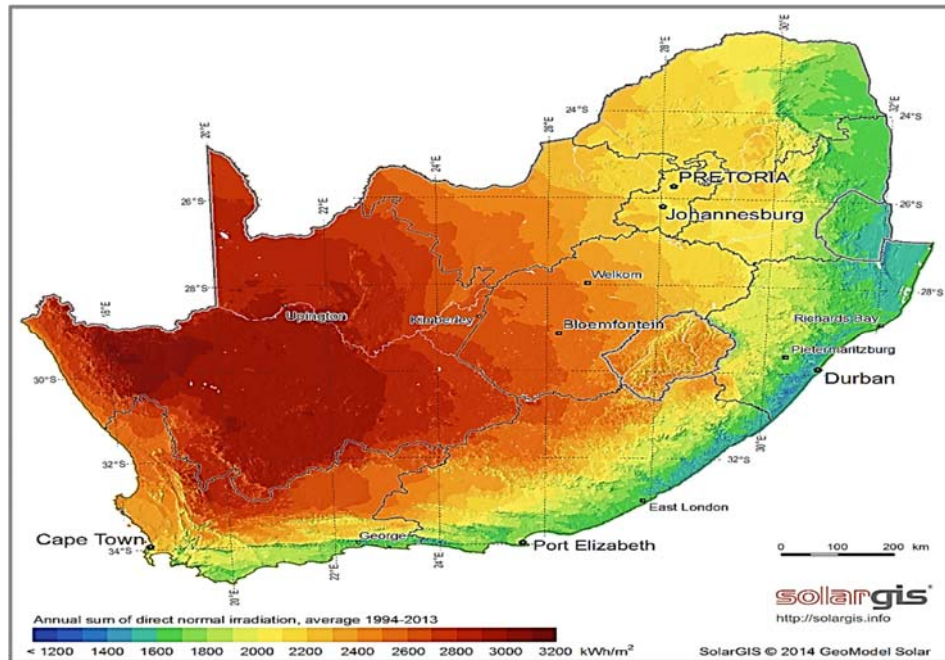


Figure 3-3: Annual DNI average for South Africa (Source: <http://www.solargis.com/>)

Whereas, the yield of electricity by wind turbine and wind speed were taken into consideration. The study conducted for this research thesis purely affirms and provide awareness regarding a huge opportunity of the

high prospect of RE availability in South Africa. According to the research performed, it is clear that the available RE sources that can be able to afford electricity supply looking at Saldanha Bay and South Africa as a whole are wind, solar and hydro energy. Nonetheless, for the purpose of this report, the possible evaluated renewable energy sources that are available in Saldanha Bay/Vredenburg are solar and wind energy. On the following sub-sections, the details of the two RE sources (i.e. wind and solar) are explained. Global Horizontal Irradiation (GHI) measured in kWh/m² is the most crucial factor to be considered during the calculations of the production of electricity by solar PV where the Diffuse Horizontal Irradiation (DHI) and Direct Normal Irradiation (DNI) are taken into account during the calculations.

3.2.2.1 Solar resource

The daily GHI of Saldanha Bay was extracted from the National Aeronautics and Space Administration's (NASA) surface meteorology and solar energy database using POWER data access viewer. POWER is a software for the prediction of worldwide energy resource with higher resolution daily time series. Additionally, HOMER energy simulation software that is explained on the sub-section 3.2.2 was used to simulate the data illustrated on Figure 3.4 which represents Saldanha Bay's average daily radiation and clearness index for the period of July 2017 to June 2018.

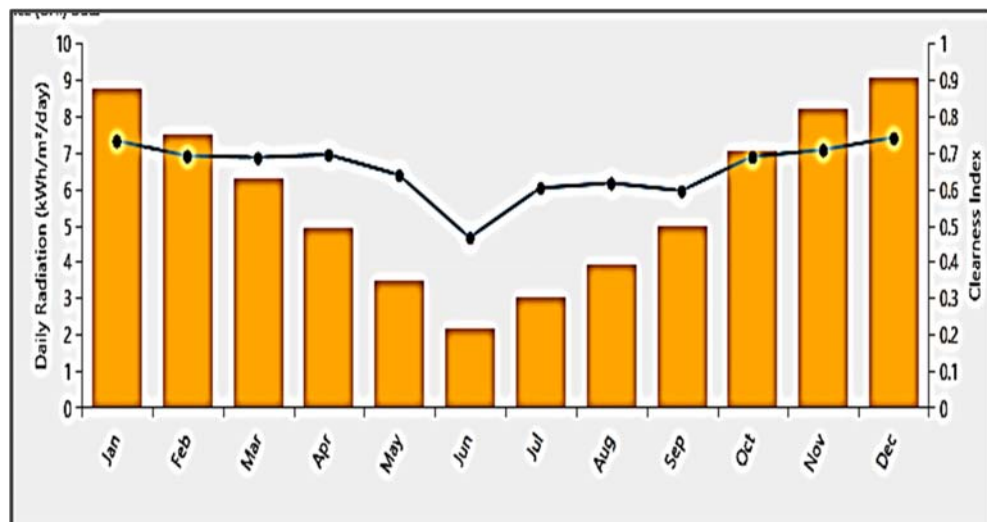


Figure 3-4: Daily radiation and Clearness Index for Saldanha Bay from July 2017 to June 2018
(Source: <http://www.solargis.com/>)

The yearly availability of solar radiation shows the steadiness and is verified by those two solar parameters. The annual average solar radiation for this region is 5.78kWh/m² per day and approximately 2150kWh/m² per year of GHI which is greater than most parts of the U.S.A. and Europe which are the countries that have most of solar and wind technologies. Therefore, solar radiation in this part of South Africa can be considered as alternative source for hybrid microgrid system in Saldanha Bay (Slann, 2013).

3.2.3 Wind Energy

The high-pressure system of the Atlantic Ocean and the strong winds that are caused by deep troughs lows in West Coast, thus the south-easterly winds in the south-Western Cape where Saldanha Bay is found, are

caused by that ridging of the Atlantic Ocean (Kruger, 2010). Furthermore, the Western Cape is exposed to an average wind speed of 6 meters per second (m/s), yearly and this is one of the reasons engineers believe that installing wind farms in this region is of high possibility (Slann, 2013). Therefore, the renewable energy source except solar with the most potential for use in Saldanha Bay is arguably wind energy (Slann, 2013). The recorded data obtained from the NASA surface meteorology and solar energy website assessed a 10 year averaged annual wind speed for Saldanha Bay to be 4.65m/s at the same 10m height.

Figure 3.5 illustrates the monthly averaged wind speed at Saldanha Bay and as mentioned earlier, the wind speed was measured in 10m height. It is observable that the maximum measured wind speed is within the period of October to February, reaching a monthly average wind speed of 4.5m/s in December, while it is lowest in July. Thus, the afore mentioned information about wind speed in Saldanha Bay proves that wind energy can be utilized in generating supporting energy together with solar and/or diesel stations in most of the months per year.

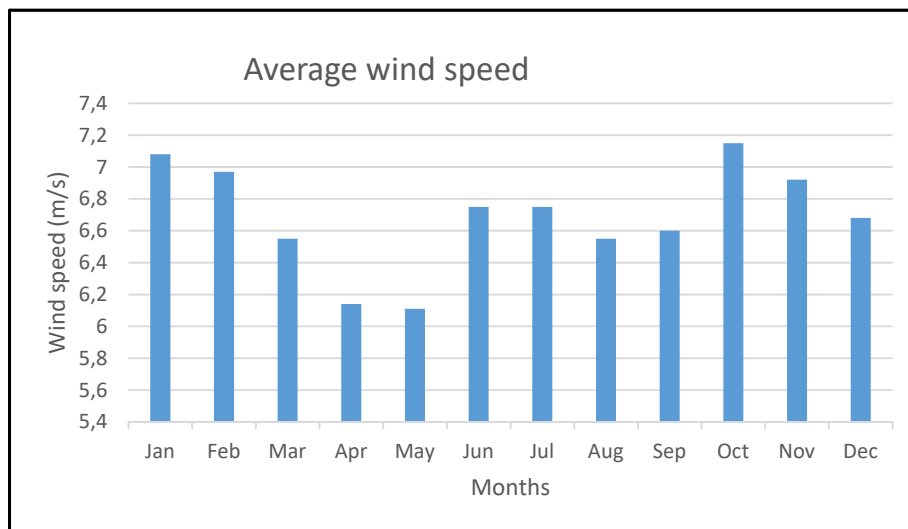


Figure 3-5: Monthly Average wind speed for Saldanha Bay from July 2017 to June 2018
(Source: <http://www.nasa.gov/>)

3.3 MG Design Specifications

This section of MG system design specifications outlines the development of different types of case studies used to model the designed MG system in this research thesis. Afterwards, the hardware components and software used are described by giving their specifications. Then finally, this section provides the critical limitations and suppositions of this research thesis.

3.3.1 Case Studies

The assumed rail freight shunting yard load that is modelled for this research thesis is primarily described in detail at section 3.1.1 and as mentioned that the location will be potentially Saldanha Bay. It is expected that the wind turbine farm and/or PV solar farm would be near the rail yard in a land where there will be no

drawbacks posed by the installation of these two renewable energy technologies. Furthermore, with regard to financial benefits and resource availability, building these two systems in places where there are less physical destructions is more feasible, especially for the wind resources (Thompson and Duggirala, 2009).

On the modelled MG system, the load is assumed to be operated in both off-grid mode as well as grid-tied mode and both the schematic diagrams of the autonomous MG system and grid-connected MG system are shown on Figure 3.6. In-order to assess the outcomes of PV solar and wind energy resources in the rail freight shunting yard in Saldanha Bay, two scenarios were modelled with different rates of PV solar and wind penetrations on the last scenario of RE penetration case. The case studies are described below.

- **Grid power only scenario:** In the grid power only case, Saldanha Bay municipality using 11kV_{AC} transformer to Salkor rail yard distributes electricity and hence in Salkor rail yard there is no backup power system used. However, the centralized traffic control (CTC) building is the only critical building on this yard and is the only building that has a generator for backup purposes. Therefore, this backup system used will not be considered as it is only supplying one building instead of the whole rail yard and hence other rail yards do not have CTC building.

- **RE penetration scenario:** Large quantity of PV solar and wind capacity are required in-order to introduce the RE (PV solar and wind turbines) to replace the 11kV_{AC} grid power from the municipality. Wind and solar are intermittent sources and due to that reason, as much as one wind turbine of 3MW capacity is required for this research. In addition to that, during the optimization process of simulation as seen on table 3.2, a 1.5MW of PV resource was considered.

The lithium-iron is added to the developed model to act as a peak solver for times when wind and solar are unavailable. In the RE penetration case, the off-grid and grid-tied scenarios were considered and it is vital that the system should work in both cases due to the unforeseen circumstances that can arise on power grid when the system is acting as backup or when the system is acting as the first method of supply. However, on the case where PV solar system is working with the grid only as shown on table 3.2, the amount of 3MW PV solar capacity is required and the power grid is considered to work as backup power supply.

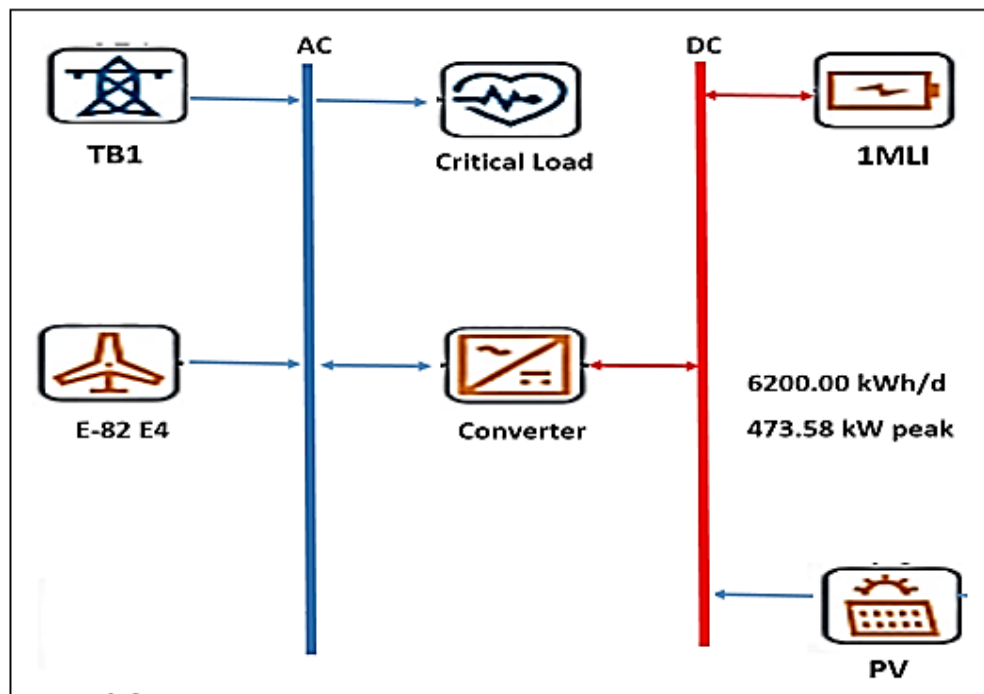


Figure 3-6: Microgrid system schematic diagram designed in HOMER

3.3.2 HOMER Simulation Software

Homer software was used to conduct the economic viability of this study. Furthermore, HOMER is software that was developed by National Renewable Energy Laboratory (NREL) of United State and was selected for modelling microgrid system due to its availability and ease to use by the public. With Homer software, the life cycle that includes operation and installation costs of the physical microgrid system can be modelled and compared with different models of MG designs focusing on technical and economic characteristics.

Homer software as illustrated on Figure 3.7 is mainly structured to focus on three different phases namely simulation, optimization and sensitivity analysis. The most essential Homer software process is simulation phase where the designed microgrid system is simulated for long-term operation and variety of system configurations. The results of the systems configuration that are simulated are then optimized in-order to find the best configuration system looking on the costs and variables of the designed system such as the number of PV array and wind turbines. Finally, the optimum results from the optimization process are then subjected to sensitivity analysis in-order to find the sensitivity of the systems' outputs to the changes made in the inputs.

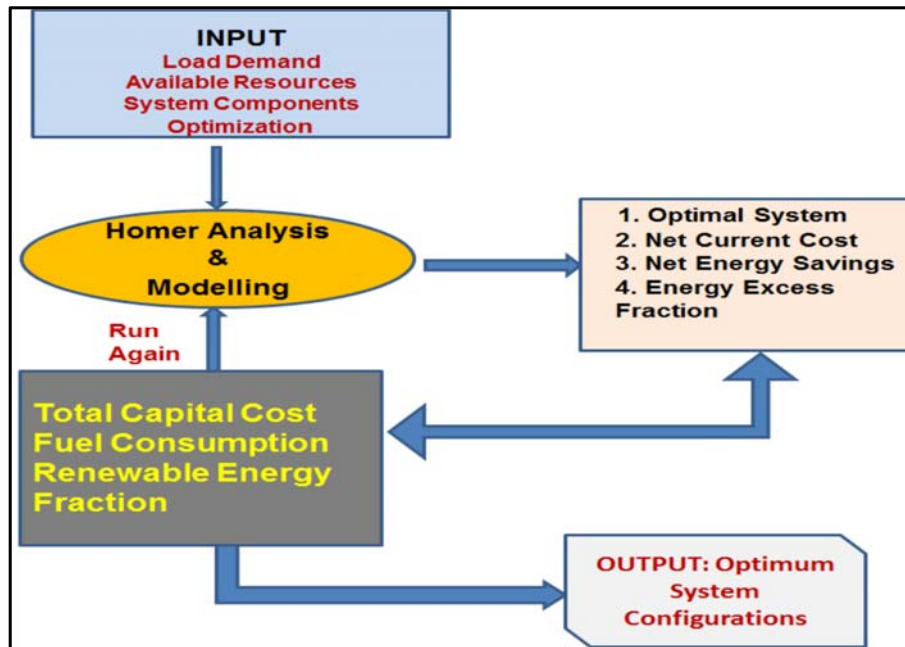


Figure 3-

Architecture of HOMER software (Belu et al., 2014)

7:

3.3.2.1 Simulation Settings

Due to the close proximity that is assumed between the modelled industrial load and power generated, Homer models a scenario that has no dissipation of electrical energy. The cycle charging mechanism is one of the discharging strategies that were considered on this research where the minimum state of charge (SOC) parameter of the battery is 30% and forces the grid power. PV solar panels and wind turbine to start at the SOC. Additionally, the maximum set point of SOC is 90% and in this research the grid power, wind turbine as well as PV solar panels will charge the battery bank until it reaches that maximum set point SOC. This is to prolong the lifespan of storage system (i.e. lithium-ion batteries by avoiding deep discharges and also be able to maintain the high load of supply.

3.3.3 MG Hybrid System Components

There are four hybrid system components that were designed for this research study of renewable energy-based microgrid system and they are PV modules, wind turbine, power converters as well as energy storage system, which is made up of Li-ion battery banks. This research attempts to find the best optimal option that will be suitable to supply power to the rail freight-shunting yard called Salkor yard in Saldanha Bay using the mix of those components sizes. Therefore, the following hybrid system components were designed to meet the AC load of the above mentioned rail freight yard.

3.3.3.1 PV Solar

On the designed microgrid system, there were various PV capacities that were considered and therefore, the maximum of 1.5MW PV capacity was allowed. During the low levels of load demand, the power generated by PV system was assumed to charge the batteries and support the load. It is always critical to consider worst case scenarios during designs and in this microgrid system that aspect was considered where the

lifetime of the PV operation was assumed to be 5 years less than NREL's data which indicates 20 years' period of lifetime. Thus, the assumptions that are made on the research that can affect the PV system performance were compensated. However, the monthly average temperature was considered and the derating factor of 80% to each PV solar panel was activated. The power point tracking was assumed not to be installed; this is to avoid any unnecessary costs. The PV array was expected to be installed with the same inclination angle, which is equal to the site's latitude, and lastly, the ground reflectance was assumed to be 20%.

3.3.3.2 Wind Turbine

For this research, a GE1.5xl and GE 1.5sle wind turbine which is manufactured was used. The capital cost of one turbine is R153 130. The replacement cost is assumed to be the same as capital cost, with an estimated annual operating and maintenance (O&M) costs of R1 701/yr.

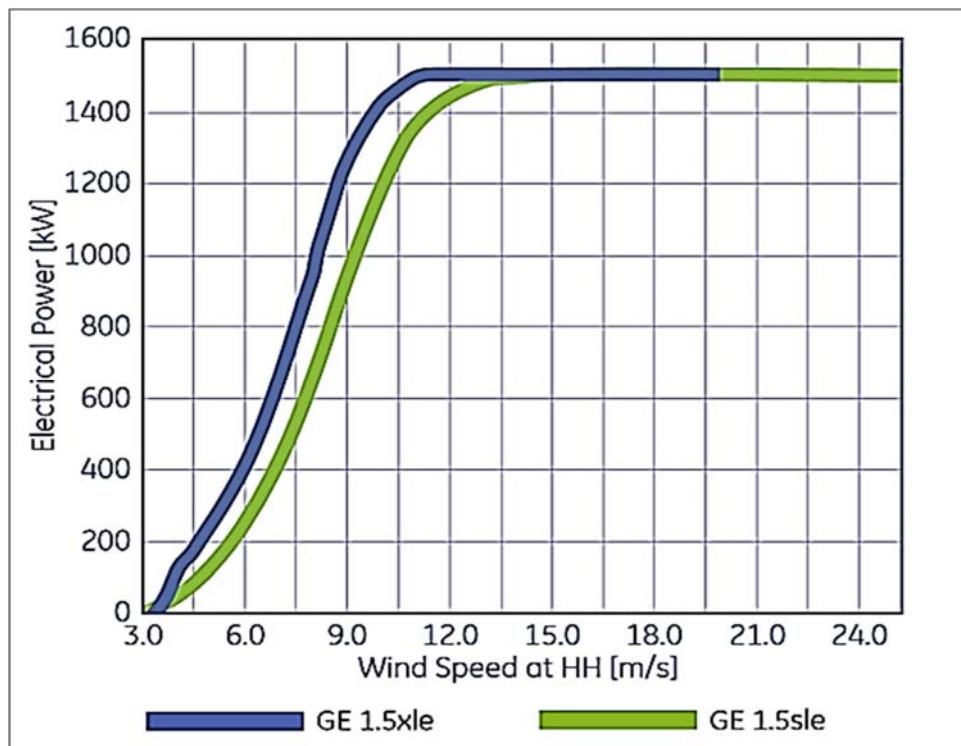


Figure 3-8: Power Curves for GE1.5xl and GE 1.5sle wind turbines (Zobaa and Bansal, 2011)

The characteristics data of this wind turbine was inserted on Homer software and the power curve shown on Figure 3.8 was resulted. According to the specifications of this wind turbine, the hub height is 120m and it was assumed that this wind turbine will serve 20 years which is 5 years less than the normal lifetime of the model. Lastly, the several units (1-8 wind turbine consideration) were inserted in-order to take to account the optima sizing.

3.4 Chapter Summary

The Salkor rail yard facilities-load requirements were used to perform simulations with the maximum load peak of 5MVA and the power factor of 90% for the whole rail yard and the power outages were averaged to be one to three days per year. The average daily electricity usage for Salkor rail yard was compared to the January 2012 – January 2013 for Stamford railway yard. Thus, proved a slightly higher demand in winter. According to the research performed, the available RE sources used for electricity supply for Saldanha Bay and South Africa as a whole are wind, solar and hydro energy, however, the PV solar and wind turbine were used in this thesis. The daily GHI of Saldanha Bay was extracted from the NASA surface meteorology and solar energy database using POWER data access viewer. Moreover, the recorded data obtained from surface meteorology and solar energy website assessed a 10 year averaged annual wind speed for Saldanha Bay to be 4.65m/s. Therefore, the wind energy can be utilized in generating supporting energy together with solar energy in most of the months per year. The microgrid system outlined the development of different types of case studies used to model the designed microgrid system in this research thesis.

CHAPTER 4: Technical Specification Modelling and Results

4.1 Overview

This chapter of the thesis covers all the technical specifications of the different components used on the developed microgrid system. It also entails all the simulated results of the performance of the components used on the designed microgrid using MATLAB/Simulink.

4.2 MATLAB/Simulink software

MATLAB software is a programming language and development software in high level that is used for technical computing. In this research project, MATLAB/Simulink was used to perform modelling and simulation of the designed MG system in-order to identify and analyse the technical issues that are significant to the operation of the renewable power units generated by MG system designed. The embedded functions and capabilities of MATLAB/Simulink allows the tasks that require an extensive amount of computation to be solved quickly, thus this makes it the most important characteristic of MATLAB/Simulink (IEEE, 2009). Additionally, MATLAB/Simulink software easily expresses the mathematical notations in simple and recognizable formats by integrating the computation, visualization and programming in an easy-to-use environment and however, typical uses of MATLAB software includes modelling, simulation and prototyping, data analysis as well as visualization etc. Because microgrid system is part of electricity system, which is divided into two systems namely, consumption and production, therefore MATLAB software is able to simulate and analyse different parts of electricity system such as electricity consumption, electricity generation as well as electricity distribution. Moreover, the usage of Simulink tool in this software assisted in all modelling and analysis that supports linear and non-linear system occurring at the same time. The reliability and simulation during tests were essentially increased by Simulink tool in MATLAB.

4.3 MG Components Modelling Methodology

As mentioned above, the toolbox used for all the analysis of electricity simulation and modelling was MATLAB/Simulink and its Sim Power Systems (SPS) for the mechanisms of the strategies for power balancing and real-time simulation. The Figure 4.1 illustrates the detailed architectural design of the microgrid system for this study in-order to show the dynamic components behaviour of the circuit. The microgrid system uses the distributed energy sources (i.e. PV system and wind energy system), utility grid and BES for storage in case of the outages of utility.

The model of the microgrid system designed consists of five important sections classified as blocks in RT-LAB as seen on Figure 4.1: 1. PV system, 2. Wind energy system, 3. Li-ion battery storage system, 4. Main utility grid, and 5. Energy management System. Therefore, section 1, consists of PV modules (542kW). The DC-AC boost converter steps up the voltage to $11kV_{AC}$, which is connected to the PCC via a Voltage Source Inverter (VSI). The VSI was used in this study to control the active and reactive power, independently and to provide high efficiency by minimizing the harmonics generated. The Maximum Power Point Tracking

(MPPT) was used to control the DC-DC boost converter in order to make sure the maximum power is generated by the PV modules at all times.

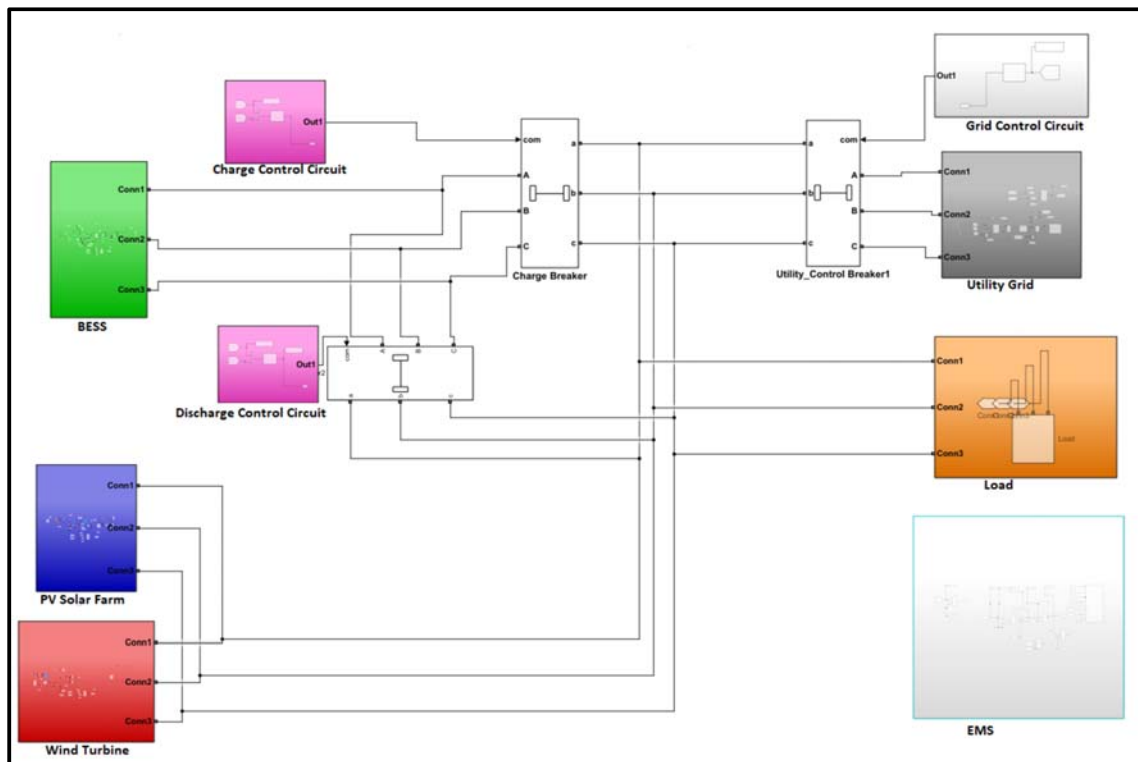


Figure 4-1: Architectural Design of the developed Microgrid System

Section 2, comprised of wind turbine (1.5MW) connected to the AC-AC converter that is connected to the step up transformer supplying the 11kV_{AC} PCC. Section 3, comprises of ideal Li-ion batteries that are connected to the bi-directional voltage source converter, (i.e. able to act as an inverter or a rectifier mode). This combination is connected in series to the DC-AC inverter and transformer to step-up the voltage from 11kV_{AC} to 400V_{AC}, which is feeding the PCC via utility grid control circuit breaker 1. Section 4, consists of the utility grid behind a fixed impedance fed through a step-down transformer (5MVA, 11kV_{AC}) connected to 11kV_{AC} PCC bus via utility grid control circuit breaker 1.

Section 5 is made up of the 3-Phase distribution feeder connected from the 11kV_{AC} PCC voltage and feeds the loads via CB3. Thus, CB3 is connected to the 1600 kVA transformer, which steps down the incoming voltage from 11kV_{AC} to 400V_{AC} for LV equipment and 500kVA transformers that step down 400V_{AC} to 220V_{AC} and 110V_{DC} for control and instrumentation. The system is designed to supply the two types of loads that therefore total to a maximum of 5MVA the critical load and non-critical load using both islanded and grid-tied modes.

4.3.1 PV Solar module

4.3.1.1 Modelling Design and Results

Originally, in order to figure out the design performance of a PV solar cell, it is obtained by considering it as a diode in which the electron-hole pair is generated by appropriate energy levels in the form of photons of the light energy. Therefore, the set electric field on the junction separates the electron-hole pair generated. The photovoltaic modules are implemented as an array, thus forming the strings of modules that are connected in parallel and in series. Moreover, the built array block of PV module allowed a simple model designed for a PV solar module consisting of the five model parameters, namely: a current source I_L or I (light-generated current), I_d (diode current), I_{sh} (ground-shunt current), R_s (series resistance), and R_{sh} (shunt resistance) to show the irradiance- and temperature-dependent I-V characteristics of the modules as depicted on Figure 4.2.

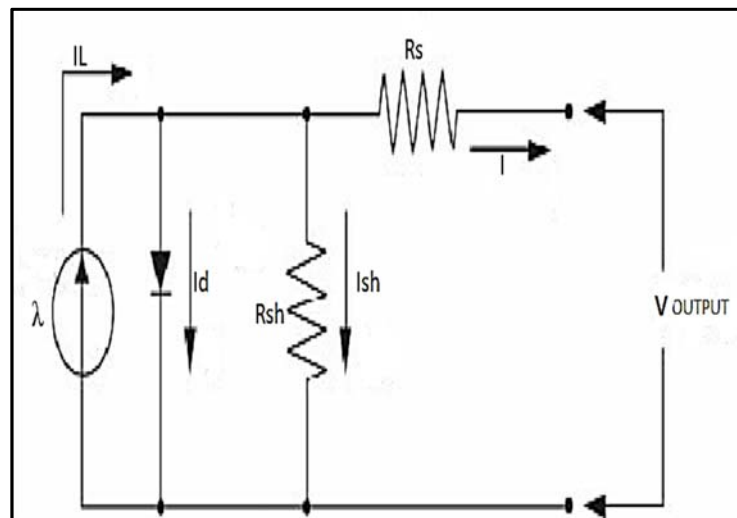


Figure 4-2: Ideal PV Model characteristic (Tarak Salmi, 2012)

The PV solar cell, as seen on Figure 4.2 is made up of various components, as mentioned above. The resistance R_{sh} component is connected in parallel to the diode thus make it inversely proportional to the shunt leakage current to ground (i.e. $R_{sh} = \infty$: no leakage to ground). On the circuit below of the PV solar cell, the leakage resistance was assumed to scope infinity without leakage current to ground and therefore, the varying resistance does not have much effect on PV array. Nevertheless, the output power of the PV array will be affected, significantly by the small variation of the series resistance R_s which represent the internal resistance to the current flow (i.e. $R_s = 0$: no series loss). In the equivalent circuit of the PV solar cell in Figure 4.2, the supplied current to the external load equals the current I generated by the illumination and thus, less than the diode current I_d and the ground-shunt current I_{sh} .

The output characteristics of the PV model was designed and built using MATLAB/Simulink where the demonstration of non-linear I-V and P-V outputs of the generalized PV model were proven. A single diode junction together with a series resistance connected in parallel with a shunt resistor was used to model an equivalent circuit of a PV cell as shown on Figure 4.2. In the PV modelling, the PV cell characteristics were

taken into consideration because of its effect by the two parameters namely, ambient temperature and cell temperature. The equation of the voltage-current (I-V) characteristic of PV solar cell model is mathematically indicated on Equation 4.1 (Jung & Ahmed, 2010; Chowdhury et al., 2008 and Salmi, 2012).

$$I = I_L - I_S \left(\exp \frac{e(V + IR_S)}{mKT_C} - 1 \right) - \frac{(V + IR_S)}{Rsh} \quad (\text{Equ 4.1})$$

Here, I; PV output current (A), I_S ; series current (A), V; output voltage (V), R_S ; series resistance (Ohms), K; Boltzman constant (1.38×10^{-23} Joule/°KT), T_C ; cell temperature (K) and Rsh; shunt resistance (Ohms).

The operating temperature of the PV cells and solar radiation as shown on equation 4.2 controls the photo current. Where I_L ; current generated by incident light (A), I_{SC} ; short circuit current in standard testing condition (@1000 W/m², 25 deg C), λ - current solar insolation, K_i ; short-circuit current temperature coefficient, T_C ; cell temperature (K), T_{Ref} ;

$$I_L = \frac{(I_{SC} + K_i(T_C - T_{Ref})) \lambda}{1000} \quad (\text{Equ 4.2})$$

The cell temperature fluctuates together with the saturation current as represented on equation 4.3. Here, I_S ; series current (A), I_{RS} ; reverse saturation current (A), T_C ; cell temperature (K), T_{Ref} , q; Electron charge (1.6×10^{-19} Coulombs), K; Boltzman constant (1.38×10^{-23} Joule/°KT) and A; ideal factor of the PV usually (1-1.5).

$$I_S = I_{RS} \left(\frac{T_C}{T_{Ref}} \right)^3 \exp \left(\frac{qE \left(\frac{1}{T_{Ref}} - \frac{1}{T_C} \right)}{KA} \right) \quad (\text{Equ 4.3})$$

On the PV ideal model circuit shown on Figure 4.2, the PV output current (I) is the difference of the current generated by light incident (A) (I_{PH}), less than the diode leakage current (A) (I_O) and the reverse saturation current (A) (I_{RS}) as seen on equation 4.4.

$$I = I_{PH} - I_{RS} \quad (\text{Equ 4.4})$$

The appropriate elaboration of the PV solar cell model is shown on equation 4.5; where I; PV output current, I_L ; Current generated by incident light (A), I_o ; diode leakage current (A), V; output voltage (V), K; Boltzman constant (1.38×10^{-23} Joule/°KT), T_c ; cell temperature (K), R_s ; series resistance and q; electron charge (1.6×10^{-19} Coulombs).

$$I = I_L - I_o \left(\exp \frac{q(V + IR_s)}{mKT_c} - 1 \right) \quad (\text{Equ 4.5})$$

Table 4.1, was used to determine the array current as represented on equation 4.6 where the array has 106 parallel (N_p) and 16 series (N_s) cells on the PV solar array. Each PV module used consists of mono crystalline silicon with 96 cells. The values were tested in standard test conditions of irradiation 1000W/m^2 and cell temperature 25°C as seen also on table 4.1. In equations 4.1 to 4.6 above, the source model of the single-diode equivalent current was used in order to describe the I-V characteristics of the solar cell. Referring to the symbols used on equations 4.1 to equations 4.6, the symbols are explained.

$$I_{PV} = N_p I_L - N_p I_s \left(\exp \frac{q \left(\frac{V_{PV}}{N_s} + \frac{I_{RS}}{N_p} \right)}{KT_c m} - 1 \right) - \frac{\left(\frac{N_p V_{PV}}{N_s} + I_{RS} \right)}{R_p} \quad (\text{Equ 4.6})$$

Table 4-1: Standard Test Condition (STC) of SunPower SPR-320E-WHT-D PV module @ 1000W/m^2 Irradiation and 25°C temperature.

Parameter	Value
Maximum Power Point (Pmpp)	320.542W
Maximum Power Point Voltage (Vmp)	54.7V
Current at MPP (Impp)	5.86A
Short Circuit Current (I_{sc})	6.24A
Open Circuit Voltage	64.8V
Short circuit current temperature coefficient	0.061747
Open circuit voltage temperature coefficient	-0.2727

The detailed parameters as well as the procedural calculation for R_s and R_p of the PV solar cell model are obtainable from the PV module.

- K- Boltzman constant (1.38×10^{-23} Joule/ $^{\circ}$ KT)
- I_L - Current generated by incident light (A)
- V_{PV} = Output voltage (V)
- I_{PV} - PV output current (A)
- T_C - Cell Temperature in Kelvin
- q- Electron charge (1.6×10^{-19} Coulombs)
- I_{RS} - Reverse saturation current (A)
- I_d - Diodes leakage current (A)
- R_P - parallel resistance (Ω)
- N_S and N_P - Series and parallel numbers of solar cells

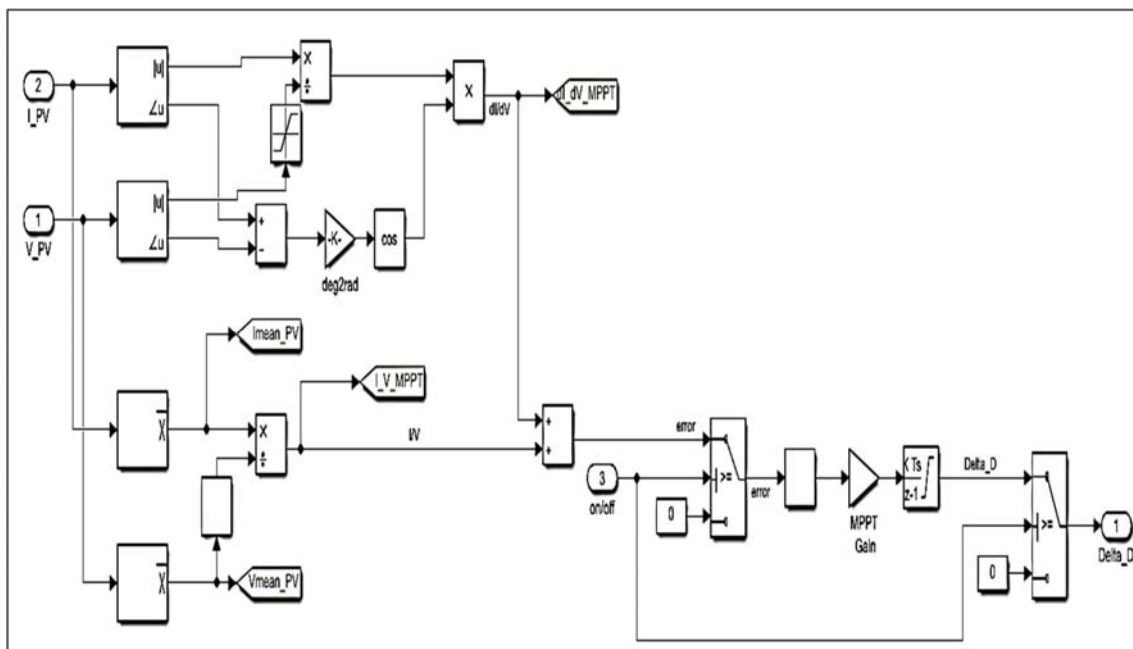


Figure 4-3: MPPT Controller designed on MATLAB/Simulink

The modelled PV solar system is precisely made up of a simple circuit formed by the PV array and an MPPT. The MPPT consists of a 5kHz boost DC-DC converter and the MPPT control using an incremental conductance and integral regulator technique as shown on Figure 4.3. To ensure that the voltage is increased and maintained on the PV system, a boost type DC-DC converter circuit was used in this hybrid microgrid system with the initial duty cycle of 50%. However, the effect caused by the solar radiation and the ambient temperature on the PV system's output performance was also considered, thus assuring that the PV output power is provided at maximum power point by the system at all times.

The PV array curves illustrated on Figure 4.4 is based on the SunPower SPR-320E-WHT-D module from the Simulink library with the P-V and I-V characteristic curves. Thus, allowing the plot of I-V and P-V characteristics for one module and for the whole array.

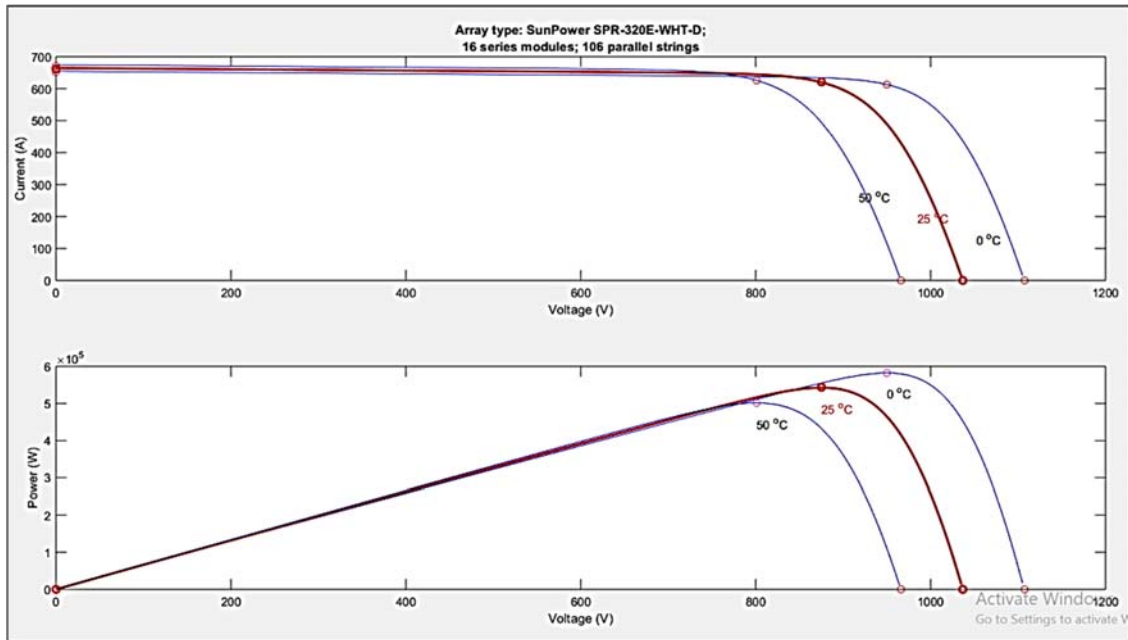


Figure 4-4: I-V and P-V curves of SunPower SPR-320E-WHT-D Solar Panel simulated on MATLAB/Simulink

4.3.1.2 PV solar plant description

The PV solar array on the microgrid designed is connected with the main grid parallel to one another and supplies the produced electricity using three-phase current to the grid conditionally to the energy management system. Moreover, the energy produced by the PV solar plant and the electrical power generated to the rail yard simultaneously controls the energy flow. Due to the intermittent nature of solar energy, the solar absence-period (i.e. night time) causes the lack or shortage of energy production by the PV solar plant. Therefore, the utility grid and the BES will supply the energy to the rail yard depending on the load demand, and thus, that particular working system is called the grid-tied mode and is managed by the EMS as per the load demand. For the detailed PV solar production energy model as illustrated on Figure 4.5, each PV module has 320.542W and there are 1696 modules that composes the PV solar generator, thus the system has approximately a maximum power of 542kW at 1000W/m² sun irradiance. The array consists of 106 strings of 16 series-connected modules connected in parallel (106*16*320.542 W= 543.639 kW). As explained on the sections above, the DC-DC boost converter and a three-phase three-level VSC are used to connect the utility grid consisting of 11kV_{AC} to the PV solar array. The technique of incremental conductance plus integral regulator was applied on the DC-DC boost converter from the Simulink model.

The DC-DC boost converter of 5kHz increases the voltage generated by the PV solar. Moreover, the MPPT controller used on the model successfully optimized the switching duty cycle, wherein the duty cycle is automatically varied by the MPPT system to extract the maximum power by generating the voltage required. The PV solar array consist of two inputs that assist in fluctuating the temperature and irradiance of the sun, thus the signal builder block defines connected to the PV solar array the profiles of these two inputs. There

are two loops that are used by the VSC for control system, namely internal control loop that regulate active (I_d) and reactive (I_q) grid currents, as well as external control loop which therefore, regulates DC link voltage. The technical requirements of the converter and the controller for the transfer of power in the microgrid system from the PV solar plant system to the distribution grid were very critical aspects to consider. This is because, the values of the voltage and current were made to comply and be compatible with those between the PV plant and the input to the converter, while the converter output values were made to comply and be compatible to those of the system common connection to the grid as explained on the system modelling section.

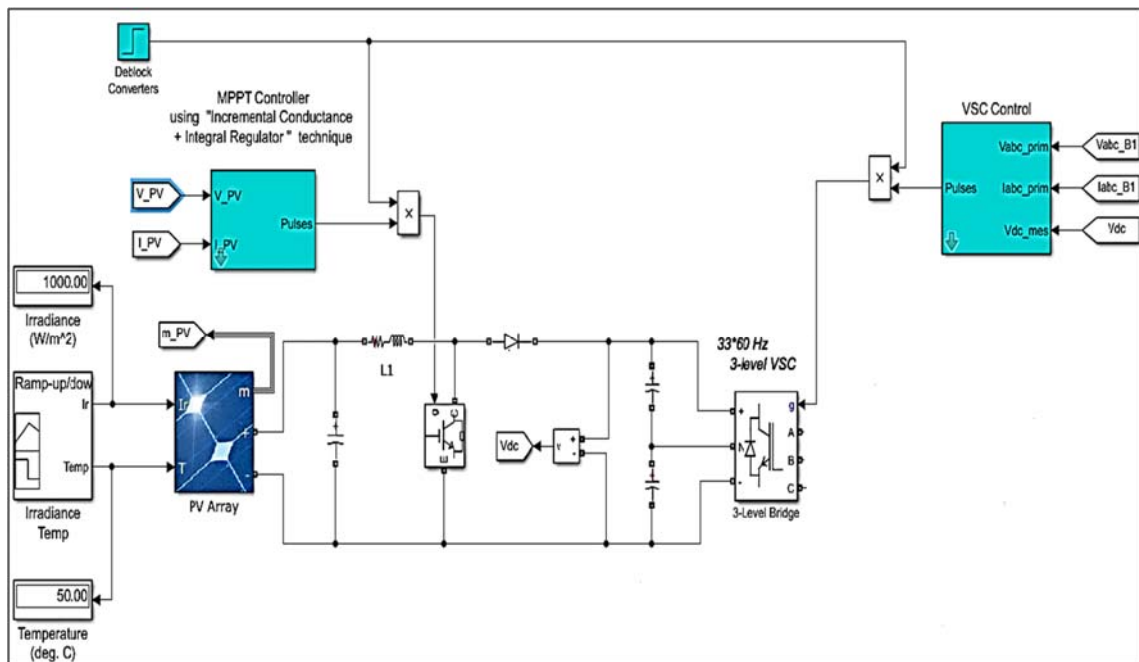


Figure 4-5: PV Solar Array modelled designed on MATLAB/Simulink

4.3.2 Wind Turbine

4.3.2.1 Wind turbine plant and Technical description

This part of the section provides the modelling and specification information regarding the wind turbine model with its associated components. The wind turbines are made up of four major components namely; turbine blades, a generator, rotor and the coupling device as seen on the typical wind energy conversion system drawn on Figure 4.11. However, the generating components that include a gearbox, braking assembly, generator and drive train are composed in a housing called a nacelle, while the rotor that is connected to the blades with a steel hub is assembled in the slow shaft end. For the wind turbine modelling purposes of this study, the type of the generator used for this particular wind turbine is an asynchronous double-fed induction generator (DFIG) consisting of slip rings. The use of asynchronous generators has many advantages such as able to be operated at various operational conditions, has low operating costs as well as being simple in construction.

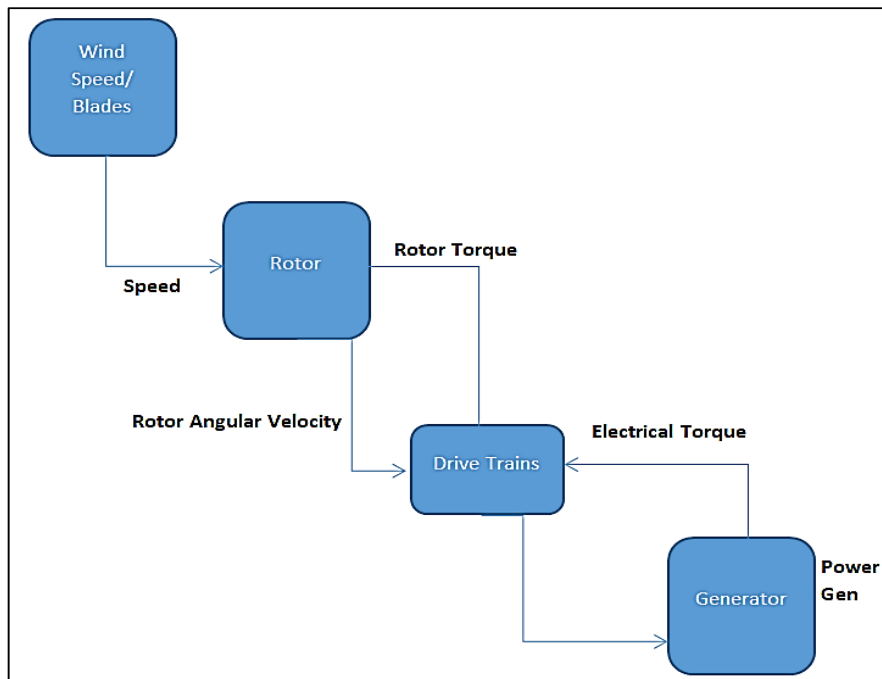


Figure 4-

6: Wind

Turbine General Schematic

4.3.2.1.1 Major Components

The type of the used wind turbine is called 50Hz/60Hz GE wind energy 1.5MWsle that accommodates a rotor of 77m in diameter. Notably, the converter used by GE wind turbine 1.5MWsle is an AC-DC-AC power electronic converter as illustrated in Figure 4.12.

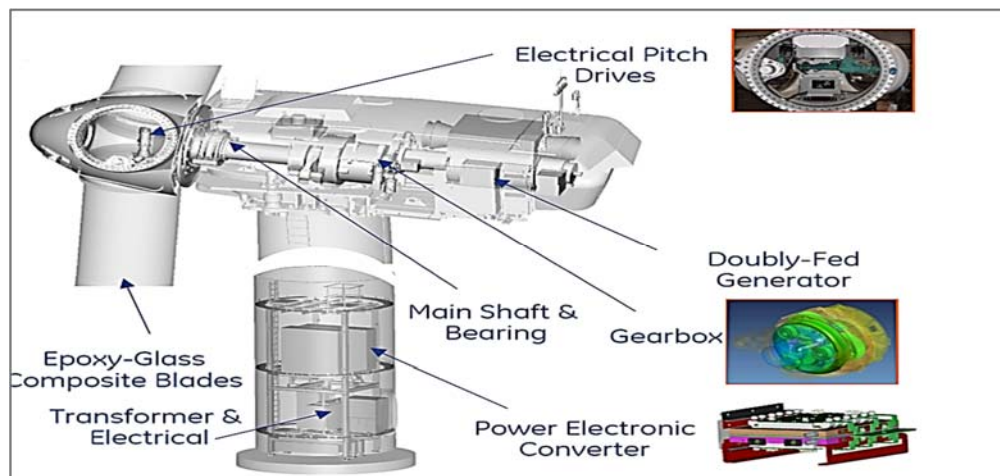


Figure 4-7: Schematic of GE 1.5MWsle Wind Turbine (Zobaa and Bansal, 2011)

Moreover, this type of a wind turbine operates in two different power factor categories, namely; lagging and leading power factors. The outstanding function of the DFIG technology used for this type of wind turbine is to extract more energy coming from the wind irrespective of the speeds that is available at that particular period. Furthermore, during low gusts of wind speed, the DFIG operationally minimizes all the mechanical stresses on the turbine, thus optimizes the wind speed. Diversely, as drawn in Figure 4.13 the

drive train of the used GE type wind turbine features the gearbox and yaw drives main shaft bearings, thus providing the regulation of the turbine rotor speed and therefore, producing the nominal values of 60Hz and 575V of electric power. However, the key distinction is that this machine is equipped with a solid-state voltage-source converter AC excitation system

The aerodynamic forces exerted when the wind blows through the blades turn the rotor of the wind turbine. Consequently, the speed of the rotor is transformed to complement the operational speed of the generator. Moreover, a wind turbine operates by extracting kinetic energy from the wind passing through its rotor. The power developed by a wind turbine is derived on equation 4.8:

$$P = 1/2 C_p \varrho V_w^3 A \quad (\text{Equ 4.8})$$

where: P = Power (W)

C_p = Power coefficient

V_w = Wind velocity (m/s)

A = Swept area of rotor disc (m²)

ϱ = density of air (1.225 kg/m³)

The square of the wind speed and the force withdrawn from the rotor are proportional to one another, however, hence the wind turbine has its cut-off speed, it is important to design to withstand the extreme wind forces. The amount of energy withdrawn by the wind turbine is measured using the power coefficient C_p and it varies with the design of the rotor. The maximum value of this measure is approximately 0.4 and it depends relatively to the speed of the wind which is known as tip speed ration and rotor. Whereas, the generator converts the mechanical energy into the usable electricity, thus making it an important aspect of the system to consider.

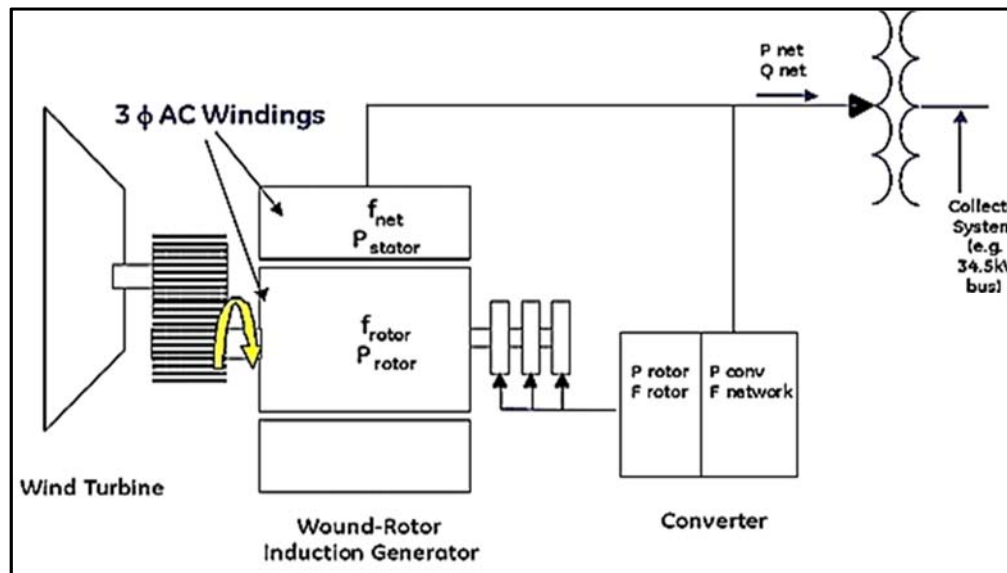


Figure 4-8: Major Components of Doubly-Fed Wind Turbine (Zobaa and Bansal, 2011)

4.3.2.1.2 Wind Turbine Specifications

The frequency and voltage values are individually isolated by the frequency AC-DC-AC converter, which presents an intermediate DC circuit. This frequency AC-DC-AC converter carries out the energy deployed to the utility grid according to the nominal values of the electric grid. According to the design and technical specifications of the wind turbine used in this project as outlined in table 4.2, during the over speed of the wind turbine or emergency, the wind turbine uses the drum brakes with cutting speed of 25m/s in order to stop the blades.

The wind turbine plant of the microgrid designed with the total power of 3MW is connected with the main grid parallel to one another and supplies the produced electricity using three-phase current to the grid conditionally to the energy management system. Moreover, the energy produced by the wind turbine plant and the electrical power generated to the rail yard dependently controls the energy flow. Due to the intermittent nature on wind and the wind energy absence-period that causes the lack and shortage of energy production by the wind turbine plant, the utility grid and the BES supplies the energy to the rail yard depending on the load demand. Thus, that particular working system is also called the grid-tied mode. The plant will consist of: wind turbine, energy conversion and electricity meter.

The technical requirements of the converter and the controller for the transfer of power in the microgrid system from the wind turbine plant system to the distribution grid were very critical aspects considered. This is because, the values of the voltage and current were made to comply and be compatible with those of between the wind turbine plant and the input to converter, while the converter output values were made to comply and be compatible to those of the system common connection to the grid as explained on the system modelling section.

Table 4-2: 1.5MW Wind Turbine Specification

Parameter	Value
Rated Capacity	1.5MW
Cut-in wind speed	3.5m/s
Cut-out wind speed	25m/s
Rated wind speed	14m/s
Frequency	50/60Hz
Voltage	690V

4.3.4 Energy Storage System (ESS)

The model of the energy storage system used on the designed hybrid microgrid system consists of both, the inverter model and the standard Lithium-ion (Li-ion) battery model obtainable in Simulink library. However, the primary part of this section consists of the design and model of a standard Li-ion cell that acts as a basic building block of battery cell. Simulink calculated the resistance of the battery (R_o) automatically, using the combination of the cell model connected in series and parallel, as seen on the equivalent battery circuit model in Figure 4.20.

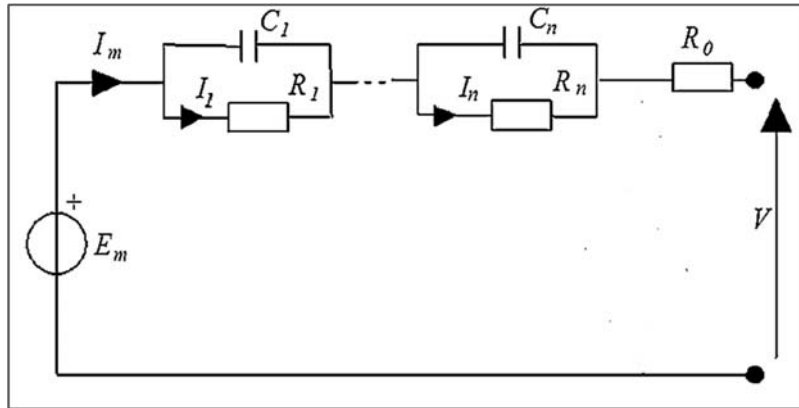


Figure 4-9: Equivalent Circuit Model of Battery Model in SimScape

Lithium-ion batteries were used as the battery storage system for this microgrid system as mentioned due to their good advantages towards other types of batteries as stipulated on the literature, above. The considerable advantages of Li-ion battery when used as a storage system of a microgrid system include:

- High rated capacity of 90% and above,
- Improved life cycle,
- Less maintenance that is ensured and monitored by the BMS that automatically balances the process of equally charging the battery bank,
- Improved efficiency, thus making Li-ion battery more economic.

The Li-ion battery is a high efficiency with much more life span type of energy storage technology, was used in this thesis for storage of hybrid energy (Al-Sakkaf et al., 2019). The equations 4.9 and 4.10 represent the fundamental expressions during the modelling of a generic Li-ion battery, thus representing the Li-ion battery during discharge and charging, respectively.

1. Equation of Lithium-ion Battery Discharging:

$$f_1(it \ i^*i) = E_0 - K \cdot \frac{Q}{Q - it} (i^* - it) + A \cdot \exp(-B \cdot it)$$

2. Equation of Lithium-ion Battery Charging:

$$f_2(it, i) = E_0 - K \left(\frac{Q}{it + 0.1Q} \cdot i^* - \frac{Q}{Q - it} \cdot it \right) + A \cdot \exp(-B \cdot it) \quad (\text{Equ 4.10})$$

Moreover, the last parameter that is important during the modelling of the Li-ion battery is its SOC. The SOC of the generic Li-ion battery as modelled for this research thesis is represented in equation 4.11 and form part of the indication for the reserving energy. The three expressions represent the three significant parameters that are useful in determining the state of the battery when performing the battery optimization model.

$$SOC = 100 \left(1 - \frac{\int_0^t i dt}{Q} \right) \quad (\text{Equ 4.11})$$

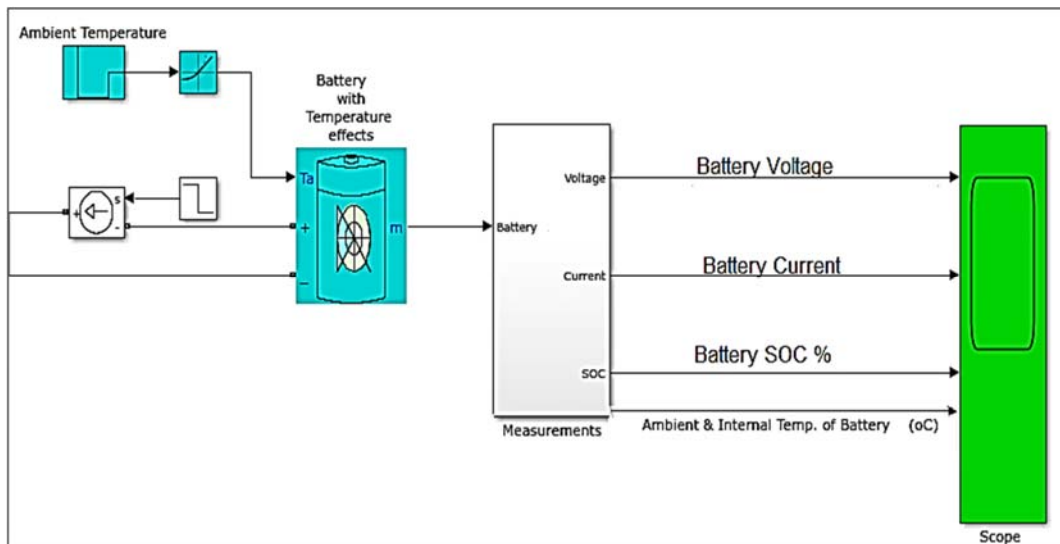
The symbols used on the above equation 4.9 and equation 4.10 and equation 4.11 represent the following:

- E_0 : Initial voltage (V)
- i_i : Capacity extraction of the battery (Ah)
- i : Low frequency dynamic current (A)
- B : Exponential capacity (Ah^{-1})
- K : Polarization voltage (V)
- Q : Battery capacity (C)
- A : Exponential voltage (V)

The inverter model used in charging the battery was the same as the PV solar array setup, nonetheless, due to its charging capabilities; the changes were made on the inverter. Notably, the battery operates in charging and dis-charging modes that take place during the specified constant power of the VSC control block and thus called constant power mode. Moreover, the characteristics of the battery for charge and dis-charge modes were presumed to be the same, thus, the self-discharge in the battery model was not included hence most of the Li-ion battery model was not included on the parasitic bridge of the equivalent circuit model on Figure 4.10, above.

The energy storage system for this designed microgrid system was designed to:

- Distribute the stored energy to the load and the grid when connected.
- Relative to the specified duty cycles, it is expected to store the energy from the grid for applications that comply and match the operation system of the distribution and the transmission.
- Ensure that the energy produced by the wind turbine and the PV solar plants is optimized according to the specified duty cycles.



- Ensure that, when the system is acting as an off-grid mode, the energy is efficiently distributed to the critical and non-critical freight rail yard load as required.

The various changes on Li-ion battery model on Simulink software were done on the battery specification in order to optimize it as illustrated on Figure 4.10. The changes made on battery model include, rated ampere-hour (Ah) of the battery, nominal battery voltage, type of the battery and the state of charge in percentage. Based on the capacity of the Li-ion battery model of 1MWh and the nominal voltage of 600V_{DC}, there were three strings of batteries connected in series that were used, as that will be elaborated and shown below.

Figure 4-10: Lithium-ion Battery Model from Simulink

The ESS designed comprises of the two major subsystems called battery energy storage system (BESS) as well as the power control system (PCS). The BESS which is the electronic system is made up of the battery pack as well as the controlling system called battery management system (BMS) that ensures the operation of recharging the batteries and their status is monitored and managed at all times. Figure 4.11 illustrate an ideal BESS configuration and its subsystems.

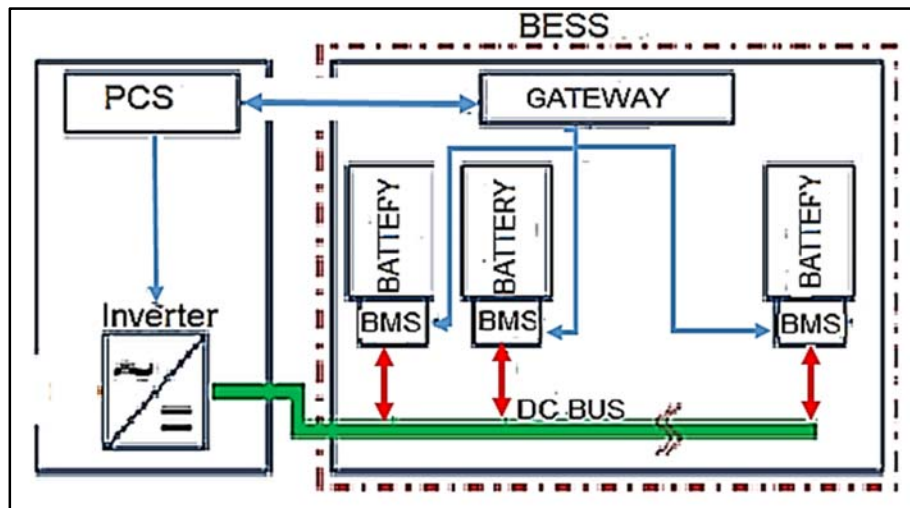


Figure 4-11: Ideal BESS Configuration

The most suitable battery technology used on this study was chosen after taking critical consideration on the data related to the distributed energy resources used for the microgrid and the load of the freight rail yard. Notably, the BESS of the microgrid system designed on this study meet the system requirements as stipulated below:

- i. The BESS stores the energy produced by the PV solar plant and the wind turbine with the total of the nominal power of the two DER plants of 4.5MW.
- ii. It is able to handle the peaks that are over 4MW as required by the load.
- iii. During the outage of the PV solar and wind turbine energy supply, the BESS supplies the load with power for at least 24 hours.

The table 4.3 represents the values during the discharge of the battery, whereas Figure 4.23 and 4.24 illustrate the nominal current discharge characteristics at the nominal discharge current of 70.014A. These discharge values were determined from the actual nominal parameters of the battery as noted above.

Table 4-3: Battery Discharge Values

Parameter	Value
-----------	-------

Maximum Capacity	166Ah
Cut-off Voltage	450V _{DC}
Fully-charged Voltage	698.3923V _{DC}
Nominal Discharge Current	70.01400A
Capacity at Nominal Voltage	1507.5478Ah
Internal Resistance	0.0035993ohms

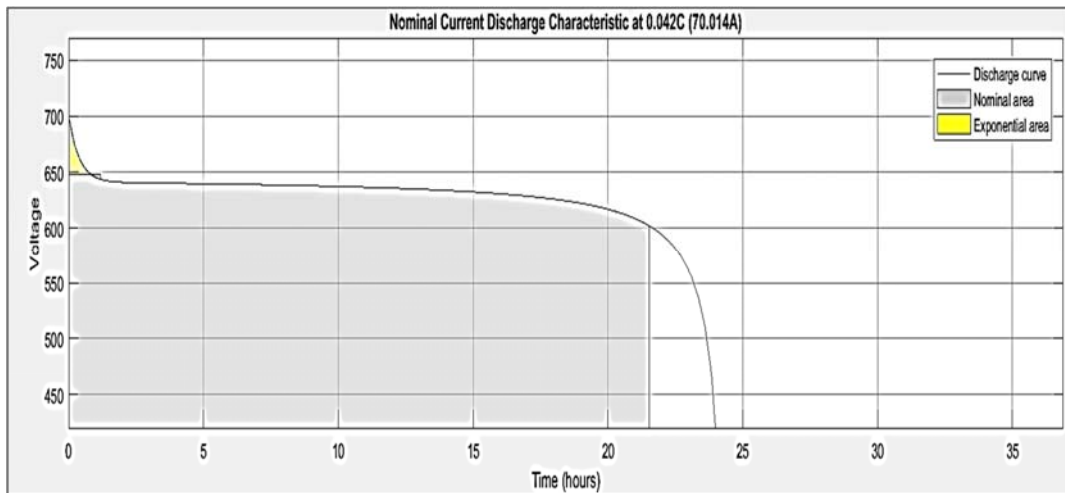


Figure 4-12: Battery Discharge Characteristics (Voltage vs Time) generated on MATLAB/Simulink

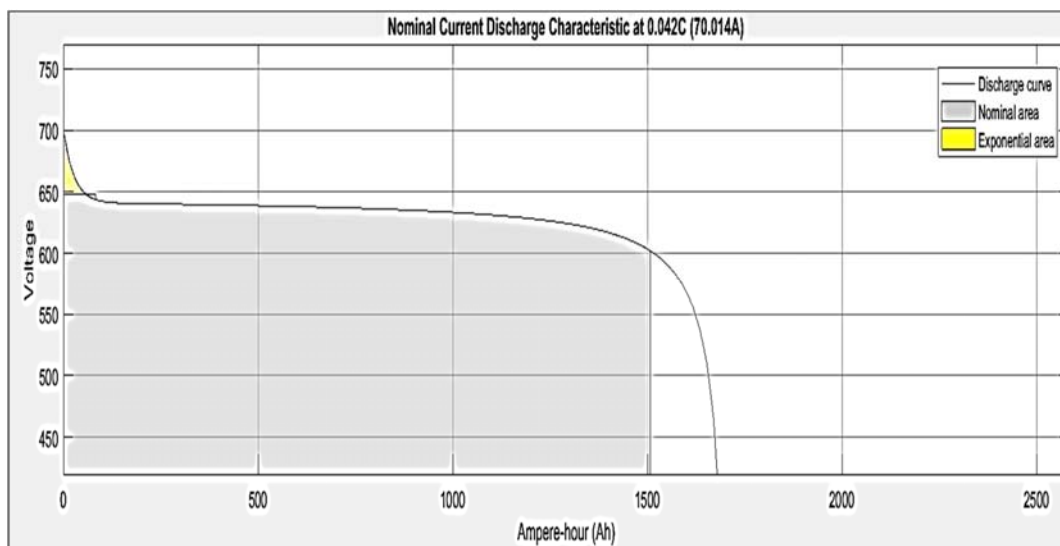


Figure 4-13: Battery Discharge Characteristics (Voltage vs Ampere-Hour) generated on MATLAB/Simulink

The results of the calculated battery bank capacity, C-rate, run-time, charge and discharge current for the Li-ion battery consisting of 3 string as mentioned earlier on this section is shown on table 4.4. However, Figure 4.25 illustrate the SOC and current of the modelled Li-ion battery.

Table 4-4: Lithium-ion battery Simulation Results

Parameter	Value
Voltage of one battery	600VDC
Rated capacity of one battery	1667Ah
Rated capacity of one battery	1000200Wh
C-rate	0.042
Charge or Dis-charge current	70.014A
Time of Charge or Dis-charge	24hrs

The total power generated is less than the total load before 1000s and greater than the total load after 1000s. It can be seen on Figure 4.25 that the battery operates in discharging mode before 1000s and charging mode after 1000s. The SOC decreases and increases before and after 1000s, respectively.

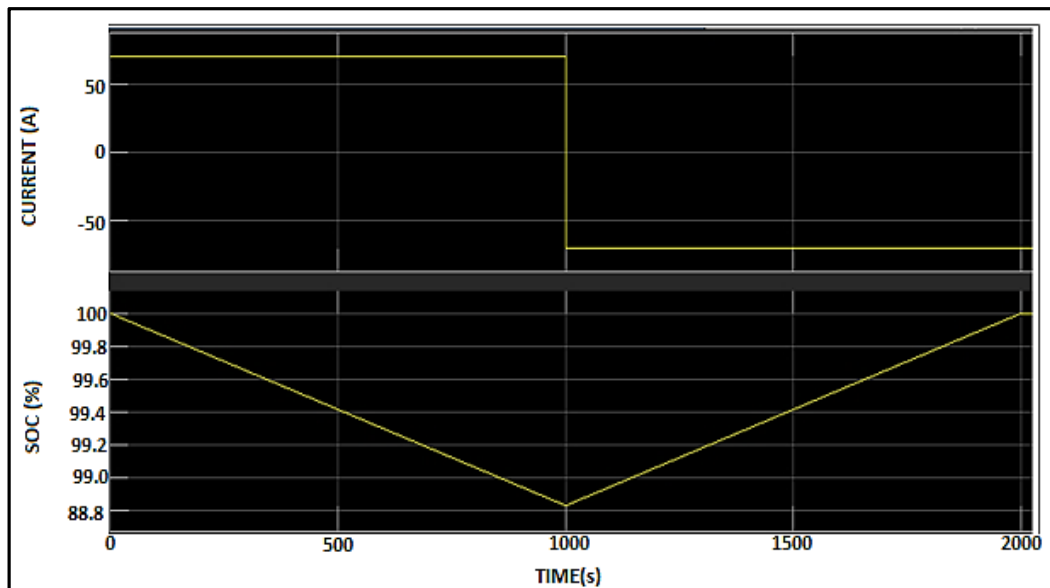


Figure 4-14: Lithium-ion Battery SOC and Current simulated on MATLAB/Simulink

4.4 Chapter Summary

MATLAB/Simulink was used to perform modelling and simulation of the designed MG system in-order to identify and analyse the technical issues that are significant to the operation of the renewable power units generated by MG system designed. The modelled microgrid system comprised of five important sections namely, PV system, Wind energy system, Li-ion battery storage system, Main utility grid and energy management system. Thus, section 1, consisted of PV modules (542kW). Section 2, comprised of two wind turbines of 1.5MW connected to the AC-AC converter that is connected to the step up transformer supplying the 11kV_{AC} PCC. Section 3, comprised of Li-ion batteries with the capacity of 1MWh that are connected to the bi-directional voltage source converter. Section 4, consisted of the utility grid behind fixed impedance fed through a step-down transformer (5MVA, 11kV_{AC}) connected to 11kV_{AC} PCC bus via utility grid control circuit breaker 1. Section 5 was made up of the 3-Phase distribution feeder connected from the 11kV_{AC} PCC voltage and feeds the loads. The system is designed to supply the two types of loads that therefore total to a maximum of 5MVA the critical load and non-critical load using both islanded and grid-tied modes. The PV module used had 320.542W and there were 1696 modules that compose the PV solar generator, thus the system has approximately a maximum power of 542kW at 1000W/m² sun irradiance. The array consists of 106 strings of 16 series-connected modules were connected in parallel ($106 \times 16 \times 320.542 \text{ W} = 543.639 \text{ kW}$). The DC-DC boost converter and a three-phase three-level VSC are used to connect the utility grid consisting of 11kV_{AC} to the PV solar array. The technique of incremental conductance plus integral regulator was applied on the DC-DC boost converter from the Simulink model. The various changes on Li-ion battery model on Simulink software were done on the battery specification in order to optimize. The changes made on battery model include, rated ampere-hour (Ah) of the battery, nominal battery voltage, type of the battery and the state of charge in percentage.

CHAPTER 5: Modelling Hybrid Energy Management System

5.1 Introduction

This chapter outlines the methodology used for the developed EMS consisting of the RES and the BESS as explained on the previous chapters of this research. In general, the aim of the developed EMS was to ensure that the RES and the peak load demand are always balanced and managed properly ensuring the energy use of the microgrid system is efficient. Thus, ensuring the different modes of operation for the designed microgrid system are consistently maximized at all times. Moreover, the strategic control system of the EMS included on the microgrid system was also proved to be effective in the management of the intermittent RES.

The studies show that the implementation of the fuzzy logic controller (FLC) for the EMS in a microgrid system is effective. Fuzzy logic shows an efficient control for microgrid, especially when multi-functions is performed on the microgrid. The successful optimization, battery management and the distributed energy management of the EMS are fairly controlled by the FLC designed algorithm. Thus, the FLC ensures that the RES throughout the normal availability of their MPPT trackers constantly supplies the load demand and also the power is sold or purchased from the utility grid when needed.

In this thesis, FLC system was developed as a controlling system of the EMS for the microgrid system, where the rate of charging and discharging by the BESS was determined according to the two parameters, namely: State of Charge (SOC) and Renewable Energy Sources (RES). Thus, the life span of batteries will be maintained by the developed FLC system as well as to optimally ensure that the power utility grid is equalized. The FLC can also be used for controlling and predicting different tasks in a microgrid, for example, the status of the load consumed, the wind velocity as well as to check the sun radiation for PV solar system. Therefore, the FLC ensures multiple tasks and actions are controlled, effectively.

Furthermore, the main objectives of the developed controlling FLC algorithms satisfy the below summary of rules for the implemented EMS and the general operation of hybrid microgrid characteristics:

- i. Rule 1: Only one renewable energy system of the microgrid system (PV solar and wind turbines) was considered to provide the acceptable generated power output.
- ii. Rule 2: Both the renewable energy systems (PV and wind turbine) fail to generate and supply power according to the load demand.
- iii. Rule 3: The Islanded mode of the hybrid microgrid system is two out of three (2oo3) system.
- iv. Rule 4: The generated output power exceeding the load demand.
- v. Rule 5: When the wind turbines reach their maximum rotating speed of 25m/s, the WT system should continue generating the maximum power of 3MW then switches off. Therefore, the wind speed and the wind turbine must be monitored. In that period, scenario 1 and scenario 2 are activated.

5.2 Model Development

As discussed above, the designed EMS system was modelled in order to optimize the produced energy according to the demand by the load as well as to ensure the SOC of the battery preserved so as to provide support to the load demand when there is not enough power produced by the RES. Moreover, the battery of the system is discharged and charged routinely; using the fuzzy logic, thus ensuring the battery is not insufficiently charged as that could decrease the life span of the battery system. The fuzzy logic system contains 25 empirical rules that assure the positive effect on the BESS. Figure 5.1, illustrates the developed EMS model with the fuzzy logic controller design. MATLAB/Simulink was used to build the model of the fuzzy logic system, where the DG system is controlled to its optimum operation, and therefore the operation of the designed FLC is explained on the sub-section, below.

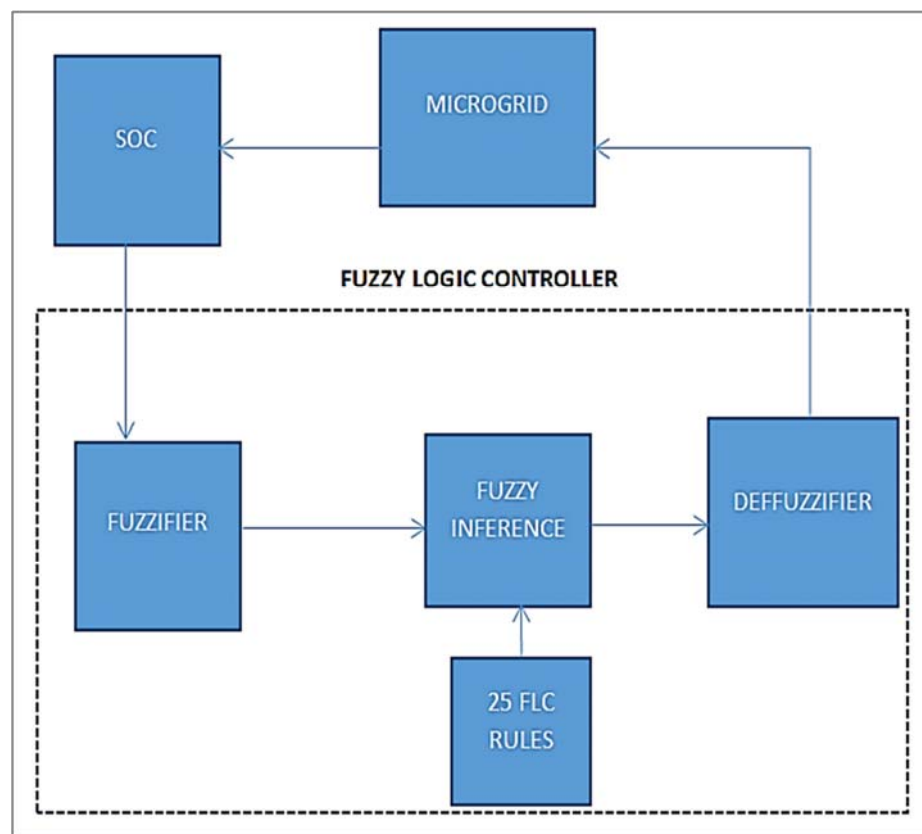


Figure 5-1: Basic Fuzzy Inference System Diagram

The operation of the developed FLC system for the BESS ensures that, the BESS is successfully charging when the load demand is below the power supplied by the RES and discharging when it is above. However, in a case of emergency, it is very important to consider the operation of this BESS, because it assists for emergency supply when it is charged to its full maximum capacity limits. Thus, ensuring the continuous availability of power during power outages as well as the reduction in the generation of RES. The capacity of current for the ESS is depicted by the SOC in percentage form, where 100% represents fully charged and 0% represents fully discharged. P_{RES} is the renewable power generated from the two RES connected as depicted in equation 5.1. Then equation 5.2 derives $P_{Equilibrium}$ which is the surplus/shortage of power

between P_{RES} and P_{LOAD} . Therefore, P_{Grid} is the difference in power sold/bought to/from the grid, as depicted by equation 5.3.

$$P_{RES} = P_{WT} + P_{PV} \quad (\text{Equ 5.1})$$

$$P_{Equilibrium} = P_{RES} - P_{Load} \quad (\text{Equ 5.2})$$

$$P_{Grid} = P_{Equilibrium} - P_{BESS} \quad (\text{Equ 5.3})$$

5.3 Fuzzy Logic Controller Design

The microgrid system comprises of 3MW wind turbine and 1.5MW solar module with lithium-ion battery considered as BESS for this developed system. The BESS was assumed to initially have 30% of the SOC with the highest value of 100%. The load was considered to be 4MW. The FLC of the developed EMS controller system is made up of the four important parameters namely; fuzzifier, 25 FLC rules, fuzzy inference and defuzzifier as shown on Figure 5.1. However, the four parameters used to design and develop the FLC system are briefly explained in this section.

- i. **Fuzzifier:** On this section of the FLC system, the membership function (MF) is used to portray the real inputs from the SOC and $P_{Equilibrium}$, thus the MF proposes the inputs that are not in the same range. However, the system's designer on MATLAB/Simulink designated the MF to be used. Figure 5.2 and Figure 5.3 together with their constraints equations, depict the optimized $P_{Equilibrium}$ and SOC trapezoid MF used for this developed FLC system, respectively. Therefore, the trapezoids MF's are nonlinear as mentioned earlier and are distributed uniformly.

$$P_{Equilibrium} \begin{cases} P_{Load} > P_{RES} & \text{if } 0 \leq P_{Equilibrium} \\ P_{Load} = P_{RES} & \text{if } P_{Equilibrium} = 0 \\ P_{Load} < P_{RES} & \text{if } P_{Equilibrium} \leq 0 \end{cases} \quad (\text{Equ 5.4})$$

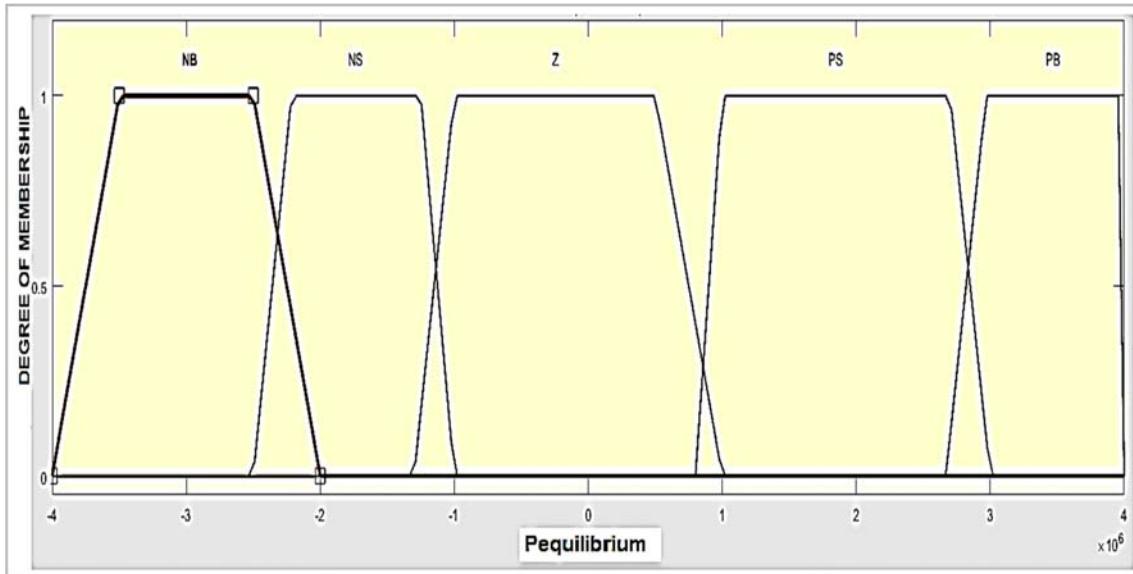


Figure 5-2: $P_{Equilibrium}$ Membership Function generated on MATLAB/Simulink

In Figure 5.3 battery SOC_{BESS} is divided into range of membership functions (Low level, Medium level, Medium High level, High level and Maximum Level) based on its available charged capacity (i.e. %) at any instance time.

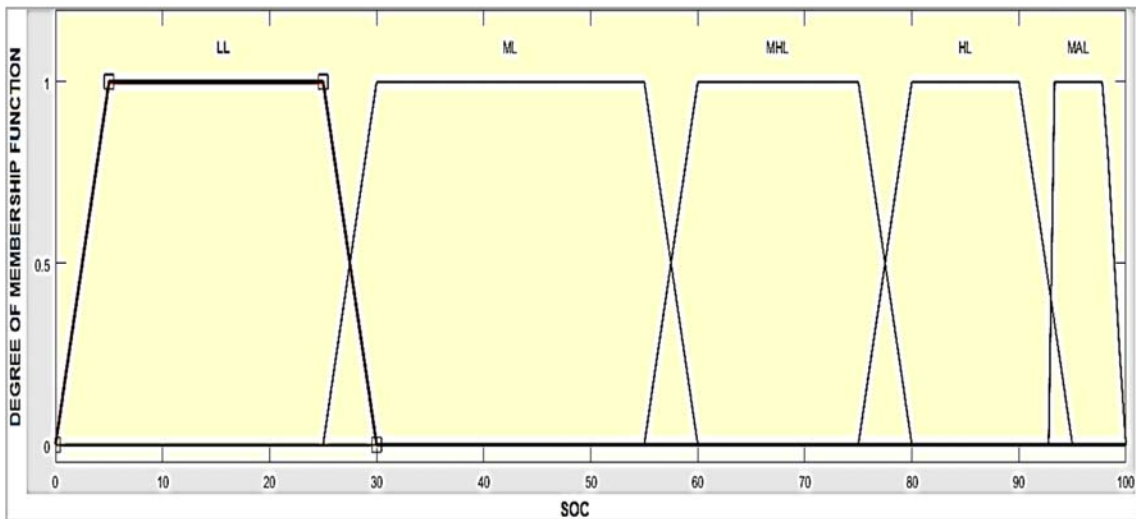


Figure 5-3: SOC Membership Function generated on MATLAB/Simulink

$$\left. \begin{array}{l} \text{Active} \\ \text{Non-active} \end{array} \right\} SOC_{BESS} \quad \begin{array}{l} \text{if } 4 \leq SOC \leq 90 \\ \text{if } SOC \leq 4 \text{ or } 90 \leq SOC \end{array} \quad (\text{Equ 5.5})$$

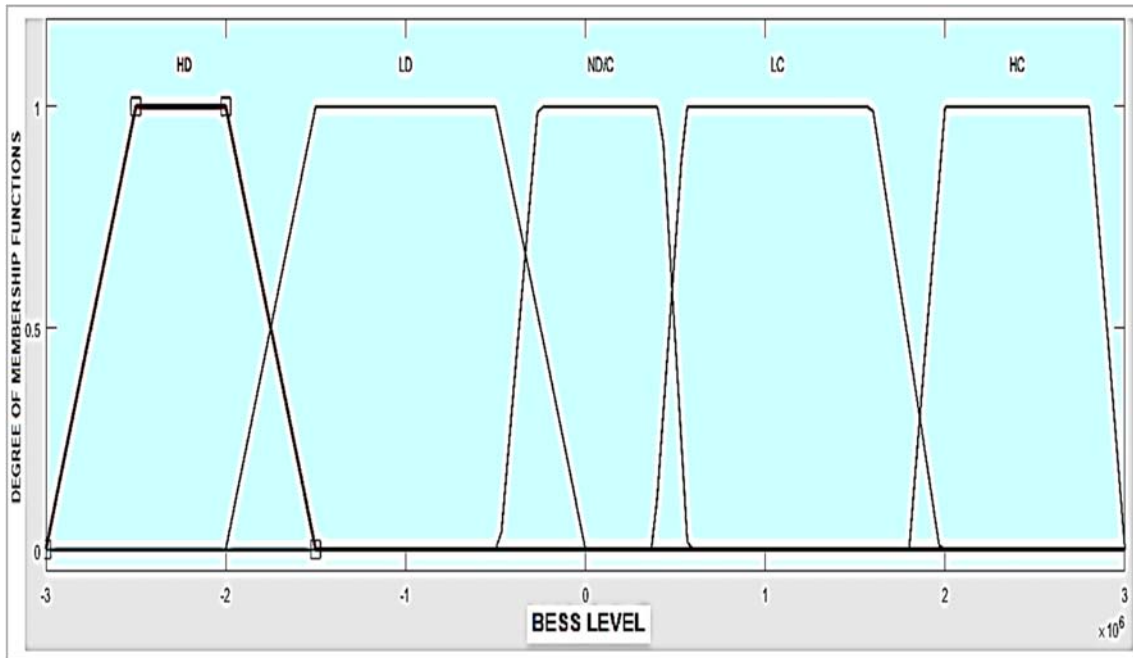


Figure 5-4: P_{BESS} Membership Function generated on MATLAB/Simulink

P_{BESS}	Discharging	if $P_{BESS} \leq 0$	(Equ 5.6)
	Inactive	if $P_{BESS} = 0$	
	Charging	if $0 \leq P_{BESS}$	

- ii. **FLC Rules:** In this section, the FLC rules are explained, where the inputs from the controller are fuzzified in order to create generic rules that is based on human language. Thus, these rules are built in statements that contain IF-THEN collection statements that can be interpreted very easy. The developed FLC is set to follow the constraints, objectives and rules below, based on the scenarios as outlined on the above section. The constraints and are as follows:
- The BESS alone supplies the load demand until it reaches not less than 60% of its SOC (the charging and discharging of the BESS must be monitored), then the main grid must be activated to supply power to the load as per the demand is concern with a delay of 30 seconds.
 - If one of the two power generating systems of the microgrid system (PV and WT) with the BESS fails to provide enough generated power, the system is converted to grid-tied mode and the SOC of the BESS should be in charging mode until it reaches 95% of SOC.
 - The BESS is constantly charged by the voltage bus where all three systems are connected and the limits of its SOC are monitored as stipulated in scenario 1 and scenario 2.

- The WT system should continue generating the maximum power of 3MW then switches off after 60s. Therefore, the wind speed of the wind and the wind turbine must be monitored. In that period, scenario 1 and scenario 2 are activated.
- The exceeded power must be sold to the main grid. However, when the generated output power is less than its minimum acceptable limits, scenario 2 takes place.

Furthermore, referring to equation 5.4, equation 5.5 and equation 5.6, the constraints and objectives of the developed FLC system were taken into account when the fuzzy inference system (FIS) was designed in order to minimize the possible variations on the utility grid while the constraints are satisfied and are outlined below:

The use of P_{GRID} (i.e. power to and from utility grid) is decreased and increased based on:

$P_{Equilibrium,min} \leq P_{Equilibrium} \leq P_{Equilibrium,max}$: the maximum and minimum parameters of the difference between the RES and load demand.

$P_{BESS,min} \leq P_{BESS} \leq P_{BESS,max}$: the maximum and minimum charging/discharging rate allowed for the BESS

$SOC_{min} \leq SOC \leq SOC_{max}$: the maximum and minimum SOC limits of the BESS.

During the minimum levels of the SOC and the absence of the REG, the microgrid system is compensated by the controlled output of the FLC. The threshold of the SOC on the BESS varies from 10% to 95% of its limits. Table 5.1, shows the 25 rules of the fuzzy control system, where the following SOC and $P_{Equilibrium}$ are the inputs of the developed FLC and P_{BESS} is the output of the FLC system. The abbreviations LL, MLL, ML, MHL and HL of the SOC stand for: low levels, medium low levels, medium levels, medium high levels and high levels, respectively. Whereas the abbreviations NB, NS, ZE, PS and PB of the $P_{Equilibrium}$ stand for: negative big, negative small, zero, positive small and positive big, respectively. Thus, the abbreviations that represent the output variables of P_{BESS} for the FLC system are HD, LD, ND/C, HC and LC, respectively stand for: high discharge, low discharge, no discharge/charge, high charge and low charge.

The five output variables for P_{BESS} are briefly explained below:

The output variable HC on the FLC system signifies that the P_{BESS} must charge with a very high rate. E.g. when the input variable of SOC LL, meaning the SOC of the battery is at low levels and $P_{Equilibrium}$ is NB, meaning there is an extreme demand from the load. The output variable LC means that the P_{BESS} must charge with a low rate, a rate that is lower than HC. E.g. this occurs when the levels of the SOC is in medium low and of the $P_{Equilibrium}$ is negatively small, meaning there is not much of demand from the load perspective. Then, ND/C simply signifies that the P_{BESS} is in neither charging mode nor discharging mode. Thus this occurs when the load demand and the RES power are balanced. HD output variable means that, the BESS system is discharging at a high rate. Whereas LD, implies that the BESS rate of discharging is very low which occurs when the RES is balanced with the load demand and the SOC of the battery is in its medium high limits.

Table 5-1: Fuzzy Logic Controller Rules for BEMS

BESS		P _{Equilibrium}				
		NB	NS	ZE	PS	PB
SOC	LL	HC	LC	LC	LC	LC
	ML	LC	LC	LC	LC	LC
	MHL	HD	LD	LD	ND/C	ND/C
	HL	HD	LD	ND/C	ND/C	ND/C
	MHL	HD	LD	ND/C	ND/C	ND/C

- iii. **Inference System and Defuzzifier:** The implemented fuzzy inference system (FIS) for the developed battery energy management system (BEMS) for maintaining the power produced by the RES on the designed microgrid was designed using MATLAB/Simulink. The inference system is the process of simulating human decision based on fuzzy concept. It is the mapping from a given input(s) to an output(s). The FIS will work towards the objective of minimizing variation in the grid while satisfying all the constraint. A total of 25 rules are set based on expert knowledge as shown in table 5.1.

The centroid technique was used as a defuzzifier to compute the FLC output based on the output generated by the inference system. Notably, the Figure 5.5 shows surface diagram of the 25 optimized simulated FLC rules with its inputs using the Mamdani type of simulation system. The surface diagram in Figure 5.5 represents the values of the two inputs (i.e. SOC and P_{Equilibrium}) and BESS with their respective classes of the membership functions. The BESS, is the rate of power to charge and discharge the battery, thus the high-negative levels of the BESS implies that the battery is discharging whereas the high-positive values implies that the battery is charging. The SOC of the battery is set to comprise the low value of 50%, thus the fuzzy controller maintains all the necessary constant values of the SOC limits of the battery. However, the highest value of the SOC is set to be 95%, therefore, the battery discharges when reaches more than its highest value. The control based fuzzy algorithm gives first priority to the selling and to maintain the SOC of the battery.

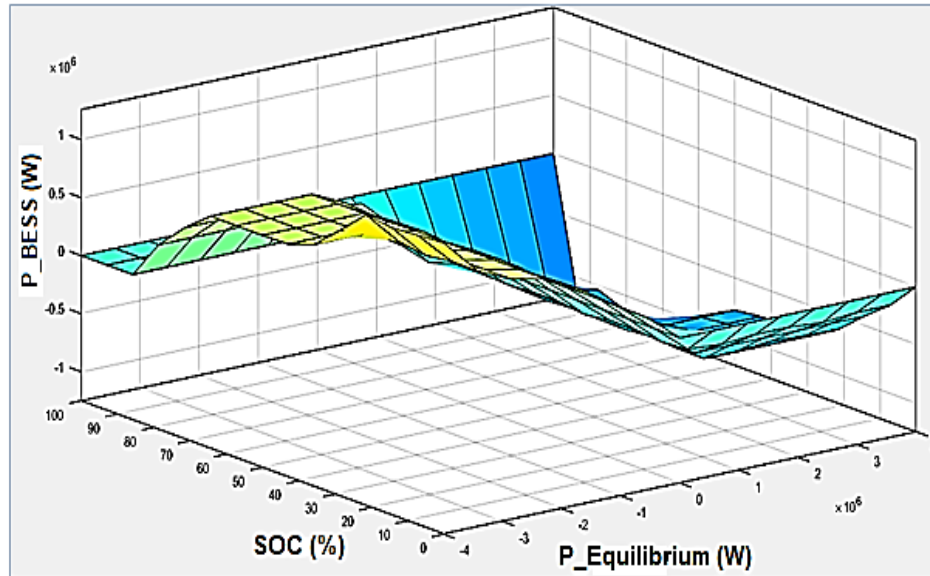


Figure 5-5: Fuzzy Rules surface diagram generated on MATLAB/Simulink

5.4 Chapter Summary

The EMS of the microgrid system was controlled using an FLC system that was made up of the four important parameters namely; fuzzifier, 25 FLC rules, fuzzy inference and defuzzifier. The rate of charging and discharging the BESS was determined according to the two parameters, namely: State of Charge (SOC) and Renewable Energy Sources (RES). The EMS contained 25 empirical rules that ensured the positive effect on the BESS for the general operation of hybrid microgrid characteristics. The battery system was discharged and charged routinely, ensuring the battery was not insufficiently charged. The capacity of current for the ESS was depicted by the SOC in percentage form, where 100% represents fully charged and 0% represents fully discharged. The SOC of the battery is set to comprise the low value of 30%, thus the fuzzy controller maintains all the necessary constant values of the SOC limits of the battery. However, the highest value of the SOC was set to be 95%, therefore, the battery discharges when reaches more than its highest value. The control based fuzzy algorithm gives first priority to the selling and to maintain the SOC of the battery.

CHAPTER 6: Real-Time Modelling

6.1 Real-time Modelling and Simulation Overview

6.1.1 Introduction

This section of the thesis outlines the overview of the real-time simulation. Then, the concepts of real-time simulation, the operation of OPAL-RT simulator are explained consequently and then validation process of the developed scenarios of microgrid system model. The real-time simulator manufactured by OPAL-RT technologies that is called OP4510 simulator, which is the target PC as seen on Figure 6.1, was used. The required RT-LAB software version v11.3.1.314 along with MATLAB (R2015b) is installed on the host PC. The RT-LAB software helps the MATLAB to create real-time simulation environment. This software provides a channel to the computer and RT simulator for communication.



Figure 6-1: OPAL-RT OP4510 Simulator (OPAL-RT Technologies, 2016)

The reasonable simulation results performed in real-time essentially produce the outputs and variables that are in the same period as that of the physically built model. Thus, this ensures the length of time-step needed to perform the computation of the simulation is shorter than that of the clock's duration of the time-step. Moreover, the focus of the RT-LAB simulator concentrates on real-time simulation of electrical networks; hence, the test controllers that ensure stability of networks are required. Therefore, this is achieved by ensuring that a real-time simulator performs the simulation of the modelled system's equations and states accurately, thus, proving the correspondence of its performance and operation to be similar to that of its physical resemblance.

6.1.2 Real-Time Simulation Concepts

OPAL-RT system is a software system that has a real-time platform called RT-LAB that was used in this study to allow the real-time simulation for the developed microgrid system model. RT-LAB enables the models that are designed and built in MATLAB/Simulink environment to be tested their dynamics in-order to get accurate hardware-in-the-loop (HIL) simulations in real-time as well as reducing the risks, costs and

delays of the built power systems of the microgrid system. Therefore, RT-LAB tool fully works together with MATLAB/Simulink.

RT-LAB is a more flexible platform of simulating power system models that can be used to design, test and optimize control as well as protection systems for power grids and power electronics, thus allowing the computing power together with control systems applications to be virtually simulated when needed. Therefore; hence, RT-LAB is more scalable and flexible, non-linear systems such as power systems that are in real-time and much complex are simulated using this type of software environment. RT-LAB uses simulating tools, namely; RT-Events and Advanced Real time electro Mechanical Simulator (ARTEMis) that are based on Simulink modelling environment. These modelling tools enable the modelling of high-speed and real-time simulation to be performed in multi-core processors.

The real-time simulations are advantageous because, the simulated models developed in real-time perform the execution at exactly the same rate as the actual physical model. Thus, in particular, the real-time system forms as part of ensuring the verification of accuracy and a controller performance. However, as stated on the above section, the critical key point and motive of performing real-time simulation was to allow the implementation of HIL and CIL simulations for the studied and developed microgrid system. Furthermore, this research thesis contains the microgrid system development model using Simulink and realised in real-time with the use of ARTEMis-SSN solver. The advantage of using ARTEMis-SSN solver for the developed and designed microgrid system was effectively to decouple the developed power system state space into lesser groups. Further, this solver assisted the modelled microgrid system to accurately provide simulations that are fast in real-time. However, the several state-space (SSN) groupings found in the computation of the subsystem were assigned by performing the parallel execution using ARTEMis-SSN solver.

6.1.2.1 ARTEMis Modelling Tool

The accuracy of the simulated results can be affected during the real-time simulation by the numerical number of oscillations. Therefore, in-order to bypass this effect on a simulation, the ARTEMis distributed transmission line model was used. ARTEMis modelling tool as it was developed by OPAL-RT ensures that the add-on for the SPS are provided. The add-on provided for the SPS are used to optimize and ensure the accuracy of the computation by implementing the solvers that are unique. Therefore, these special tools provided by the SPS in-order decouple complex circuits in real-time simulation. This real-time modelling tool supplies a stability that is in high degree to allow the state-space models to be in discrete time and enabling the electric circuits on the central processing unit (CPU) cores that are different to be performed in parallel computation; thus allowing a huge number of switches to be simulated in real-time. The Figure 6.2 (a) shows the simulation model of the developed microgrid system using OPAL-RT digital simulator. Nonetheless, during compilation of the model in the building stage in RT-LAB, the simulated model encountered an error related to the number of cores used by the target PC as explained on sub-section, below. Furthermore, sub-section 6.1.6 explains the solution to the error, thus the model was re-done as a

solution to the error as shown on Figure 6.2 (b). In order to ensure the decoupling of the large electrical components used on the developed microgrid system with the ARTEMiS-SSN solver tool on RT-LAB, the microgrid system was simulated using time step of $20\mu\text{s}$ on E3 4-core, 3.5GHz processor speed RT-LAB simulator. Finally, the parallel tasks can be built from Simulink model using RT-LAB.

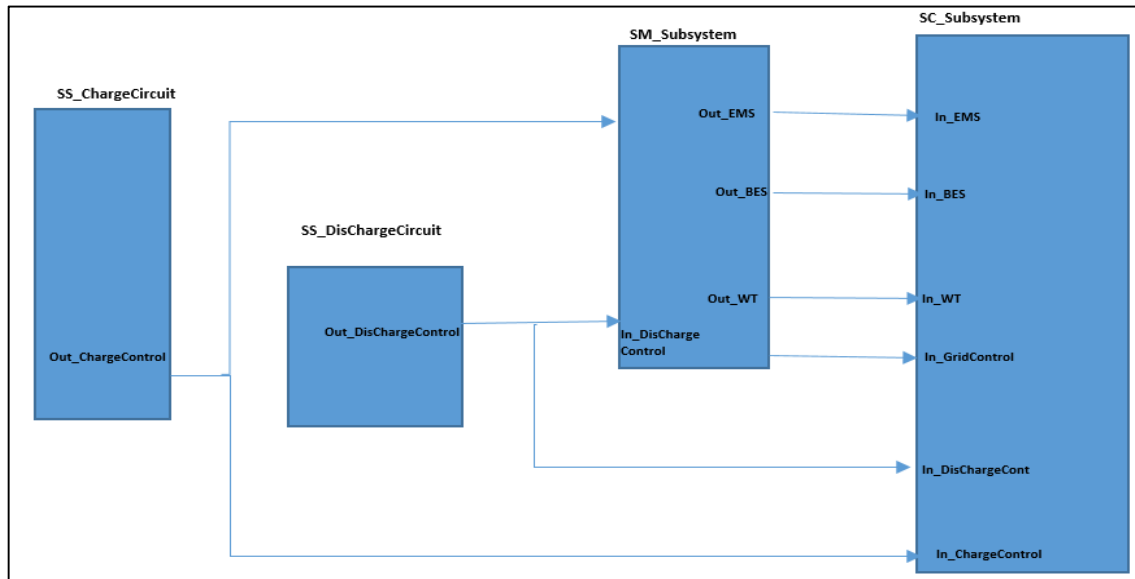
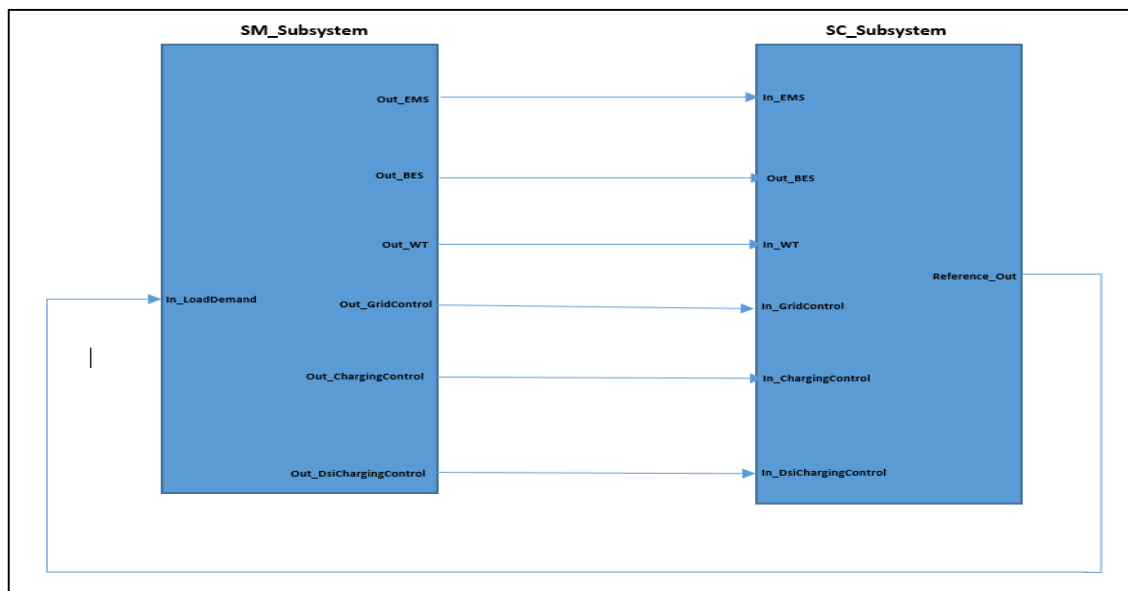


Figure 6-2(a): Real-Time Simulation Setup using OPAL RT Simulator

Figure 6-2(b): Real-Time Simulation Model on RT-LAB



6.1.3 Timing Mechanism

The timing mechanism is a real-time simulation tool needed when performing any simulation in real-time. In this thesis, the duration of time steps of the simulation were assumed as discrete-time that is constant. In

discrete-time constant simulation also called fixed time-step, the forward movement of time during the simulation is set to be fixed step size. However, although this is not the only time-simulation method that can be used in Simulink, it is the only method that is suitable for real-time simulation. The computation of the time-step for the simulation performed produces not only mathematical model but also ensures that the time of the input and output (I/O) ports are efficiently driven. As depicted on Figure 6.3, before the simulation finished its computation, it is critical to ensure that the idle time of the time-step simulation is not lost and due to the overrun in the simulated model, the computation for the next step on the model is not affected and frozen. In order to avoid overruns and idle time on the real-time simulation, the computation and receiving of data on one cycle was performed within the duration of the time step given on the simulation set up.

Figure 6.3 depicts the time-step timing mechanism used for the real-time simulation. In Figure 6.3, the idle time is disorientated, thus ensuring the completion of both the I/O and computation during the set time-step $T_1=1s$ and $T_2= 2s$. Furthermore, Figure 6.3 proves that, at time-step $T_3=3s$, when the output sent and the during the computation performance are not responding according to the set time-step, the overruns in the simulation occurs. Thus at time-step $T_4=4s$, the computation of the simulation model is stopped, due to the overrun occurred at $T_3=3s$. Therefore, causing the computation of the simulated model to be omitted due to the lost time-step $T_4=4s$ as shown in Figure 6.3.

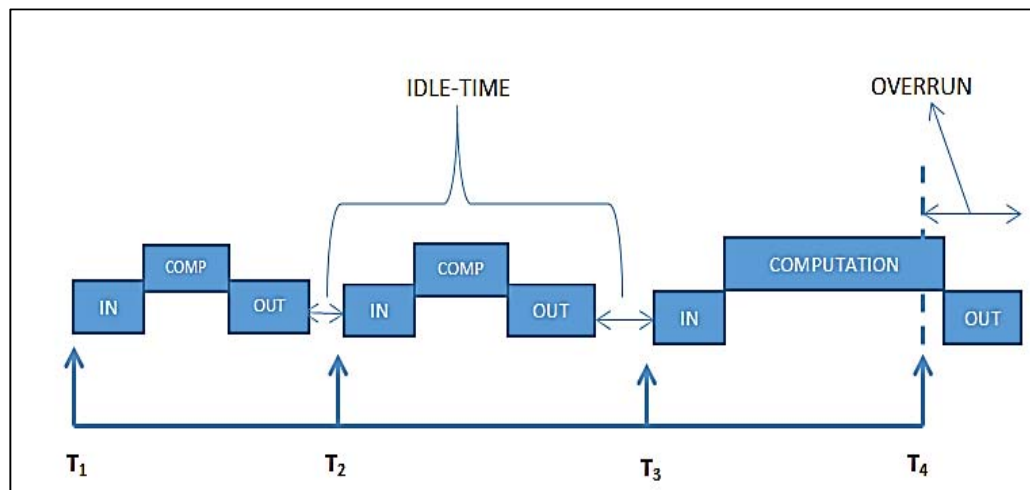


Figure 6-3: Time-step timing mechanism in RT-LAB

6.1.4 OPAL-RT Architecture

The OPAL-RT simulating equipment present at the CDPES laboratory that was used in this study is shown on Figure 6.4. This real-time and high speed simulating equipment uses a MEGAsim simulation system containing a host PC and a target PC. The host PC includes a 1Gbps LAN card for real-time communication with the target PC, thus operated based on Windows to allow the compilation of the model to be easily performed and downloaded to the target PC.



Figure 6-4: Real-Time Simulation Setup PCs

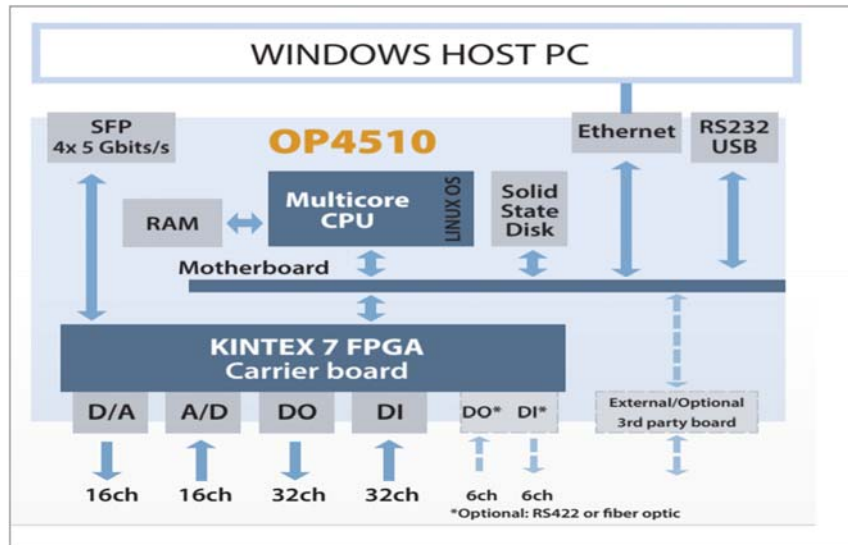
Furthermore, the host PC provides three major purposes namely, compilation of the model with RT-LAB, graphical user interfacing (GUI) as well as the edition of Simulink model. Whereas, the real-time target computer of OP4510 real-time simulator consisting of a 3.5GHz processor cores, with four cores activated provides the file transfer protocol (FTP) and Ethernet TCP/IP, UDP/IP communication with the host PC, input/output (I/O) and real-time model execution as well as the Linux operating system. The MEGAsim simulation system is applicable in running protection systems, power system controls, modular multilevel converter (MMC), microgrid on-board power systems, hybrid and electrical transportation. The software and hardware requirements used for the simulation in this study are shown on table 6.1.

Table 6-1: Software and Hardware equipment used

Hardware	Software
OPAL-RT OP4510	MATLAB/Simulink
LG 29WK600 UFHD LED Monitor	RT-LAB
	Windows operating system

In Figure 6.5, the architectural design of the target PC connected with the host PC shows that the OP4510 real-time simulation machine, which is the target PC is integrated by RT-LAB. Thus, the Simulink from the industry, LABVIEW software as well as the FPGA chips have all the great performance, hence integrated with eFPGAsim, which is the real-time platform from OPAL-RT machine (OPAL-RT Technologies, 2016). The architecture that is shown on Figure 6.5 is able to accurately perform the HIL simulations and applications. Moreover, the time-step of approximately $7\mu\text{s}$ for the sub-system that is operating on INTEL CPU is enabled by the FPGA as shown on the architectural design (OPAL-RT Technologies, 2016). Tuning is easy because it is possible to change parameters during real-time simulation. Lastly, the OP4510 target

PC used in this research study is able to act as a standalone power controller thus is used to test system in power electronics models.



**Figure 6-5: Architecture of Target PC (OP 4510 Machine) Connected to Host PC
(OPAL-RT Technologies, 2016)**

6.1.5 Architecture of RT-LAB Simulator and Configuration Errors

The architectural software design of the RT-LAB software effectively provides more and clearer understanding of the developed system and ensures the efficient operation with the OPAL-RT system. The RT-LAB software application consists of the three fundamental roles for it to operate effectively that are explained below.

i. License:

The host PC contains the OPAL-RT licences that are installed for the application of real-time modelling namely RT-LAB v11.2.2.108 and v11.3.1.314 version. These software licences ensure that several features of the RT-LAB software are effectively enabled and disabled. However, there are remarkably different features matching the target PC used, with the IP address 192.168.10.102 included on the licence file automatically for configuration purposes. During the start of RT-LAB operation together with MATLAB R2017a version using the RT-LAB v11.2.2.108, the error encountered was with regard to the licence of the MATLAB R2017a version of MATLAB software. This was caused by the MATLAB licence version error as seen on Figure 6.6 which led to the difficulties when loading the model. However, the use of MATLAB R2015b version was used in solving the problem.

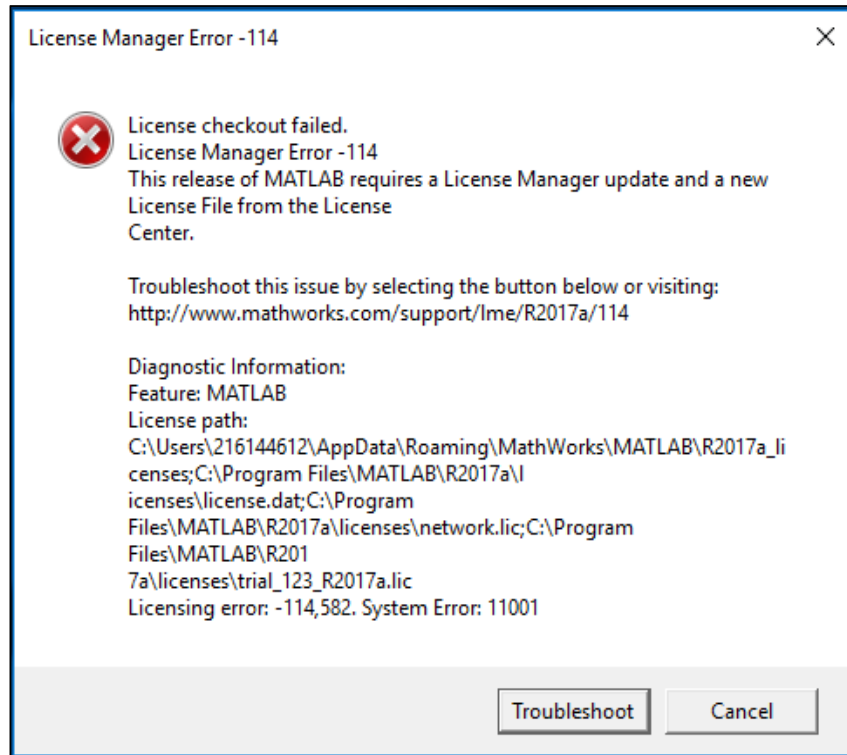


Figure 6-6: License Manager Error for MATLAB vR2017a

Moreover, during the compilation of the demo model simulation, at the beginning of the pilot simulation model, the error message shown on Figure 6.7 was encountered. Nonetheless, with the conjunction efforts with OPAL-RT technologies technical support team, the solution to the error was not a challenge, as the RT-LAB software together with the MATLAB version R2015b was re-installed to solve the error

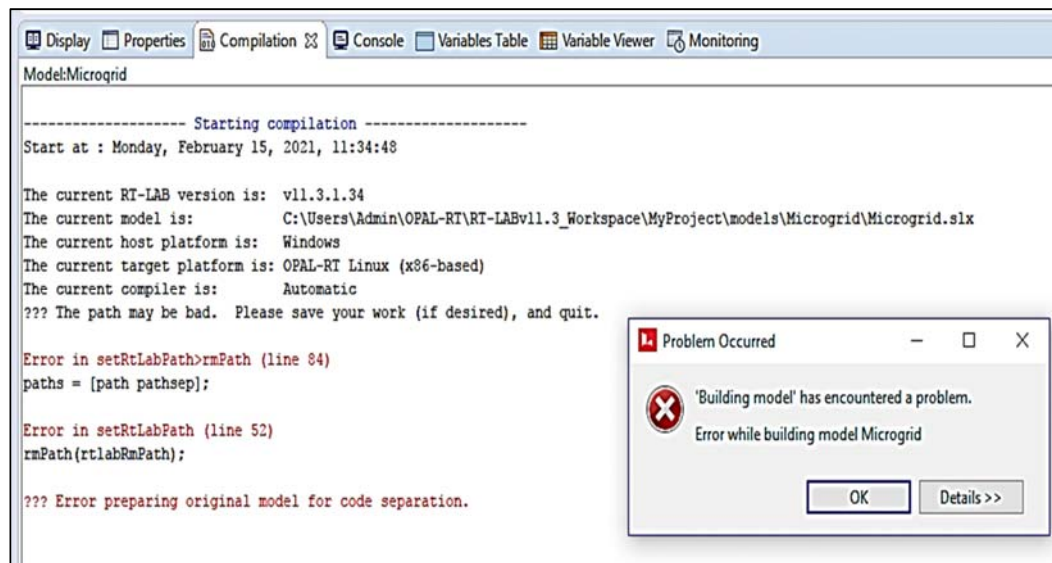


Figure 6-7: Wrong Path Installed Error

The wrong path installed for RT-LAB caused the error. During the launch of the RT-LAB re-installed software, the software was launched as an administrator, thus on MATLAB command prompt the logs proved the library and RT-LAB applications are installed.

ii. Meta Controller:

RT-LAB software application contains a main application called Meta Controller. This application operates as a server, thus allowing the user to be able to open the new models as required and allows the performance in debugging (i.e. to ensure the availability of the controller logs as well as to be able to display the controller application). Moreover, the Meta Controller application ensures that the user access the probe control, monitoring viewer, parameter as well as the dynamo panel on RT-LAB window. Remarkably, as the operating system of the host PC initiates, the Meta Controller applications will therefore begin as well.

iii. Model live viewing in RT-LAB:

The live viewing of the real-time model execution allows the user to perform the analysis of the execution process, thus ensuring accessibility of different functions and operations in RT-LAB software application. Primarily, the Meta Controller application as explained above which acts as a server in RT-LAB software, is essentially required to be running effectively, prior starting the RT-LAB window.

6.1.6 RT-LAB Model Compilation Errors and Solutions

1. Simulink Error

Figure 6.8, shows the error message caused by improperly setting the parameters on Simulink model file. The error message was due to the fuzzy logic controller files that were not saved on the same folder as the Simulink model to be modelled on RT-LAB. Furthermore, it is critically important to note that, when RT-LAB tries to build the model, the Simulink model is opened and checked if it runs offline. In order to be able to detect the error message, the simulated model should only be running on RT-LAB application software.

```

RT-LAB v11.2.2.108
File Edit Navigate Search Simulation Tools Window Help
Display Properties Compilation Console Variables Table Variable Viewer Monitoring
Model:Wind_turbine_Sim_NewVers
----- Starting compilation -----
Start at : Thursday, October 29, 2020, 11:43:27

The current RT-LAB version is: v11.2.2.108
The current model is: E:\Wind_turbine_Sim_NewVers.slx
The current host platform is: Windows
The current target platform is: OPAL-RT Linux (x86-based)
The current compiler is: Automatic
Separating model because it has never been built
Preparing original model for code separation and generation...
The current Matlab version is: v8.6 (64 Bit)

??? Error using opInitFunction>DisplaySimulinkError (line 443)
??? Simulink error :
Update diagram of Simulink model failed. Please check that the model can run offline in Simulink.

Error using opInitFunction>CompileModel (line 460)
Invalid setting in 'Wind_turbine_Sim_NewVers/SM_Subsystem/BES/Pulse Generator1' for parameter 'Period'.

Error in opInitFunction>GenerateModel (line 324)
CompileModel(model);

Error in opInitFunction (line 112)
GenerateModel(action, model, platform, preBuildCmd, postBuildCmd, listSub, StandAloneModel, SlxFormat);

Caused by:
Error using opInitFunction>CompileModel (line 460)
Error evaluating parameter 'Period' in 'Wind_turbine_Sim_NewVers/SM_Subsystem/BES/Pulse Generator1'
Error using opInitFunction>CompileModel (line 460)
Undefined function or variable 'Ts_Power'.

Error in opInitFunction>CompileModel (line 479)
DisplaySimulinkError(simulink_err);

Error in opInitFunction>GenerateModel (line 324)
CompileModel(model);

Error in opInitFunction (line 112)
GenerateModel(action, model, platform, preBuildCmd, postBuildCmd, listSub, StandAloneModel, SlxFormat);

??? Error preparing original model for code separation.

```

Figure 6-8: Improper Parameter Setting Error

2. Generated C-Code Error on RT-LAB

The error message occurred during generation of the C-Code, thus it was caused by the Simulink coder on the modelled microgrid system model as seen on Figure 6.9. However, the error was reproduced on Simulink directly, in a way of finding its root cause as well as its solution. Therefore, the afore-mentioned error was resolved by performing the above activities using the article on the link <https://www.opal-rt.com/support-knowledge-base/?article=AA-01352>.


```

----- Generating C code -----
Using System Target File (TLC file) : rtlab_rtmodel.tlc...
Using Template Makefile (TMF file) : rtlab_rtmodel.tmf...

----- Generating wind_turbine_sim_new_1_sm_subsystem C code -----
??? Error using tlc_c (line 179)
Algebraic loops are not supported in generated code. Use the 'ashow' command in the Simulink Debugger to see the algebraic loops

Error in coder.internal.ModelBuilder/make_rtw (line 633)
    [buildResult, profilingInstrumentationData] = tlc_c(h,...

Error in coder.internal.ModelCodegenMgr/make_rtw (line 8)
    buildResult = obj.make_rtw(varargin);

Error in make_rtw (line 18)
    buildResult = h.make_rtw(varargin{:});

Error in build_target

Error in build_target

Error in build_standalone_rtw_target

Error in slbuild_private

Error in slbuild_private

Error in sl (line 15)
    [varargout{1:nargout}] = feval(varargin{:});

Error in slbuild (line 61)
    sl('slbuild_private', mdl, varargin{:});

Error in rtwbuild (line 189)
    slbuild(sys, 'StandaloneRTWTarget', ...

Error in opMakeRTW

```

Figure 6-9: Simulink C-Code Generation Error

3. Inaccessible Workspace Error

The screenshot shows the Simulink RTW build console with the following text:

```

Overview | Development | Execution | Variables | Files | Assignment | Diagnostic | Hardware | Simulation Tools
Display | Properties | Compilation | Console | Variables Table | Variable Viewer | Monitoring
Model: Wind_turbine_Sim_NewVers
Corrupted Stateflow charts are recovered and placed in a subsystem named
'###Recovered Stateflow Charts###'. You can open it using
open_system('wind_turbine_sim_new_3_ss_chargecircu/###Recovered Stateflow Charts###');
Separating RT-LAB subsystem 'SS_DischargeCircuit'.
Repair completed.

*****IMPORTANT*****
Corrupted Stateflow charts are recovered and placed in a subsystem named
'###Recovered Stateflow Charts###'. You can open it using
open_system('wind_turbine_sim_new_4_ss_dischargeci/###Recovered Stateflow Charts###');

Model preparation and separation duration : 00h:00m:38s
----- Completed successfully -----

----- Generating C code -----

Using System Target File (TLC file) : rtlab_rtmodel.tlc...

Using Template Makefile (TMF file) : rtlab_rtmodel.tmf...

----- Generating wind_turbine_sim_new_1_sm_subsystem C code -----
Cannot copy file(s) : C:/Users/Admin/OPAL-RT/RT-LABv11.3_Workspace/MyProject/models/Wind_turbine_Sim_NewVers/Opcommon/wind_turbine_sim_new_1_sm_subsystem.slx
to C:/Users/Admin/OPAL-RT/RT-LABv11.3_Workspace/MyProject/models/Wind_turbine_Sim_NewVers/wind_turbine_sim_new_1_sm_subsystem.slx

```

Overlaid on the console is a 'Problem Occurred' dialog box with the following text:

Problem Occurred

'Building model' has encountered a problem.
Error while building model Wind_turbine_Sim_NewVers

Buttons: OK, Details >>

Figure 6-10: Error on Location of the Workspace in RT-LAB

The error that appears on Figure 6.10 was caused by the inaccessibility of the workspace used during the start of the RT-LAB application software. In order to ensure that the RT-LAB does not encounter such an error, RT-LAB application software was opened as Admin and the location of the workspace was also changed from Admin, thus the new workspace was created in a new location.

4. Error Caused by Number of Cores Activated by License

On the Figure 6.11, the error encountered is linked to the number of cores activated by the license as explained on the above sub-section 6.1.2.1. Initially, the model consisted of four sub-systems that ran in a dedicated core simulator. Hence, there were only two cores activated by the RT-LAB license, the RT-LAB model was allowed to consist of two subsystems that can be used in the model. However, the detailed error was rectified by reducing the number of subsystems used on the model, thus the modelled system incorporated two subsystems as seen on Figure 6.2 (b).

```

2020-11-26 10h33m31s:OpalRtMain.c      : Standard output has been redirected to /dev/null
2020-11-26 10h33m31s:OpalRtMain.c      : Standard error has been redirected to /dev/null
2020-11-26 10h33m31s:OpalRtMain.c      : Standard input has been redirected to /dev/null
2020-11-26 10h33m31s:OpalRtMain.c      : Line 1642

2020-11-26 10h33m33s:OpalRtMain.c      : Number of required cores (3) > number of available licensed cores (1).
2020-11-26 10h33m33s:ERROR: [0] ERROR_STATUS
2020-11-26 10h33m33s:OpalRtSnapshot.c   : Snapshot taken (opwind_turbine_sim_new_sm_subsystem_0.snap).
2020-11-26 10h33m33s:OpalRtSnapshot.c   : Estimated time to take a snapshot = 5 us.
2020-11-26 10h33m33s:OpalPrint.c        : Sending file name notification request for system control (cmd 30)
2020-11-26 10h33m33s:OpalHostSendIf.c   : Open file done (/home/bv-ele-a237-pl8/e/yardmicrogrid/modeling/models/wind_turbine
2020-11-26 10h33m33s:OpalHostSendIf.c   : Close file done (/home/bv-ele-a237-pl8/e/yardmicrogrid/modeling/models/wind_turbin
2020-11-26 10h33m33s:OpalPrint.c        : Sending file name notification request for system control (cmd 33)
2020-11-26 10h33m33s:OpalSyncOs.c      : clk_res = 10 us
2020-11-26 10h33m33s:OpalSyncOs.c      : clk_res_factor = 1
2020-11-26 10h33m33s:OpalTarget.c       : Sending notification request for system control (cmd 20)
2020-11-26 10h33m33s:OpalRtMain.c      : [0]: PAUSE mode, IO set to pause value.
2020-11-26 10h33m33s:OpalRtMain.c      : Total of 0 Overrun detected.
2020-11-26 10h33m33s:OpalRtMain.c      : Thu Nov 26 10:33:33 2020

2020-11-26 10h33m33s:OpalRtMain.c      : Master requests slave(s) to stop simulation.
2020-11-26 10h33m33s:OpalRtMain.c      : OpalInit: Error code 50 (License error, see previous error messages. )
2020-11-26 10h33m33s:OpalRtMain.c      : [0]: Reset
2020-11-26 10h33m33s:OpalRtMain.c      : Total of 0 Overrun detected.
2020-11-26 10h33m33s:OpalRtMain.c      : Thu Nov 26 10:33:33 2020

```

Figure 6-11: Error Caused by Cores Activation by RT-LAB License

6.2 Chapter Summary

The real-time simulator manufactured by OPAL-RT technologies called OP4510 simulator was used as a target PC. Thus, comprised of a 3.5GHz processor cores, with four cores activated provides the file transfer protocol (FTP) and Ethernet TCP/IP, UDP/IP communication with the host PC, input/output (I/O) and real-time model execution as well as the Linux operating system. This allows the real-time simulation for the developed microgrid system model. RT-LAB software was used in order to enable the models designed and built in MATLAB/Simulink environment to be tested their dynamics in-order to get accurate hardware-in-the-loop (HIL) simulations in real-time as well as reducing the risks, costs and delays of the built power

systems of the microgrid system. RT-LAB used simulating tools, namely; RT-Events and Advanced Real time electro Mechanical Simulator (ARTEMis) that is based on Simulink modelling environment. These modelling tools enabled the modelling of high-speed and real-time simulation to be performed in multi-core processors. The modelled microgrid system was simulated using time step of $20\mu\text{s}$ on E3 4-core, 3.5GHz processor speed RT-LAB simulator. The duration of time steps of the simulation were set as discrete-time constant. This real-time and high speed simulating equipment uses a MEGAsim simulation system containing a host PC and a target PC. The host PC included a 1Gbps LAN card for real-time communication with the target PC, and operated based on Windows to allow the compilation of the model to be easily performed and downloaded to the target PC. Notably, the errors encountered during the compilation and modelling of the microgrid system in real-time were; Simulink error, generated C-Code error on RT-LAB, inaccessible workspace error and an error caused by number of cores activated by license.

CHAPTER 7: Operated Modes and Scenarios in Real-Time Simulation

7.1 Introduction

The main purpose of this chapter is to perform the validation of the designed operation modes and developed case studies using OPAL-RT simulator as well as RT-LAB. However, it is vitally important to note that the use of real-time simulators was indeed applied in electrical power system models developed for any applications for the past decades. Thus, with the change of time, an increase in the use of computer technologies have gained more attention and therefore resulted in the growth on its performance as well as the proficiency in solving systems that are more complex in less amount of time. Therefore, the sub-sections of this chapter present the real-time simulation results wherein sub-section 7.2.2 designed operating modes of the developed microgrid system. Sub-section 7.3 real-time modelling with implemented case Studies and Results.

7.2 The Developed System Configuration and Operating Mode Algorithms

7.2.1 Microgrid Connection

The microgrid system modelling in this study is formed by making sure that the 4-Node distribution model is connected to the DER's on Simulink model, thus the confirmation of the attributes of the microgrid system discussed above is made on the new modelled microgrid system. The DER's, namely PV solar system and the wind turbine system, as well as the battery storage system were all connected in a 4-node DC bus feeder. Therefore, OPAL-RT was then used to simulate the designed and developed microgrid system in real-time. The PV solar inverter system and the battery storage inverter system were connected to the distribution system, whereas the inverter system of the wind turbine was integrated with the 4-node distribution system. In Figure 7.1, the microgrid switching, which exists between Conn 1 of Grid control and Conn 1 of PV solar farm was used to disconnect and connect the microgrid system developed from the 4-Node distribution system, in-order to create the off-grid mode of the microgrid system. Thus, the system uses the DER's as the first method of supplying power for the microgrid system, irrespective of the utility grid being active or not active.

Microgrid controller is a vital component needed for the microgrid system as stipulated above. However, it is required to be to maintain the system and regulatory constraints, and therefore by making sure that the logical transfer from one mode to another as well as the security of the system is maintained without any interruptions. The developed microgrid system consists of two controllers, namely, the micro-source controller that controls the DER's operation, locally, and the central controller, controlling the entire operation of the microgrid system.

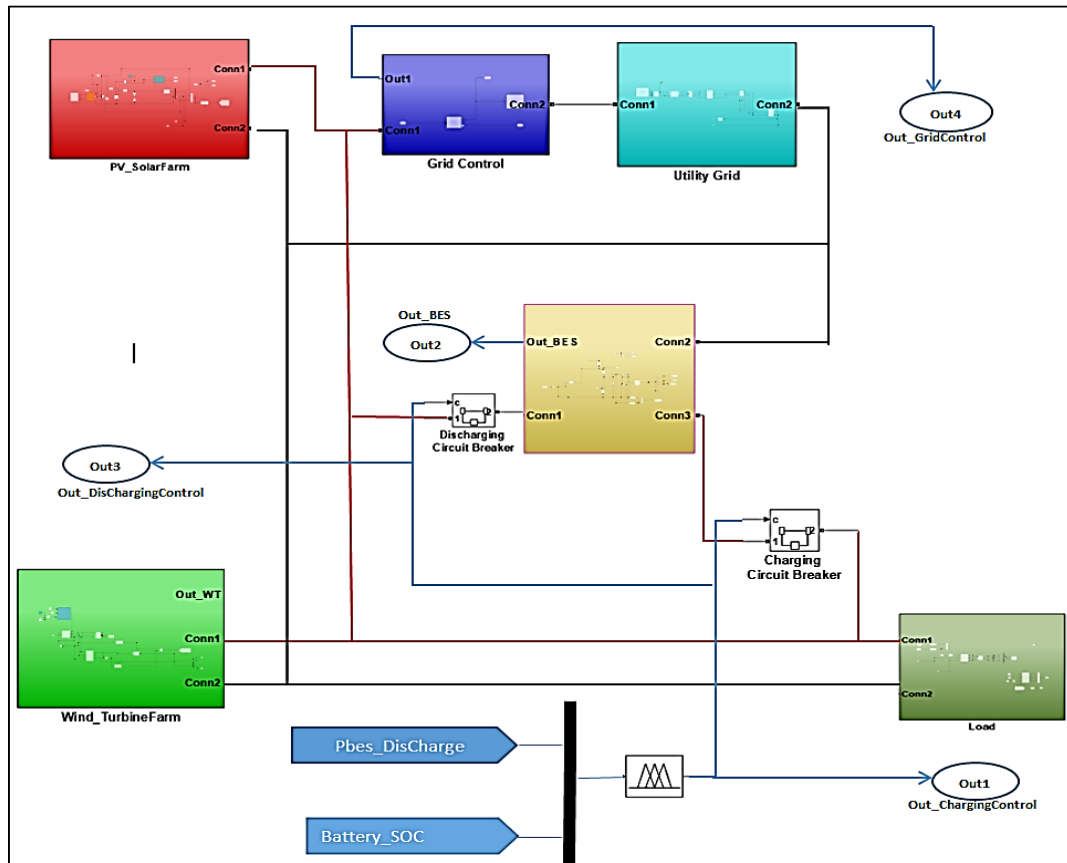


Figure 7-1: RT-LAB Microgrid System with DC Bus Connection modelled using OPAL-RT

7.2.2 Designed Operating Modes of the Developed Microgrid System

The concept of the microgrid is concluded on the previous sections, as the inter-connection of the DER's and either the combination of thermal loads and electrical loads or both with the controllable electrical limits connected and disconnected to the grid, depending on the user's demands. In order for the MG to transitionally work on the off-grid mode, the energy storage system and the system generating power must be included locally, because both systems are the bases of the off-grid mode microgrid. Additionally, the microgrid controller is the most critical component needed and used. However, with the absence of one of those two systems or both, the functioning of the MG was severely compromised.

Technologies used in microgrid systems developed were renewables and non-conventional resources for generation purposes and are integrated to generate power at distributed voltages. The afore-mentioned types of resource technologies are therefore provided with power controls and electronic interfaces to establish a powerful single system's operation. Thus, the microgrid system control as a single unit is allowed to provide the operation standards needed from the local utility supply. To ensure the local utility standards are met with the power security, compliance and reliability, the utility grid considers the MG as the single operated load that is controllable.

The developed microgrid system consists of a common DC bus voltage acting as the communication signal during the conversion of the microgrid system operation modes. In addition, for this developed modes of

operation of the microgrid system, there are many different effects of interconnection controls occurring in the power balancing of DC bus. However, these interconnecting control effects are prevented by effectively using the adaptive mode of transition among the operating modes designed on the microgrid system. Therefore, this is done by using the DC bus-signalling scheme through a decentralized control. Thus, the developed method of operation by using a decentralized control method regulates the proper function of the designed microgrid system during the input conditions that are changing indefinitely.

This section explains the mode of operation as simulated for the DER's used in the developed microgrid system. According to Figure 7.3, the amount of power produced by the RES of 300kW is greater than the load demand of 92.170kW. Therefore, the distributed generation mode of operation occurs when the load power demand is less than the power generated as seen on Figure 7.2(a), thus the microgrid system on this mode of operation is working in off-grid mode. The BESS charges during this period and is supplied by the excess power from the DER's, thus the bus voltage is regulated in order to control the voltage bus by ensuring that the MPPT is shifted to allow this process. Notably, this process of changing the MPPT control to a constant voltage for sharing the BESS will be clearly shown on sub-sections below. In this mode, AC grid is disconnected and the battery-interfacing converter regulates the bus by absorbing the excess power.

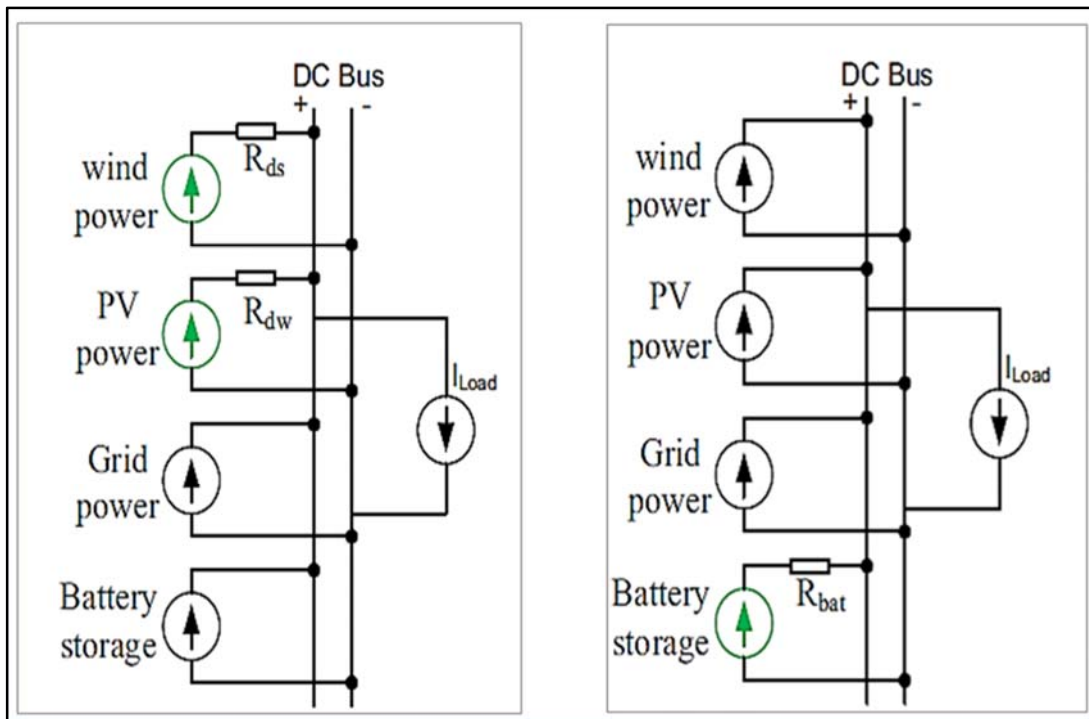


Figure 7-2(a): Off-Grid Operation Mode (Ensurma, 2019)

Figure 7-2(b): Battery Storage Mode (Ensurma, 2019)

The Figure 7.4 shows the battery storage mode of operation wherein the load demand of approximately 1.06MW is greater than the power produced by the RES of 625kW. This mode occurs during the microgrid system activation by the BESS in order to discharge power as seen on Figure 7.2(b) as well as the load demand is greater than the power generated by the DER's. However, if the power that is supplied by the

DER's and the BESS is not enough to match the power demanded by the load, the utility grid is activated, thus the microgrid system satisfies the process of buying the power from the grid as explained on the aforementioned sub-sections. During this time of discharging power to be supplied to the load, the BESS is working as the voltage source as well. This is due to the power generated by the DER's is less than the load demand, thus the battery regulates the voltage DC bus.

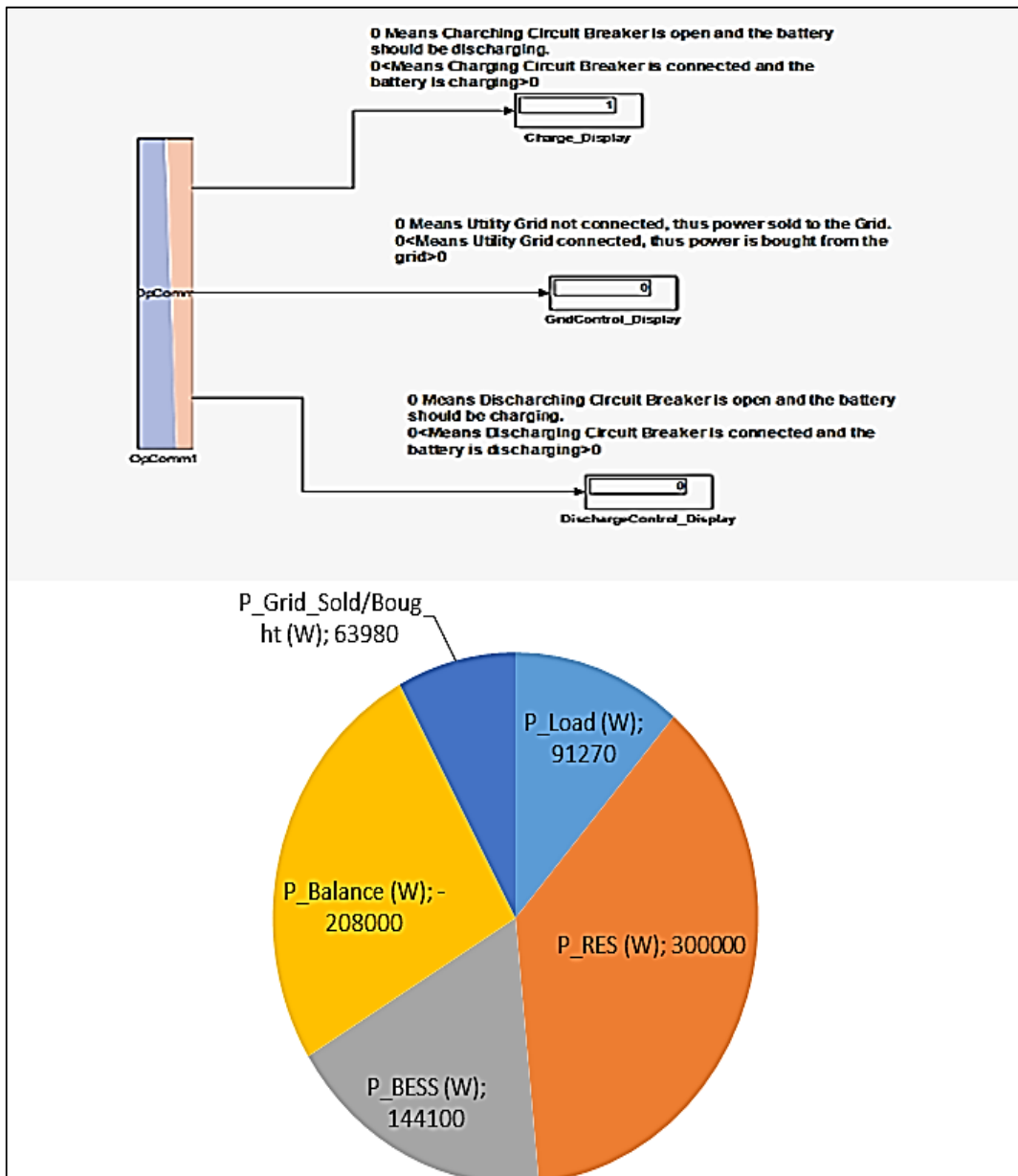


Figure 7-3: Load Demand Less than Power Generated by DER's

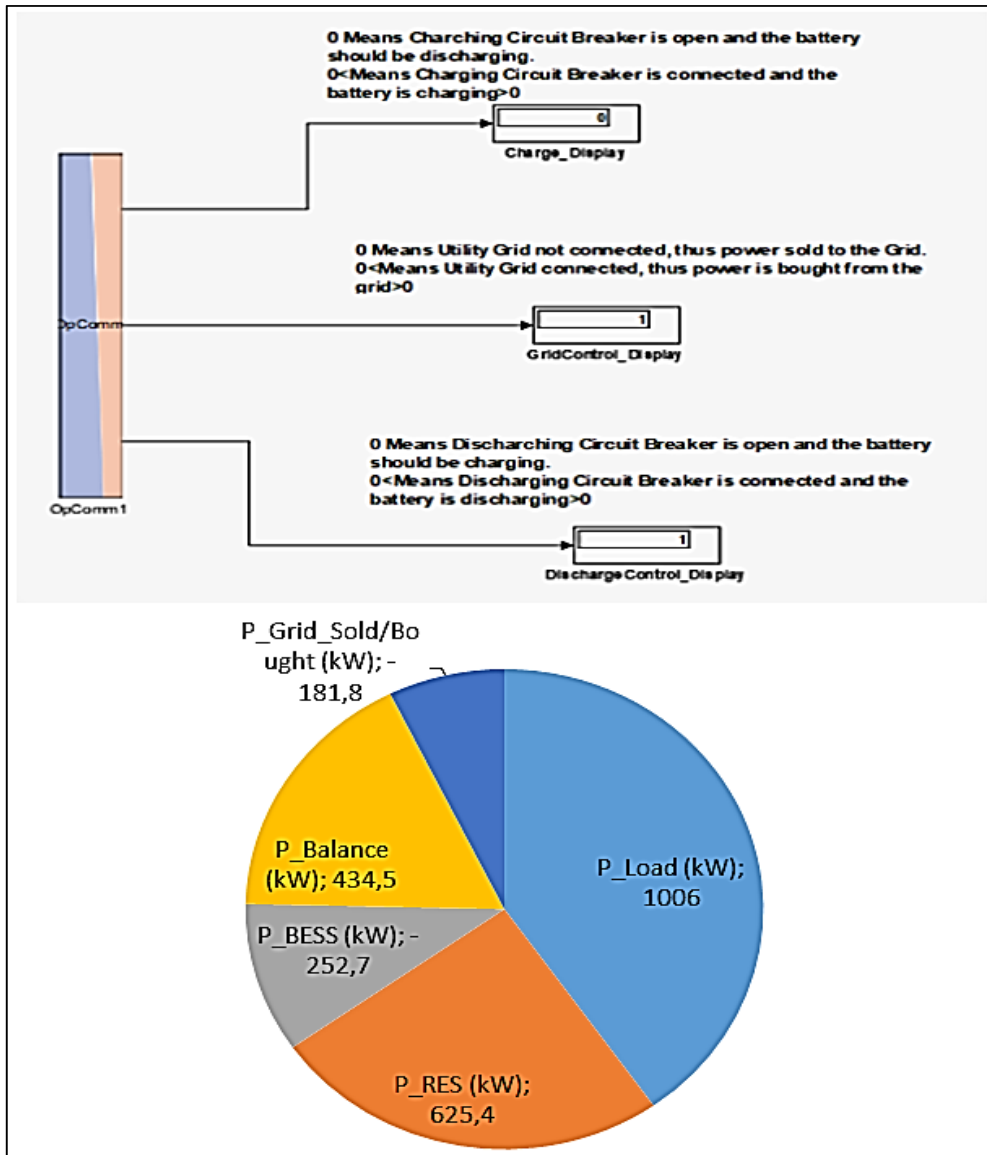


Figure 7-4: Load Demand Greater than Power Generated by DER's

7.3 Chapter Summary

The operation modes were designed and validated using OPAL-RT simulator as well as RT-LAB namely, the off-grid operation mode and the battery storage mode. The development System Configuration and operating mode algorithms of the microgrid system modelling were achieved by forming the 4-Node DC feeder and connect it to the DER's on Simulink model. The switching of the microgrid system, was created in order to disconnect and connect the microgrid system developed from the 4-Node DC distribution system, in-order to create the off-grid mode of the microgrid system. The microgrid system controller was developed comprising of two controllers, namely, the micro-source controller that controls the DER's operation, locally, and the central controller, controlling the whole operation of the microgrid system. The energy storage system and the system generating power were included locally, because both systems were the bases of the off-grid mode microgrid. The DC bus-signalling scheme through a decentralized control was created in order to prevent the interconnecting control effects using the adaptive mode of transition among the operating modes. Furthermore, the off-grid operational mode of the microgrid system occurred

when the amount of power produced by the RES was 300kW and load demand was 92.170kW; thus, the BESS was charged during this period. The battery storage mode occurred when the battery storage mode of operation wherein the load demand of approximately 1.06MW was greater than the power produced by the RES of 625kW. This mode occurs during the microgrid system activation by the BESS in order to discharge power.

Chapter 8: Results and Discussion

8.1 Overview

This chapter starts by detailing the results modelled from Homer Energy software to perform analysis on the simulated and optimized microgrid system model. Therefore, the operation and installation costs of the physical microgrid system designed is modelled and compared with different models of MG designs focusing on technical and economic characteristics. Moreover, this chapter outlines the results of the PV solar array and wind turbine per the specifications of the microgrid system designed. The chapter further provides the analysis of the results from the implemented case scenarios of the microgrid system simulated in both MATLAB/Simulink and in real-time using OPAL RT-LAB simulation software. Finally, the summary of results and their impact on railway yard is discussed.

8.2 Homer Energy Modelling Results

Table 8.1 illustrates the six case scenarios optimized and generated by HOMER energy software. The first case scenario is made up a PV solar, wind turbine, diesel generator and BESS, where the amount of the COE is approximately equal to 8% of COE in case scenario 6 which consists of a main grid supply only. Furthermore, the second case scenario illustrated on table 8.1 consists of the PV solar, wind turbine, diesel generator and a main grid. Thus, in case scenario 2 the amount of cost per initial and net present cost (NPC) differs from that of case scenario 1, although the COE is equal for case scenario 1 and case scenario 2. In case scenario 3 consisting of PV solar, wind turbine system, BESS and main grid, the COE is still lower than that of case scenario 6 with a decrease of the operating costs as compared to that of case scenario 2; thus, showing much improvement due to the diesel generator exclusion in this case scenario and be the case scenario that is outstanding for the hybrid system developed.

Table 8.1 further demonstrates case scenario 4 that is made up of a diesel generator and a grid, where the initial costs are lower than case scenario 1 and case scenario 3. However, case scenario 4 has higher NPC and COE than the previous case scenarios. Lastly, case scenario 5 consisting of PV solar, wind turbine system as well as the main grid proves that an RES-based microgrid system will always have low COE even when it is operated in grid-tied mode. However, the operating costs as well operation and maintenance (O&M) are high as compared to that of case scenario 3 causing it to be less disadvantaged hence it does not have a storage system.

Table 8-1: HOMER Cost Effectiveness Simulation Results (Dekeda and Adonis, 2019)

Case Scenarios	PV (kW)	3MW Wind turbine	Diesel generator (kW)	Li-ion battery strings	NPC (R)	COE (R)	Operating cost (R/yr)	Initial capital (R)	O&M (R/yr)
Case 1	7.64E-29	1	530	1	R7 909 015	0.12	R 299 916.1	R 4 031 845	R 79 895.21
Case 2	1.96	1	530	N/A	R8 326 056	0.12	R 386 606.5	R 3 328 193	R 100 148.9
Case 3	542	1	N/A	3	R11 200 000	0.16	R 339 362.7	R 6 839 179	R248 093
Case 4	N/A	N/A	530	N/A	R11 900 000	0.41	R 902 897.7	R 265 000	R 139 343.8
Case 5	427	1	N/A	N/A	R16 300 000	0.21	R 924 809.6	R 4 366 643	R 890 210.7
Case 6	N/A	N/A	N/A	N/A	R43 600 000	1.49	R3 371 870	R0,00	R3 371 870

8.3 Modelling design and Results of PV solar array and Wind turbine on MATLAB/Simulink

8.3.1 PV Array Modelling and Results

The Figure 8.1 and Figure 8.2, respectively illustrate the I-V and P-V characteristics curves occurring at different irradiance levels and at a fixed temperature level of 25°C. Respective to Figure 8.1, the total open-circuit voltage of PV solar array is approximately 1036V_{DC} during the sunny day when the irradiance approximately 1000W/m². Thus, that measured value corresponds with the calculated value of 16*64.8V_{DC} where 16 is the number of cells in series and 64.8V_{DC} is the open-circuit voltage. The voltage and load current of the PV array is evident that they behave inversely proportional to one another. Figure 8.1 shows that as the load current increases, the voltage decreases, therefore, thus at short circuit (V=0) the current is approximately 680A.

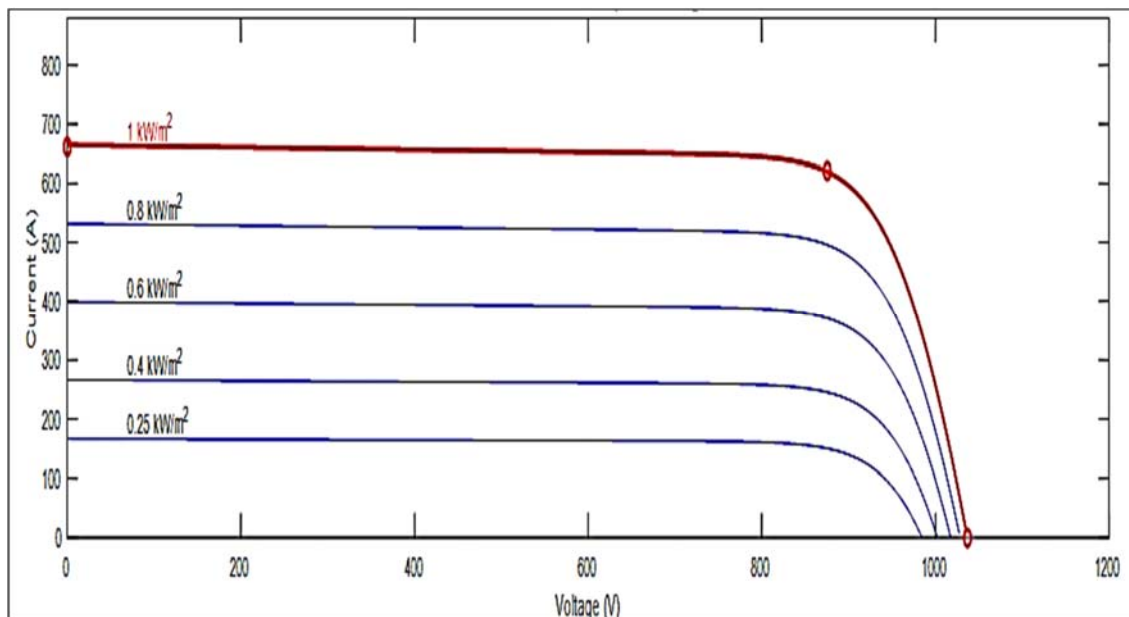


Figure 8-1: I-V characteristic for a PV array at a constant temperature of 25°C simulated on MATLAB/Simulink

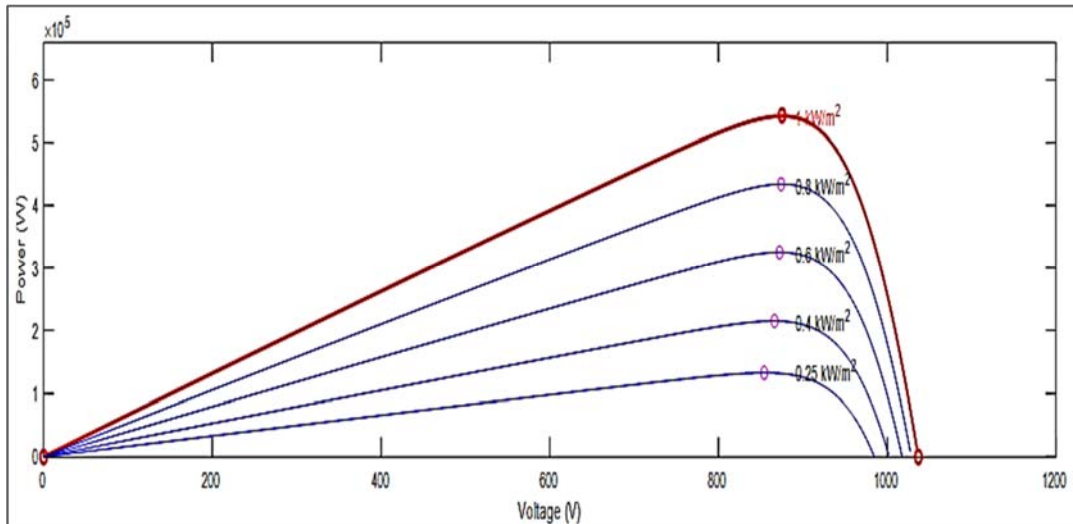


Figure 8-2: P-V characteristic for a PV array at a constant temperature of 25°C simulated on MATLAB/Simulink

The power is not produced by the PV solar array at open-circuit and short-circuits. However, the maximum power is attained from the PV solar array at maximum power point (MPP). This can be seen on the I-V characteristic curve, which is Figure 8.1, where the rectangle area part has the largest area, thus proving the maximum power generation of the PV system as illustrated on Figure 8.2 of the P-V characteristic curve. On Figure 8.2, it can be concluded that at high levels of irradiance, the amount of power generated is increased. The linear relationship between the irradiance and the short-circuit current occur when short-circuit current decreases at lower irradiation.

The PV characteristics curves shown on Figure 8.3 and Figure 8.4, illustrate the I-V and P-V curves, where the irradiance was kept constantly at 1000W/m^2 and varying the temperature from 0°C , 25°C and 50°C . As seen from Figure 8.1 and 8.2, the open circuit voltage decreases not as much, until the irradiation is very low. Nonetheless, Figure 8.3 and Figure 8.4, proves that the temperature of the PV solar cell significantly influences the open circuit voltage of the PV solar array. As seen from the illustrations below, the open circuit voltage decreases as the temperature increases, thus the output power of the PV system decreases too with a percentile margin that approximate to 15% from 0°C to 50°C . Notably, all modelling and simulations for the PV solar system were performed without linking the utility grid to the system.

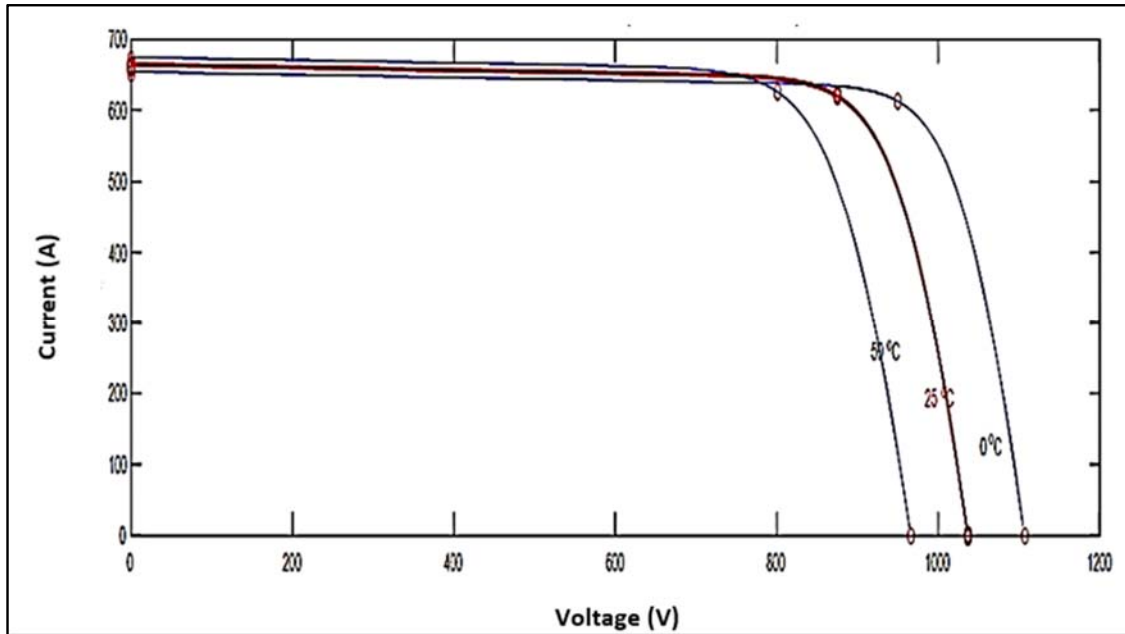


Figure 8-3: I-V characteristic for a PV array at a constant irradiance of $1000\text{W}/\text{m}^2$ simulated on MATLAB/Simulink

This section of simulation results details the behaviour of the PV solar system relative to time as set on the simulation model. As explained above, the system was modelled after finding all other possible results using the standard test conditions where the temperature and the irradiance values were 25°C and $1000\text{W}/\text{m}^2$, respectively. Starting from $t=0$ sec until $t=0.05$ sec, the system blocked the pulses to the boost converter and VSC, therefore the PV array voltage corresponded to that of calculated open-circuit voltage of $1036.8\text{V}_{\text{DC}}$ ($N_{\text{ser}} \times V_{\text{OC}}$) as seen on Figure 4.10.

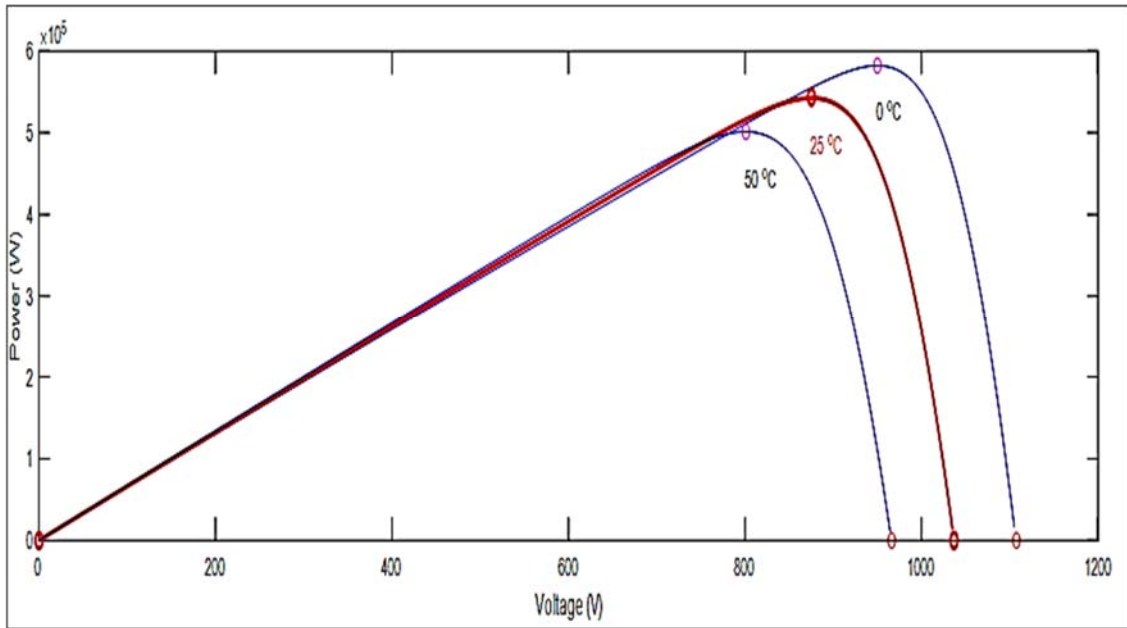


Figure 8-4: P-V characteristic for a PV array at a constant irradiance of 1000W/m^2 simulated on MATLAB/Simulink

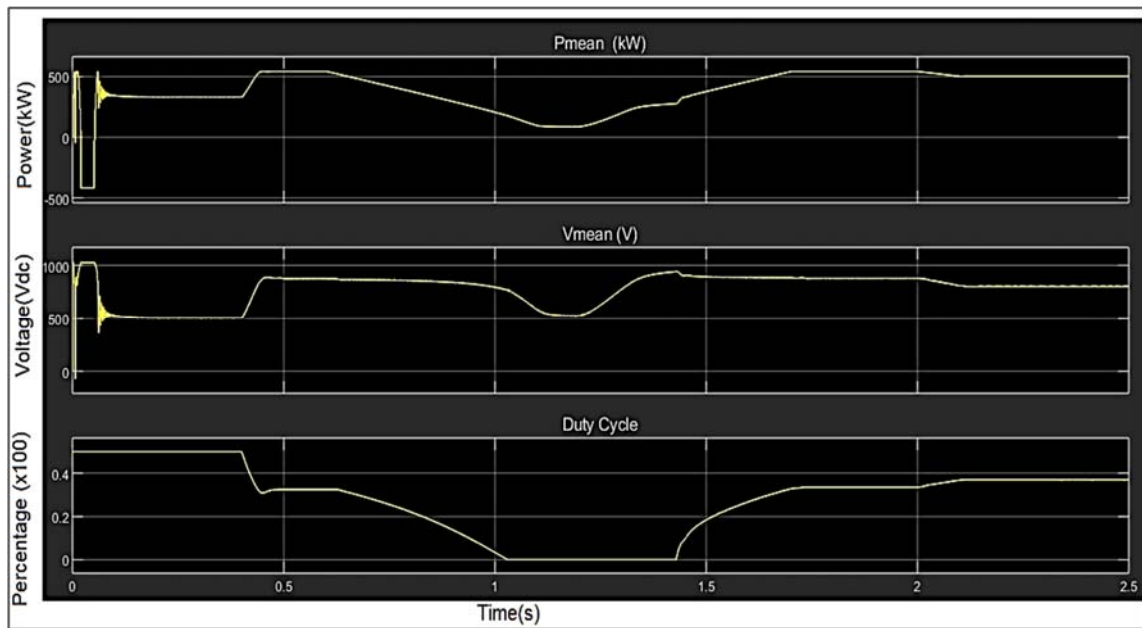


Figure 8-5: Pmean, Vmean and Duty cycle PV scopes simulated on MATLAB/Simulink

The initialization of the VSC and DC-DC boost converter starts after few milliseconds as seen on Figure 8.5 and the DC voltage is steadily regulated 500V_{DC} . Moreover, during that period, the duty cycle of the DC-DC boost converter is however steadily set at 50%. Consequently, the PV array voltage is approximately 1000V_{DC} . Therefore, the system reaches its steady state at $t=1.25$ seconds, as depicted in Figure 8.5.

8.3.2 Wind Turbine Modelling and Results

This section addresses the modelling designs and development of the 3MW wind turbine farm formed by two 1.5MW wind turbines using MATLAB/Simulink. The wind turbine projects available in MATLAB/Simulink were used in order to model the requirements of the wind turbine, instead of being designed from the beginning. Therefore, Figure 8.6 illustrates the designed wind turbine model. The output power that is attained at low wind speeds is too low and the normal starting speed of the wind turbines in generating energy is when the wind speed exceeds 3m/s to 4m/s. However, the output power of the wind turbine increases with the cube of the wind speed, thus the rated wind speed of 14m/s is reached. From Figure 8.7, which is the characteristic curve of the modelled wind turbine, it is clear that the rated power of the wind turbines is limited by the wind speeds from 14m/s to 25m/s, and therefore the pitch-control or stall-regulation provide that limitation. Moreover, the wind speed over 25m/s is called the cut-out speed of the wind turbine and it causes the wind turbine to be normally stopped in-order to prevent the mechanical loads that are high.

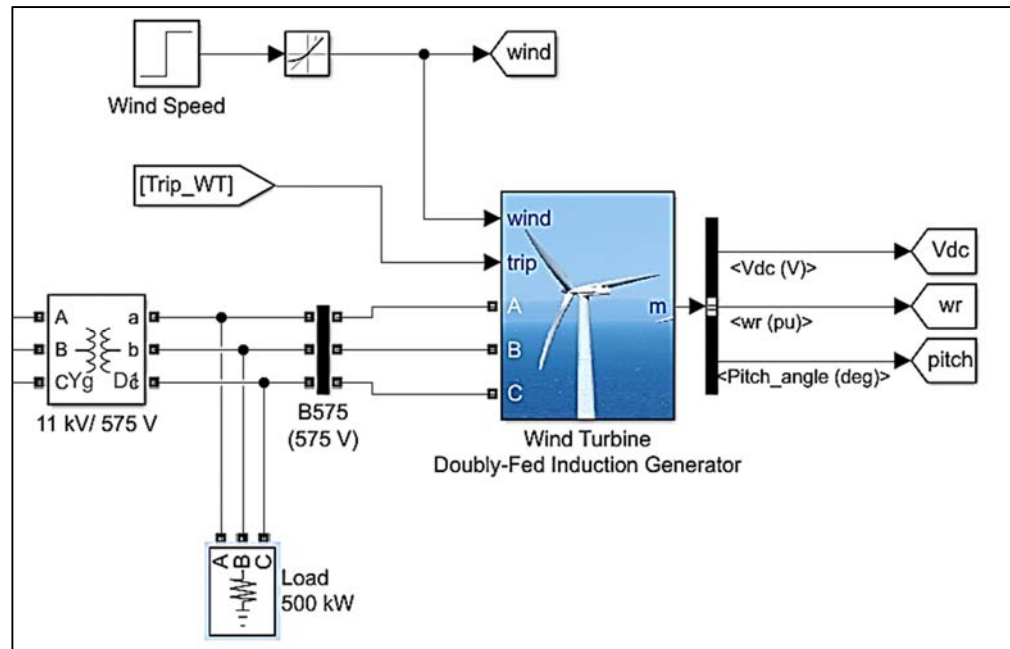


Figure 8-6: Wind Turbine plant modelled

The modelled wind turbine plant is made up of two of 1.5MW wind turbines that are connected to the 11kV_{AC} grid using 11kV_{AC} feeder line as shown on Figure 8.6. This 3MW plant of wind turbines was modelled and simulated using a pair of 1.5MW wind turbines with a DFIG as stipulated above. The pitch angle of the wind turbine used is varied in order to control and drive the rotor, thus the output power of the generator is limited during its nominal values when the nominal speeds exceeds 14m/s. However, the wind turbine plant is connected to the 50Hz operating-frequency grid, directly via a stator winding. Furthermore, the power is generated when the asynchronous speed is lower than the DFIG speed and hence on the model, the speed is controlled between 0.2 per unit (pu) at no load and 1.2pu at full load.

The Figure 8.7 which is the wind turbine characteristic curve, shows the reflection of the generated power and the aerodynamic power. It is clear that the extracted output power from the wind is too low during low wind speed as the modelled wind turbine starts producing power at approximately 3.5m/s and 4m/s wind speeds. The pitch-control ensured that during 14m/s and 25m/s the rated power of the wind turbine is limited. On the wind turbine characteristic curve, the output power-tracking characteristic from point A to point D is obtained. As seen on Figure 8.7, the power is zero from the start until the wind speed at point A. However, it can be noted that from point A tracking characteristic to point B, the speed increased. Furthermore, the maxima of the wind turbine output power and the wind speed is reached between point B tracking characteristic and point C. Finally, a straight constant line between tracking characteristics of point C and point D is reached, thus the power at point D is one per unit (1 pu) and the speed of the point D is greater than the speed of point C.

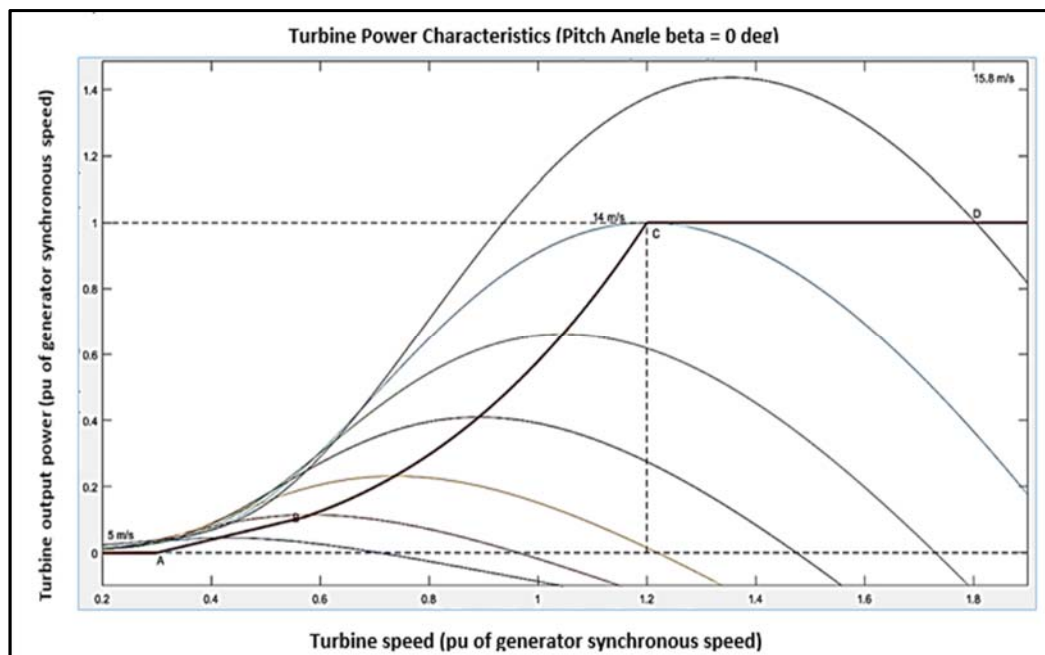


Figure 8-7: Turbine Power Characteristic Curve simulated on MATLAB/Simulink

The speed, voltage as well as the current of the wind turbines system is monitored by the protection system. On the designed microgrid system, the capacitor bank connected to the voltage bus of 400kVar moderately balances out the reactive power that is absorbed by the DFIG from the grid. Whereas, according to the design model of the wind turbine system, the 3-Mvar STATCOM provides the rest of the reactive power to maintain 11kV_{AC} voltage. As seen from Figure 8.7, the mechanical power of the wind turbine system is dependent to the turbine speed, and thus the illustrated mechanical power acts as a function of turbine speed ranging from 4m/s to 14m/s. Therefore, relative to the Figure 8.7, the nominal power of 3MW is accomplished by a nominal wind speed of 14m/s.

The examination for the functioning of the modelled wind turbine is performed in this section. As illustrated in Figure 8.8, the speed of the wind turbine is initially moving constantly at approximately 4m/s for 5 seconds. However, after 5 seconds the inclination of the signal is introduced which lasts for 27 seconds, and then followed by the constant rated wind speed of 14m/s for the duration of 23 seconds.

The active power generated by both wind turbines is shown in Figure 8.9. Both the active power and the wind speed can be seen increasing smoothly. Therefore, the active power starts increasing at the same time with the wind speed, thus reaching the total rated power of 3MW for both wind turbines in approximately when the rated wind speed of 14m/s is at around 27 seconds. Subsequently, the reactive power (Q) caused by the changing wind speed is also illustrated in Figure 8.10, and accordingly at nominal power, the generated Q value is approximately -0.3MVar, relative to the graph.

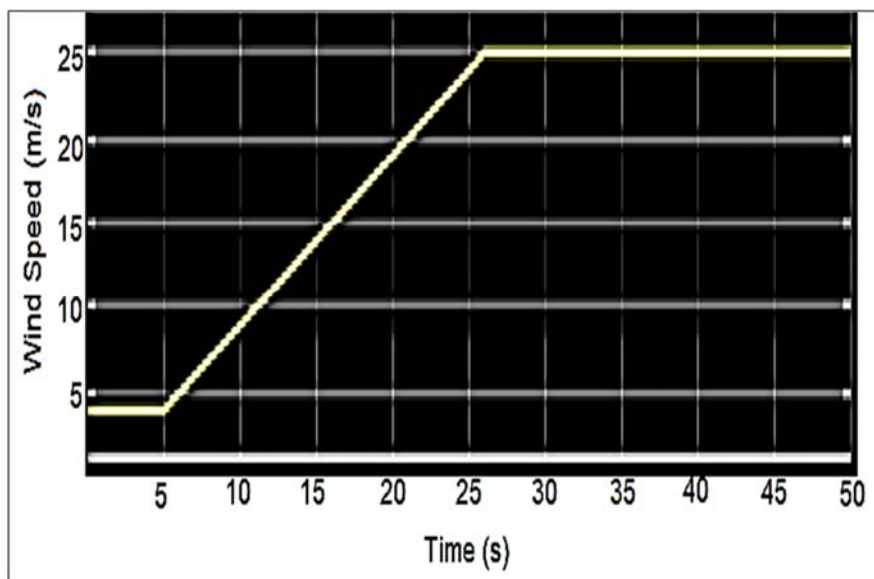


Figure 8-8: Wind Turbine wind speed simulated on MATLAB/Simulink

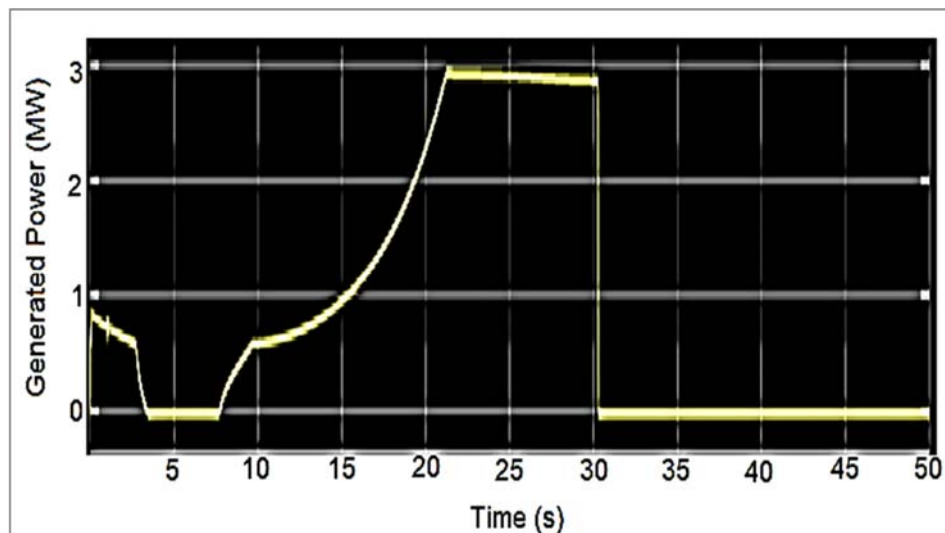


Figure 8-9: Wind Turbine generated power simulated on MATLAB/Simulink

The results of the pitch angle response are illustrated in Figure 8.11, as required by the changing wind speed. In Figure 8.7, it can be seen that the operating point of the wind turbine ended on point D, where initially the pitch angle of the wind turbine started at 0 degrees. Furthermore, the behaviour of the pitch angle response as shown on Figure 8.11, increases from 0 degrees after 28 seconds to approximately 32 degrees, thus the mechanical power of the wind turbine is limited. Figure 8.9, proves that, the nominal power of the wind turbine is reached at 20 seconds, due to the pitch angle controller that is not used which can prevent the rotor over speeding.

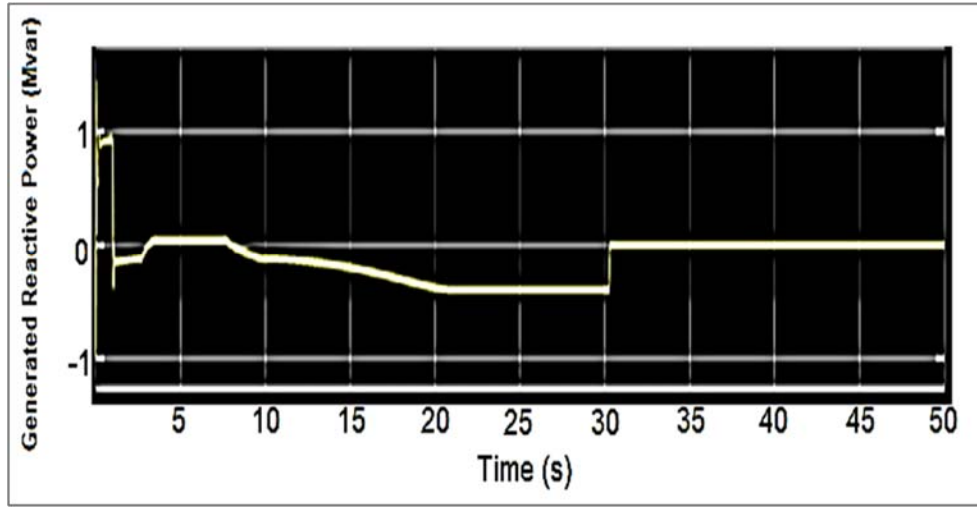


Figure 8-10: Wind Turbine Reactive Power simulated on MATLAB/Simulink

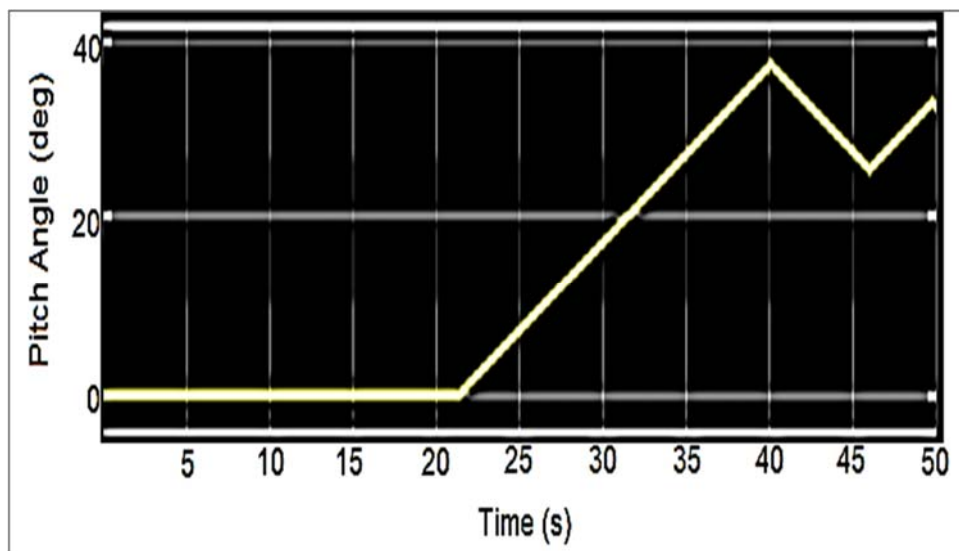


Figure 8-11: Wind Turbine Pitch Angle simulated on MATLAB/Simulink

8.4 Simulation Results of the Implemented Case Scenarios using MATLAB/Simulink

The simulation results are based on the implementation of the designed microgrid and FIS using MATLAB/Simulink to effectively verify the developed method used for the EMS. In order to assess and

examine the performance of the controller for the developed EMS in this study, there were four test cases implemented for the EMS. The simulation was performed on MATLAB/Simulink using the 24-hour period which is represented with a total of 8.64×10^4 s on the x-axis.

8.4.1 Implemented Cases Scenarios

This section explains the results of the four implemented cases that were simulated in order to prove the correct functioning and operation of the developed microgrid EMS. The developed scenarios for this exercise were thoroughly explained. Table 8.2 represents the summarised results of the simulated EMS system with the load variation taken at 95% level of the SOC of the battery. The table consist of the difference between the load and the generated power by the RES called $P_{\text{Equilibrium}}$, power expected to charge or to be discharged by the lithium-ion battery and the probability of the power bought or sold to the utility grid as per the regulations of the municipality and power utility (Eskom).

As mentioned on the section above, the initial condition of the battery SOC was set to be 95% and the demand to be 50% with the values taken at approximately on the twelfth hour of the day. On the case were $P_{\text{Equilibrium}}$ is negative, that means the load demand is higher than the produced power by the renewable energy, thus the renewable energy is not providing enough power for the load. Therefore, the lithium-ion battery should be operating in discharging mode if its SOC is enough to assist supplying power to load demand, thus P_{BESS} will be negative implying it is discharging; otherwise, the power grid must assist on the event where the battery is not supplying enough power.

Table 8-2: Summary of results taken at 95% level of SOC

Case Scenarios	$P_{\text{Equilibrium}}$ (MW)	P_{BESS} (MW)	P_{Grid} (MW)	SELL/BUY GRID POWER
1	-2.00	-0.75	-1.25	BUY
2	-4.00	-1.242	-2.758	BUY
3	2.00	0	2.00	SELL
4	0	0	0	NO SELL/BUY

On table 8.2, the first case simulated shows that, the load demand exceeded the power produced by the RES by 2MW. Therefore, the power to be discharged by the BESS was approximately 750kW at constant discharging rate. However, the utility grid added 1.25MW to the microgrid system, in-order to match the load demand. Therefore, the first case proved that, whenever there is shortage of power produced by either PV solar or wind turbine, the BESS and the main grid power will be activated. The second scenario of the simulated EMS illustrates that, neither the PV solar farm nor the wind turbine produced enough power to meet the load demand, thus the power to be discharged by the BESS increased to 1.242MW with the main

grid standing at 2.758MW so as to meet the load power demand of 4MW. As shown on table 8.2, the third case proves that, on any occasion where the power produced by the RES exceed that of the load demand, the power surplus will be sold to the grid, thus the BESS will not discharge. Noticeably, the power from/to the BESS is 0MW, indicating that the BESS is at its higher rates of SOC. Lastly, on the fourth case, the load demand and the power produced by the RES are balanced, therefore $P_{\text{Equilibrium}}$ recorded 0MW. Thus, from both the BESS and the main grid are standing at 0MW, proving that the battery is not discharging/charging and from the main grid's perspective there is no power sold /bought by the microgrid system.

8.4.2 Simulation Results of the microgrid system with changing load profile and RE system as input variables of FLC

This section of the study stipulates the simulation results for the developed EMS using the load profile that is changing over a 24-hour period. The load profile consists of a maximum of 4MW for the load demand, occurring during peak hours between 14:00 (i.e. 5.04×10^4 s) and 16:00 (i.e. 5.76×10^4 s). During the simulation, the time was kept constant and the initial rate of SOC of the battery was 95%. As mentioned on the previous chapters, the maximum output power of the wind turbine used was 3MW, while the maximum power output produced by the PV solar farm was 1MW. The lithium-ion batteries as used for BESS were occurred to be kept at 1.5MWh.

The Figure 8.12 illustrates the dynamic behaviour of the power produced by the renewables (i.e. PV solar and wind turbine). According to this research study, the maximum amount of power the renewables can produce is 4MW. As seen on the on Figure 8.12, the varying power produced by renewables is positive for the duration 24-hour period, thus implying the produced power. For the duration of eleven hours, the power produced by the RES is below 2MW, thus showing that both renewables are not producing power to their maximum capacity. Furthermore, in the course of this duration, the PV solar system was the only renewable system that was not producing power, hence the low amount of power produced. This varying renewable energy power reached the maximum rates after the 16:00th hour (i.e. 5.76×10^4 s), thus at that stage, the wind turbine was at its maximum speed and produced the maximum power of 3MW in conjunction with the PV solar farm. Due to the wind turbine speed reaching its maximum speed at the fore-mentioned hour-interval, the amount of power produced dropped drastically, causing the amount of power that can be supplied by the battery to increase.

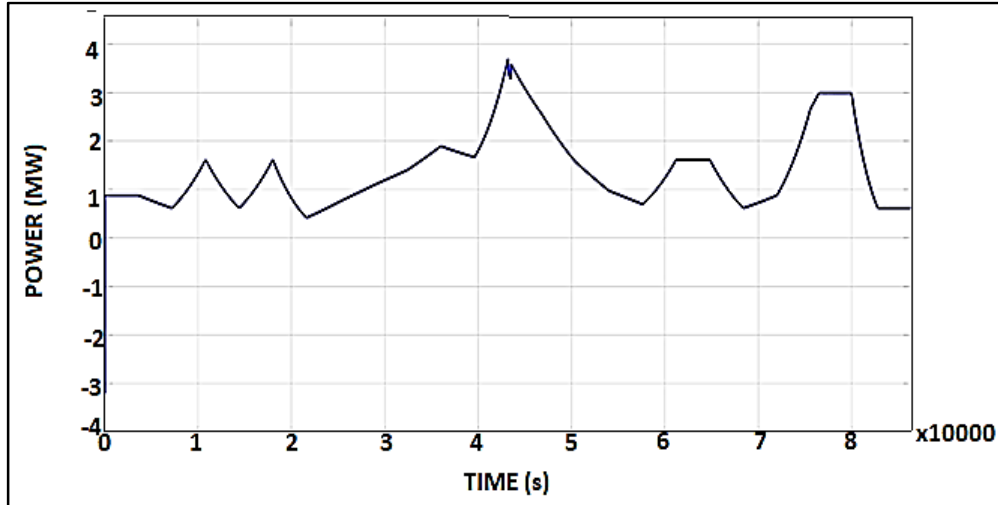


Figure 8-12: Varying power produced by RES simulated using MATLAB/Simulink

In Figure 8.13, the response of the load profile during the simulation is shown. As mentioned above, the load power consumed, solar PV modules as well as the wind turbines extract their maximum renewable energy power and are uncontrollable for this study purpose. The maximum power that the load can reach was set to be 4MW, as seen on Figure 8.13. Furthermore, the load demand reaches its maximum power at the 16:00 hour (i.e. 5.76×10^4 s). The load demand is at its lowest power demand approximately throughout the morning hours of the day, spanning to 1.98MW at 4:00 am (1.44×10^4 s). The load profile on Figure 8.13 proves that the load demand is high during the afternoon as most of the people are at work. As seen on the Figure 8.13 and Figure 8.14, the response of the graph is at its negative values showing that it is the power that is demanded by the load, whereas the power produced and supplied by the RES is always at its positive values, respectively.

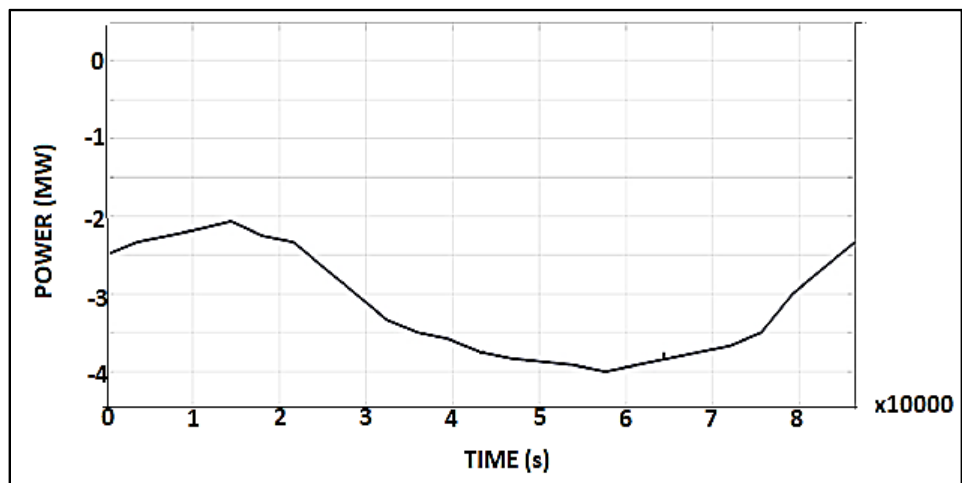


Figure 8-13: Varying power required by load demand simulated using MATLAB/Simulink

The output power response resulted from the load and the RES is shown on Figure 8.14 and is depicted by $P_{\text{Equilibrium}}$. As it can be seen, the behaviour of this output power is similar to that of Figure 8.12 which proves that it is an active power needed by the system. The output power response of the load demand and the RES mostly is on its negative values for the duration of then 24-hour period, implying that the load demand is exceeding the RES power produced. Between 5×10^4 s and 6×10^4 s the output power response shows that the $P_{\text{Equilibrium}}$ reached the maximum output power of approximately 3.25MW; thus, the power produced by the RES during that period was much less than the power needed in order to supply the load. Therefore, according to the FLC of the developed EMS, the BESS and the utility grid will assist by the supplying the power as per the set rules of the fuzzy controller.

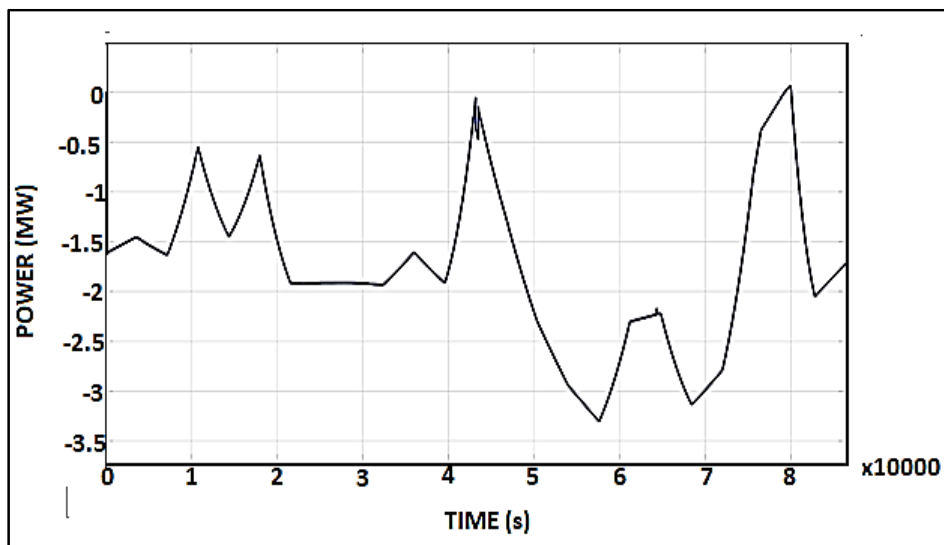


Figure 8-14: Power Balance ($P_{\text{Equilibrium}}$) from load demand and RES simulated using MATLAB/Simulink

The amount of power produced by the RES is not enough to sustain the load demand due to PV solar system unavailability of power produced, the level of $P_{\text{Equilibrium}}$ remain negative for the duration of the 24-hour period. Thus, showing the load demand is much higher than the produced power by the RES. Figure 8.14, also proves that, when the output power of the RES is increasing constantly, the rate of power on $P_{\text{Equilibrium}}$ which denotes the amount of power needed, decreases. When the WT system reached its maximum voltage before the 8×10^4 s, it is seen on Figure 8.14 dropping the amount of $P_{\text{Equilibrium}}$ to be equal to that of the load, thus when the WT system reached its maximum speed of 25m/s the wind turbine is cutting-off power produced so as to protect the WT from being damaged.

8.4.3 Simulation Results of the SOC as required by the EMS of the microgrid system

The battery lifetime was a critical aspect that was considered when the FLC for the EMS was designed. As shown in Figure 8.15, the fuzzy controller lithium-ion battery SOC is maintained just above 60% with an initial value of 95%. In order to keep the life span of the lithium-ion batteries much longer, the minimum

rate of the battery SOC was set to be 60%, thus preventing the battery not to fall below its minimum values as secured, which may compromise its life span as stipulated. Additionally, the battery SOC when discharging does not fall below 60% which further confirms that the SOC is effectively kept on secured limits.

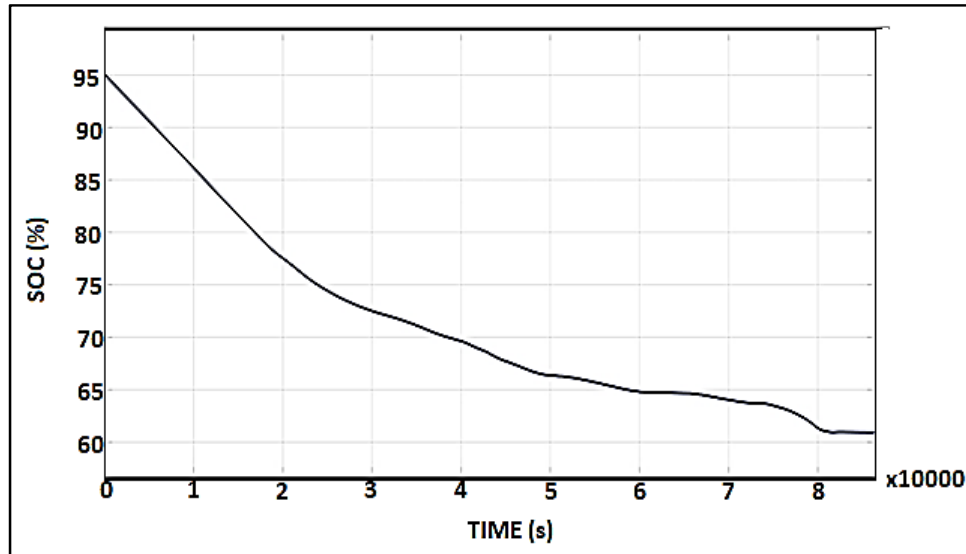


Figure 8-15: SOC of Battery Energy Storage System simulated using MATLAB/Simulink

Moreover, on the 24-hour period, Figure 8.15 verifies the correctness of the developed system with fuzzy controller that can maintain the SOC of the battery at a certain level. The FIS is able to charge/discharge at a higher/lower rate hence able to match the supply and demand better.

8.4.4 Simulation Results of the microgrid system for the output variables of FLC as per the case scenarios

To confirm the correctness and the performance of the developed EMS model during a period of 24 hours where the load demand kept changing as the day progresses, the analysis were used. In this sub-section, all the four cases are analysed in a way to verify and evaluate the behaviour of the BESS and the utility grid during the interchange of supplying power as per the AC load demand. The power from/to the grid is depicted by negative-response/positive-response of the graph, respectively. However, the power supplied by the BESS will have a negative response, showing that the SOC of the battery is discharging, whereas the positive response of P_{BESS} will depict that the BESS is charging.

8.4.4.1 Case 1: Simulation Results of the MG system with WT providing an acceptable output power and with PV and BESS unable to provide an acceptable output power

The model consists of the battery, RES (i.e. PV solar and wind turbine) and the main grid. The EMS of this model was controlled by the FLC. In this case, it was only the wind turbine system from RES that provided the acceptable amount of power generated in order to supply the load. The BESS as well as the main grid

were activated to assist during this process as seen on the initial phases of Figure 5.16, depicted by the red arrow section. The load is constantly connected to the microgrid system-bus via a three-phase circuit breaker.

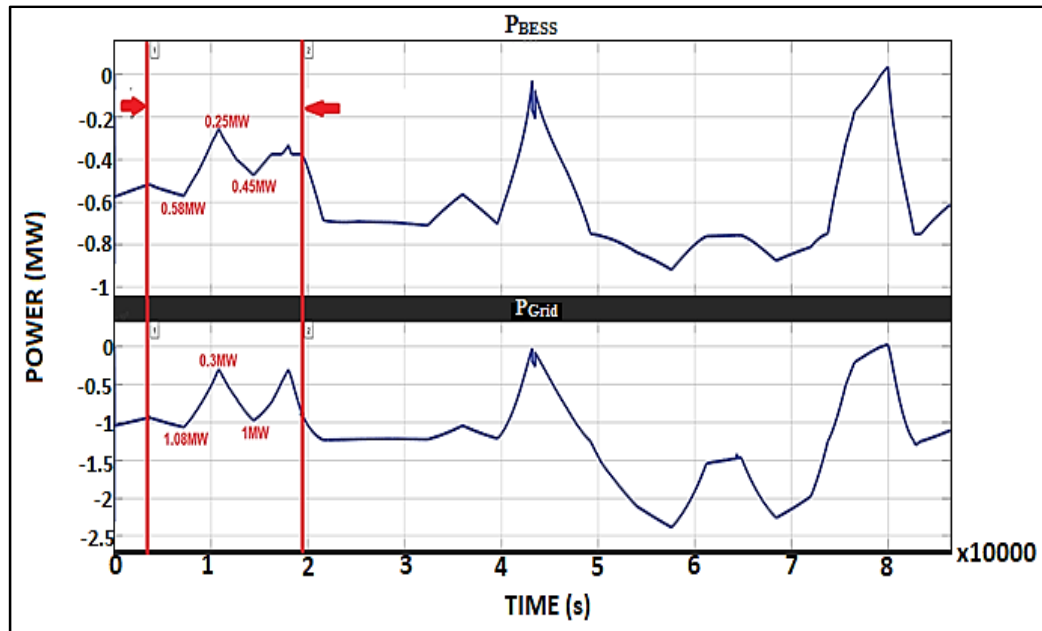


Figure 8-16: PV solar and BESS unable to provide enough Output power simulated using MATLAB/Simulink

The behaviour of power from the battery energy storage needed to assist the WT during the period when the PV solar system was unable to provide the acceptable output power as seen on Figure 8.16 between 0.4×10^4 s and 2×10^4 s. Correspondingly, the amount of power expected from the BESS is also varying depending on the load demand. However, the level power on the graph is negative, which shows that the BESS is discharging. The microgrid is operated in grid connected mode. When the power discharged by the BESS is not enough, the utility grid assists the system and this minimizes the amount of power bought from the utility grid, thus reducing the energy costs. The negative power from the grid depicts that the power is bought from the grid to add to the system to match the amount of power needed by the load. This power is needed to also charge the battery at times.

8.4.4.2 Case 2: Simulation Results of the MG system with WT and BESS unable to provide an acceptable output power

The output power response illustrated on Figure 8.17, shows the power profile of the P_{BESS} and P_{Grid} . In addition, there were many troughs and peaks the output power response experienced throughout the 24-hour period. The utilization of the BESS and the RES by the fuzzy controller was much vital as the integration of the power sources with high intermittent nature could have a great impact to the power grid. Moreover, Figure 8.17 proves that by discharging power more than required by the microgrid system will reduce the SOC to its minimum capacity prematurely. The red section with arrows on Figure 8.17, illustrate a case

scenario where the wind turbine produced a constant and a less average power output of 6.234kW, while the PV solar farm was also producing an increasing power output with a maximum of 1MW in that period of time. As it can be seen on the output power profile of Figure 8.17, the power from the BESS was constant as this depicted that both the wind turbine and the BESS were unable to provide enough power to meet the load demand. Hence, the EMS activated the power from the utility grid as well as the power that was increasing at a constant rate produced and supplied by the PV solar system. Therefore, case 2 of this study was successfully confirmed at that period of the changing output power profile where MG system with RES and BESS unable to provide an acceptable output power.

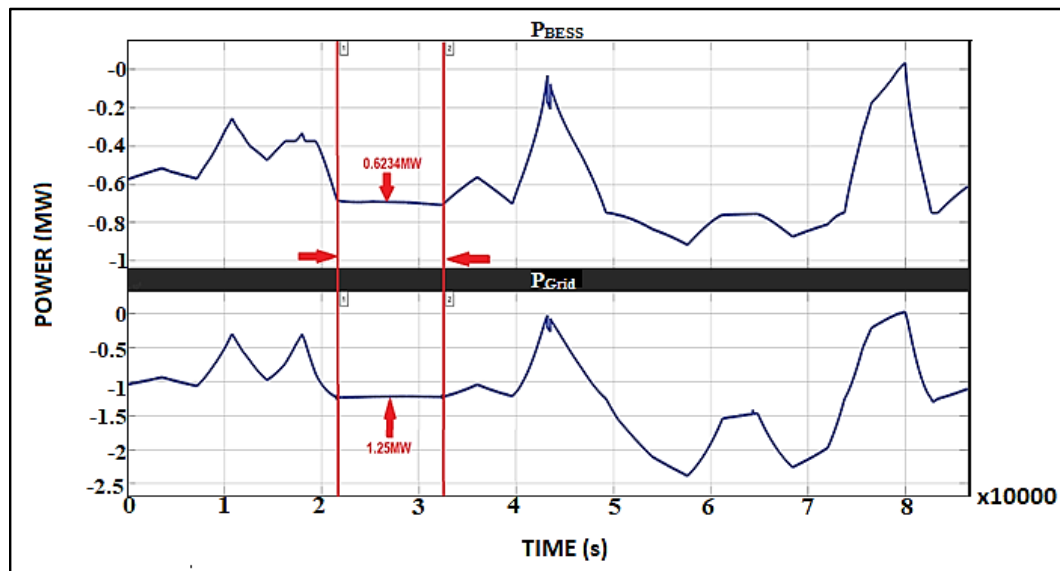


Figure 8-17: WT and BESS unable to provide enough Output power simulated using MATLAB/Simulink

8.4.4.3 Case 3: Simulation Results of the MG system when RES power reached maximum limits

The maximum limits of the RES were set to 3MW for the wind turbine system, thus depending on the maximum speed limit of 25m/s; whereas the maximum limit of the PV solar farm was set to 1MW. As stated above, the maximum power tracking system designed to assist the RES, was used to ensure the maximum power was tracked and produced for the developed microgrid system, at all times. On the Figure 8.18, approximately between the 11:00th hour (i.e. 4×10^4 s) and 13:00th hour (i.e. 5×10^4 s) marked with red section, the RES (see Figure 8.12) system tracked the maximum power output, meaning the wind turbine was moving on its maximum speed limit, hence produced maximum power of 3MW. Furthermore, the PV solar on the upper hand, also however produced the maximum power output during that period.

According to the study, one of the aspects to be simulated was that, at any given time when the wind turbine approaches its maximum speed limit, the wind turbine system should effectively be able to switch off in order to protect it from being damaged by over-speeding. Consequently, as it can be seen on the red section of Figure 8.18, the P_{BESS} and P_{Grid} power outputs constantly increased with a steep straight-line curve just

before then 11:00th hour mark (i.e. 4×10^4 s) gradually reaching 0MW. However, hence the wind turbine at that time was at its maximum speed, the output power of the RES dropped causing the BESS and the utility to increase their output power to match the load demand. As it can be confirmed by the peak of the output power response of the P_{BESS} and P_{Grid} on Figure 8.18 at any occasion when the RES produced-power capitulates, the BESS as well as the utility grid assist the microgrid system as per the fuzzy controller of the EMS.

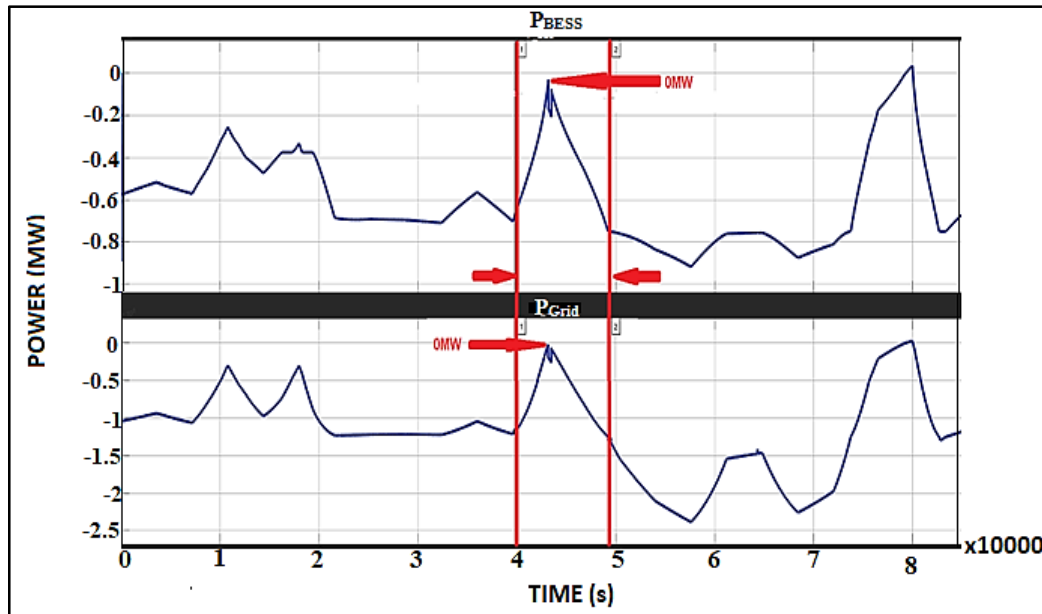


Figure 8-18: P_{BESS} and P_{Grid} graphs at RES output power of 4MW maximum levels simulated using MATLAB/Simulink

8.4.4.4 Case 4: Simulation Results of the MG system with RES unable to provide an acceptable output power

As the method of simulation of the developed EMS for controlling the power interchange for the designed microgrid system, the rest of Figure 8.19 proves that fuzzy controller is capable of maintaining and controlling the output power of the BESS and the main grid, all the time. The indicated region on Figure 8.19 illustrates a condition where the RES (see Figure 8.12) was unable to provide an acceptable amount of power during the 24-hour period. The amount of power needed to supply the load increased drastically between 5×10^4 s and 6×10^4 s, hence the output power response on the region shown on Figure 8.19 approached 0.9MW of power to be discharged to the microgrid system. Correspondently, the power bought from the utility grid approached 2.4MW in order to match the power to be consumed by the load of 4MW. Furthermore, the output power response by the BESS and the utility grid proves the effectiveness of the operation of the fuzzy controller designed in this study.

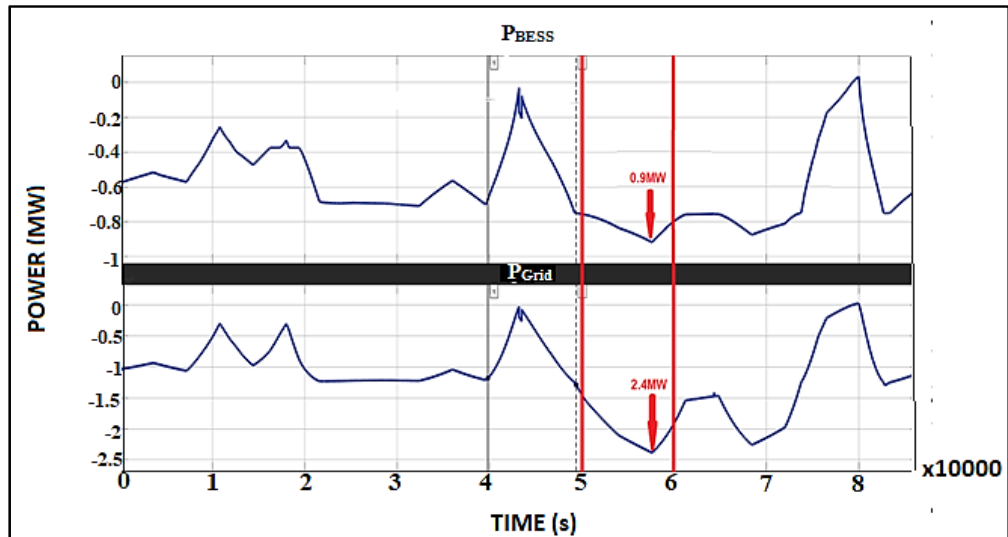


Figure 8-19: P_{BESS} and P_{Grid} graphs when RES unable to provide enough output power simulated using MATLAB/Simulink

8.5 Real-Time Modelling with Implemented Case Studies and Results

This section details the results of the modelled microgrid system in real-time, based on the three implemented case studies, although the modelled microgrid system can be modelled using various types of scenarios. Furthermore, these three-used case scenarios were examined and simulated based on the varying circumstances of the load demand, the rate of battery SOC available, the power available from the RES as well as the utility grid. Thus, all the above-mentioned aspects were used to assess the behaviour and operation of the microgrid system during the changing load demand conditions. Notably, the microgrid system developed is expected to consistently match the change in power on the system, the real-time simulation updates the behaviour and resultants of the RES power in every second. The level of solar irradiance was set to vary 1000W/m^2 and 250W/m^2 , whereas the level of wind speed varies from 0m/s to 25m/s .

8.5.1 Case Study 1

The results of the first case scenario studied are shown on Figure 8.20. This case study evaluates the designed microgrid system using the off-grid mode as the operating mode. The microgrid system simulated in this case scenario comprised of the battery system SOC initially at 80%, the generated power by the RES unable to reach its maximum values of approximately 4MW, then the varied load demand power as initially starting from lower values.

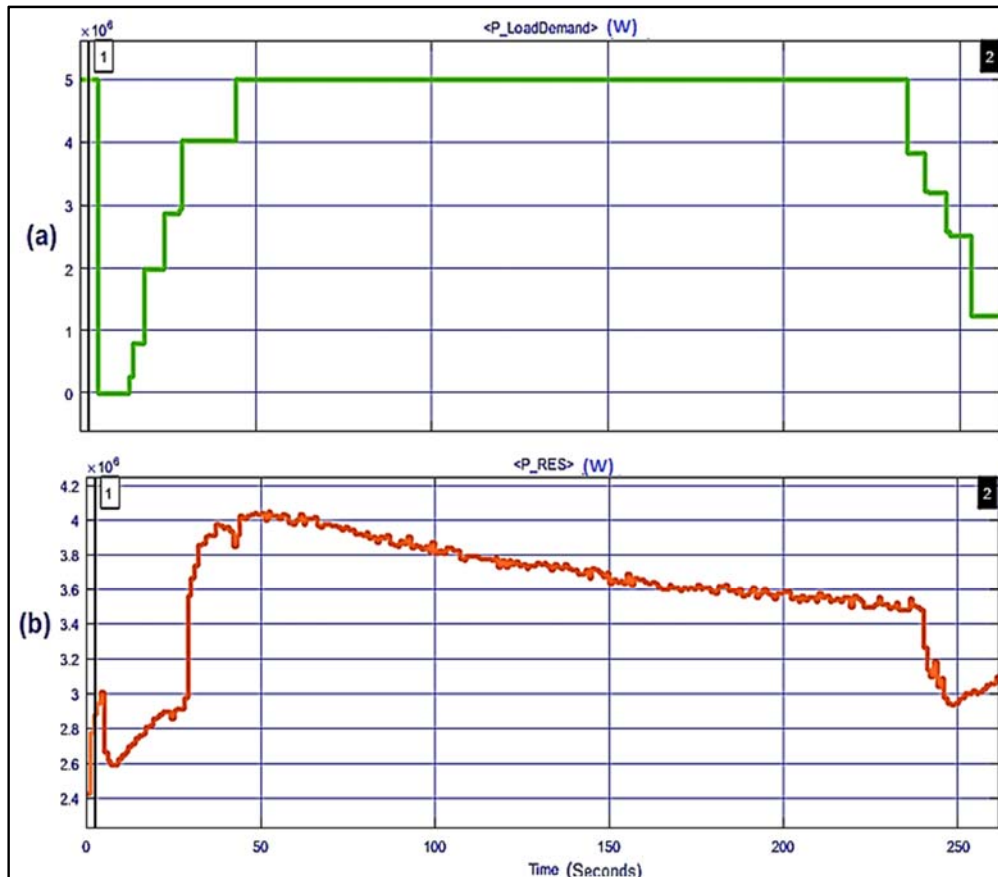


**Figure 8-20: Load Demand and RES Power
For Case Study 1 simulated using OPAL-RT simulator**

- It can be seen on Figure 8.20(a) and 8.20(b) that as soon as the load demand reaches 4MW, the RES is in its decreasing state of approximately 3.9MW, and hence the P_BESS power as well as the SOC starts to decrease depicting that the battery system is discharging in order to supply the load demand.
- According to Figure 8.20(b), the amount of power generated by the RES coupled on the studied microgrid system starts at higher rate prior reaching 50s of time then steadily decreasing to approximately 2.95MW of power. The decrease of power generated by the RES is caused by the PV solar system, thus causing the wind turbine to be the only renewable system to generate enough power in order to match the amount of load demand.
- The microgrid system is operating in off-grid mode, thus the microgrid system activated the battery system to match the load demand.
- The simulated time prior reaching 50s, the amount of power generated is greater than the load demand, thus in this instance the power generated is enough to supply the load.
- The decline of the SOC is steadily decreasing with the same gradient of declination; this is because the load demand is constantly at 5MW. Nonetheless, during this time, the RES power generated continues to provide insufficient power, thus the P_BESS continued to support the RES to match the required power by the load until the SOC of the battery starts charging again at 79.91% as depicted on Figure 8.21(a).

- The power of the battery system available is increasing as seen on Figure 8.21(b), thus the SOC of the battery is charging as well during this time.
- When initially there was insufficient amount of power generated by both the RES and the battery storage system to match the load demand, the microgrid system activated the grid to match the load, thus the amount of power bought from the grid was always less and the energy costs were improved. However, in a case where the RES generates more power as needed by the load, the microgrid system studied always operated perfectly.

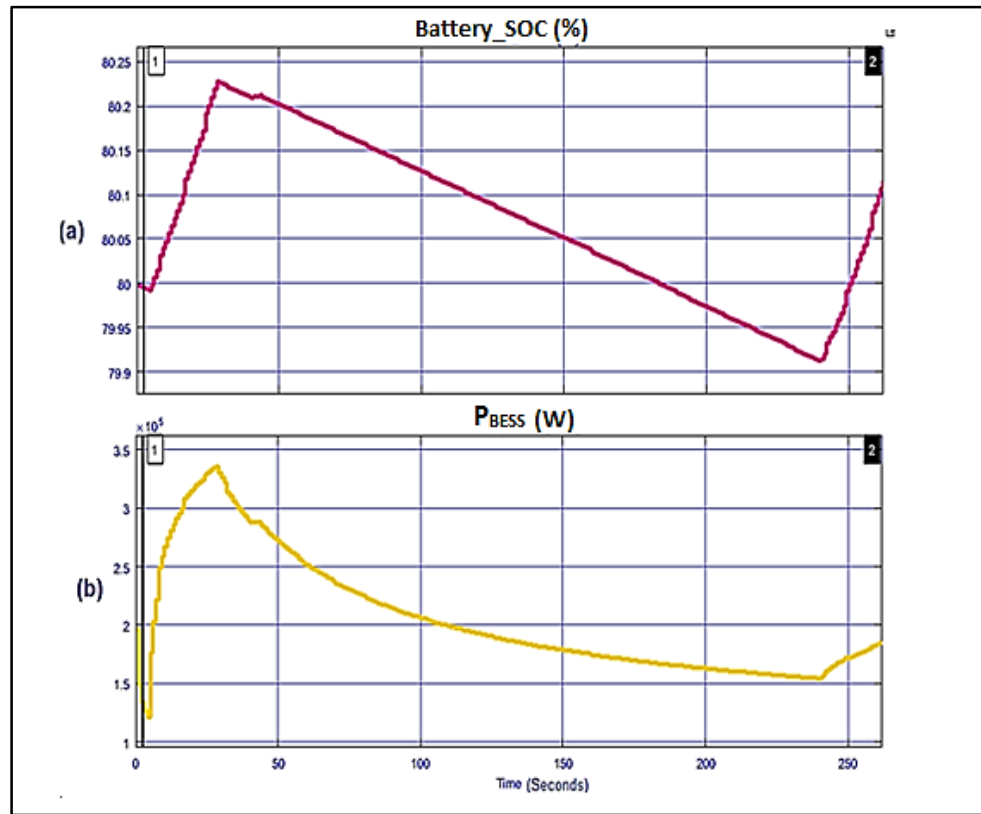


**Figure 8-21: SOC and Power of Battery Energy Storage System (P_{BESS})
For Case Study 1 simulated using OPAL-RT simulator**

8.5.2 Case Study 2

The second case scenario examined in this section, further considers the off-grid mode wherein the varied load demand initially varied from its lower values then gradually increased and the RES generated power unable to reach its maximum values of approximately 4MW. The P_{BESS_needed} is the rate of power needed by the microgrid system in order to charge or discharge the battery storage system.

- The amount of power demanded by the load of approximately 0.75MW was initially less than the amount of power generated by the RES of approximately 1.5MW and gradually increased to reach the maximum of relatively 2.8MW as seen on Figure 8.22(a) and Figure 8.22(b), respectively.
- Figure 8.22(a) and Figure 8.22(b) further depict that, for the duration of almost 85s the power generated was enough in supplying the load.

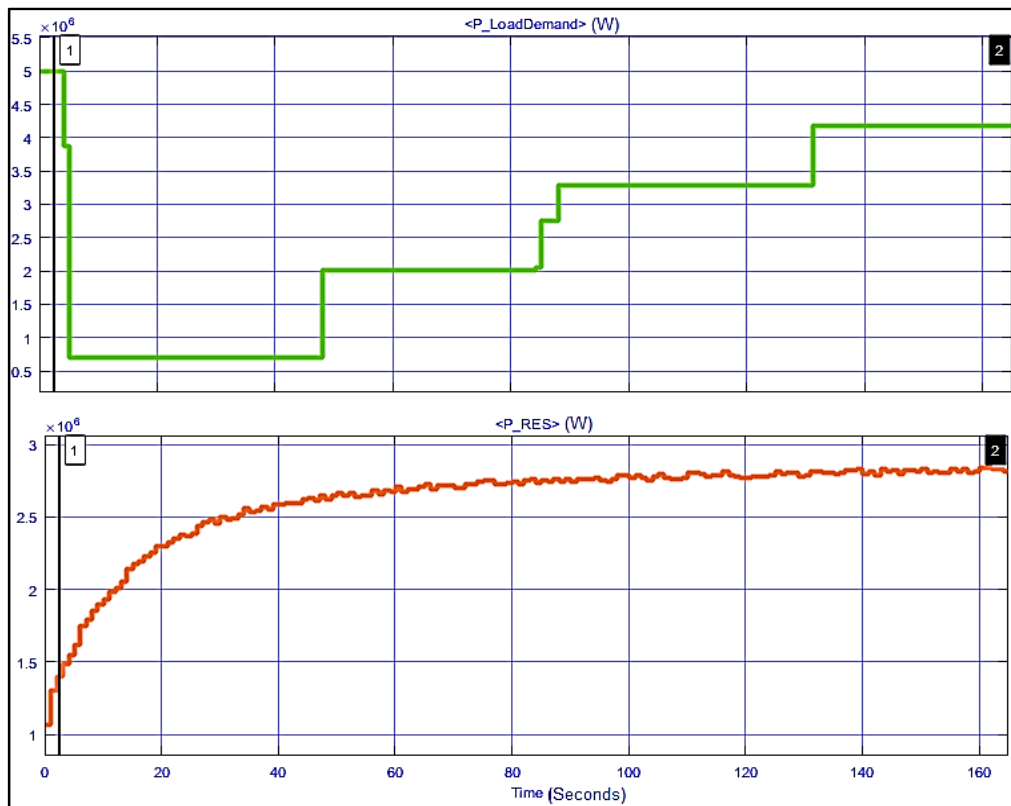


**Figure 8-22: Load Demand and RES Power
For Case Study 2 simulated using OPAL-RT simulator**

- With the increasing load demand, the renewables together with the battery system could not afford to provide and support the microgrid system, due to insufficient amount of power available and the lower levels of the SOC.
- Figure 8.23(a) represents the amount of power needed by the microgrid system for the main grid (PGrid_needed) as required by the EMS. Moreover, the positive values of PGrid_needed shows that the main grid supplies power to the microgrid system, whereas the positive values of PGrid_needed signifies the power sold by the microgrid system to main grid.
- As it can be seen on Figure 8.22(a) and Figure 8.22(b), the behaviour of both graphs are similar, thus showing that whenever there is a change of power on the developed microgrid system, the main grid power will affect the power needed from the battery system.
- At negative values of the PBESS_needed signifies a higher rate of charge of the battery system, whereas the positive values of the PBESS_needed shows the lower rate of charge during the minimum threshold values of the SOC as seen on Figure 8.23(b).

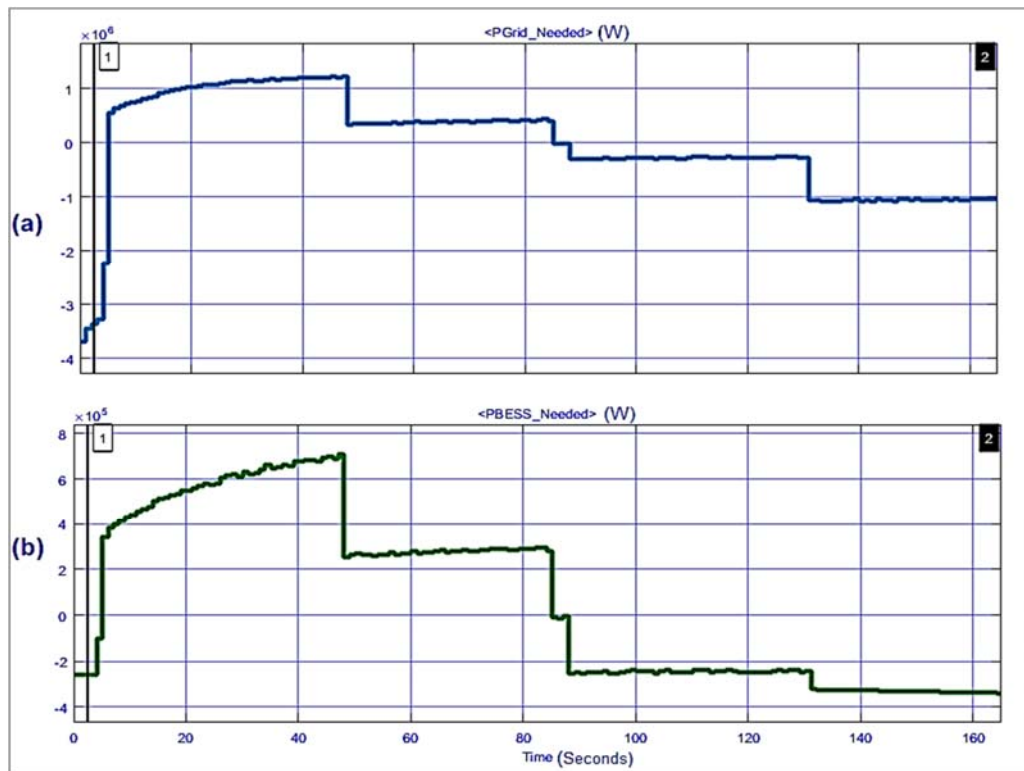


Figure 8-23: Main Grid Power needed and Battery Energy Storage System Battery needed for Case Study 2 simulated using OPAL-RT simulator

- The SOC of the battery system was initially set to 15% as depicted by Figure 8.24(a).
- However, Figure 8.24(a) proves that the battery system continues to charge despite the changes of load demand hence the microgrid system is designed not to discharge power of the battery storage system when the levels of the SOC are near the minimum values.

- Figure 8.24(b) shows the amount of power available on the BESS increasing from 270kW to approximately 380kW as the battery system charges. The modelled microgrid system satisfies the case where the renewables generate enough power to supply the load, the battery system activated to be in charging mode and continues to charge during the insufficient RES power generated if the SOC is still near the minimum threshold values of less than 50%. Thus, the life span of the battery system will be increased as well.

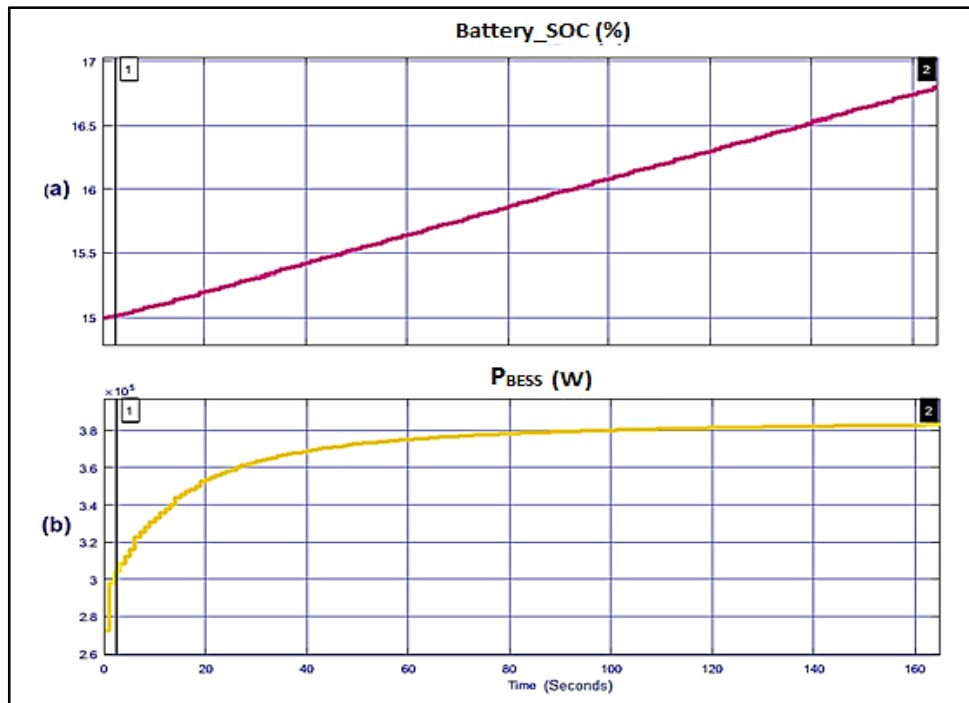


Figure 8-24: Battery SOC and Power of Battery Energy Storage System (P_{BESS}) For Case Study 2 simulated using OPAL-RT simulator

8.5.3 Case Study 3

- The last case study of the examined microgrid system model included the utility grid; therefore, the microgrid system was operated in grid-tied mode. In this scenario, the generated power by the RES of the microgrid system failed to generate and match the varied power needed by the load demand at its maximum generating point of approximately 2.9MW as depicted by Figure 8.25.
- According to Figure 8.25(a), the amount of load demand started at lower values and gradually increased to the maximum of 4.2MW then decreased again to approximately 1MW, thus indicated the high values and low values of power than the generated power by the RES, respectively.
- In Figure 8.25(b), the power produced and generated by the RES initially started at higher values than the power of the load demand. Moreover, Figure 8.25(b) shows that the maximum amount of power the RES produced was approximately 2.93MW which was less than the amount of power needed by the load between 40s and 100s of time intervals.
- Therefore, hence the load demand is greater than the power from the renewables and the SOC of the battery is in minimum values, the EMS of the microgrid system activates the utility grid to

support the microgrid system in order to match the load demand at any moment the power generated is insufficient.

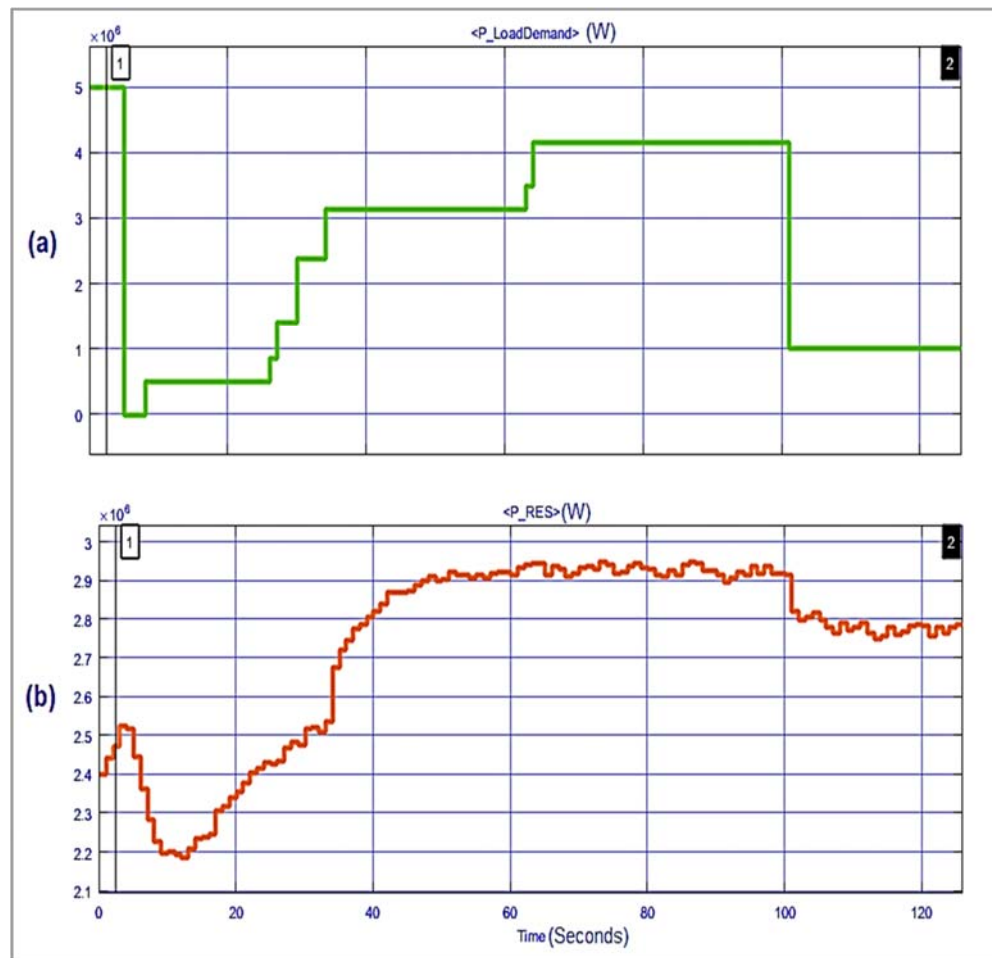


Figure 8-25: Load Demand and RES Power for Case Study 3 simulated using OPAL-RT simulator

- As shown on Figure 8.26(a), the SOC of the battery system was at 15%, which indicated the minimum threshold values of the SOC.
- Furthermore, the change in gradient of the SOC graph on Figure 8.26(a) between 35s and 100s of time, demonstrates the changing gradients of the SOC graph.
- Nonetheless, Figure 8.26(b) represents the power available from the battery system. Thus the behaviour of the graph on Figure 8.26(b) proves that, the steeper the gradient of the SOC, the greater the power available on the battery system.

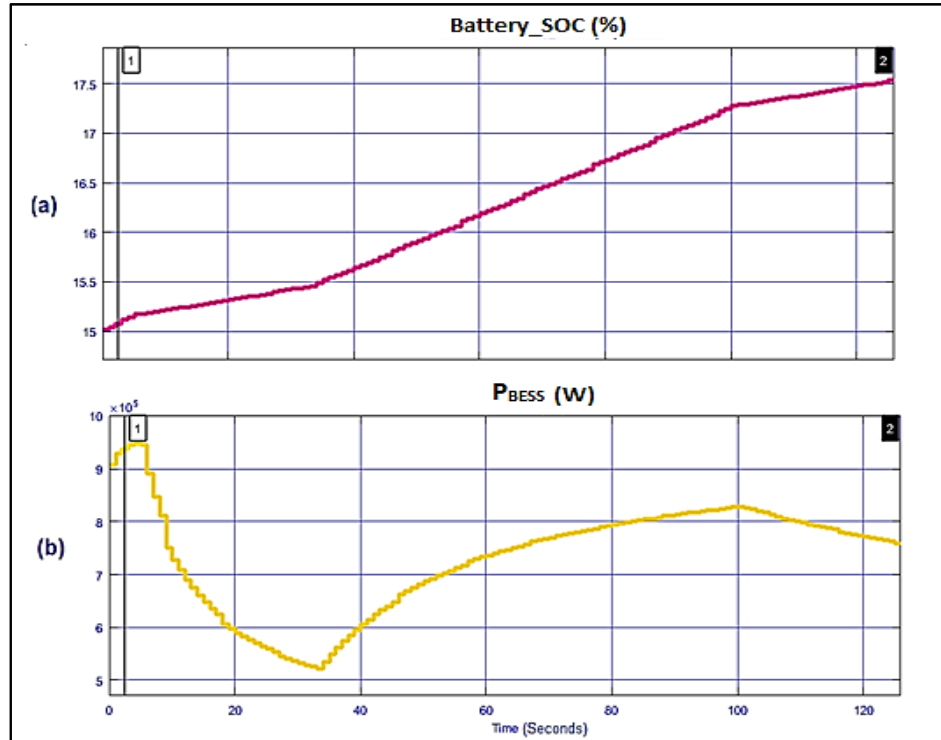


Figure 8-26: Battery SOC and Power of Battery Energy Storage System (P_{BESS}) For Case Study 3 simulated using OPAL-RT simulator

- At the time that, the maximum load demand is 4.2MW, between 62s and 100s, the generated power by the RES was approximately 2.9MW, thus the power needed from the main grid was 1.3MW as seen on Figure 8.27(a), because the battery system was in charging mode.
- Therefore, the microgrid system operating in grid mode proves that the unused power on the microgrid system is sold back to the main grid, thus the microgrid system ensures that the power generated by the RES is prioritized than the main grid.
- Primarily, during the negative values of the main grid power values, that indicates the power generated and available on the microgrid system is more than the load demand.
- Therefore, the surplus power is sold to the main grid. Nonetheless, the positive values of power indicate that the power is bought from the main grid and is used to match the load and charge the battery.
- According to Figure 8.27(b), during the positive values of the P_{BESS_needed} , the battery system is charging at lower rate, whereas during the negative values, the battery system is charging at higher rate if the SOC is near its minimum threshold values.

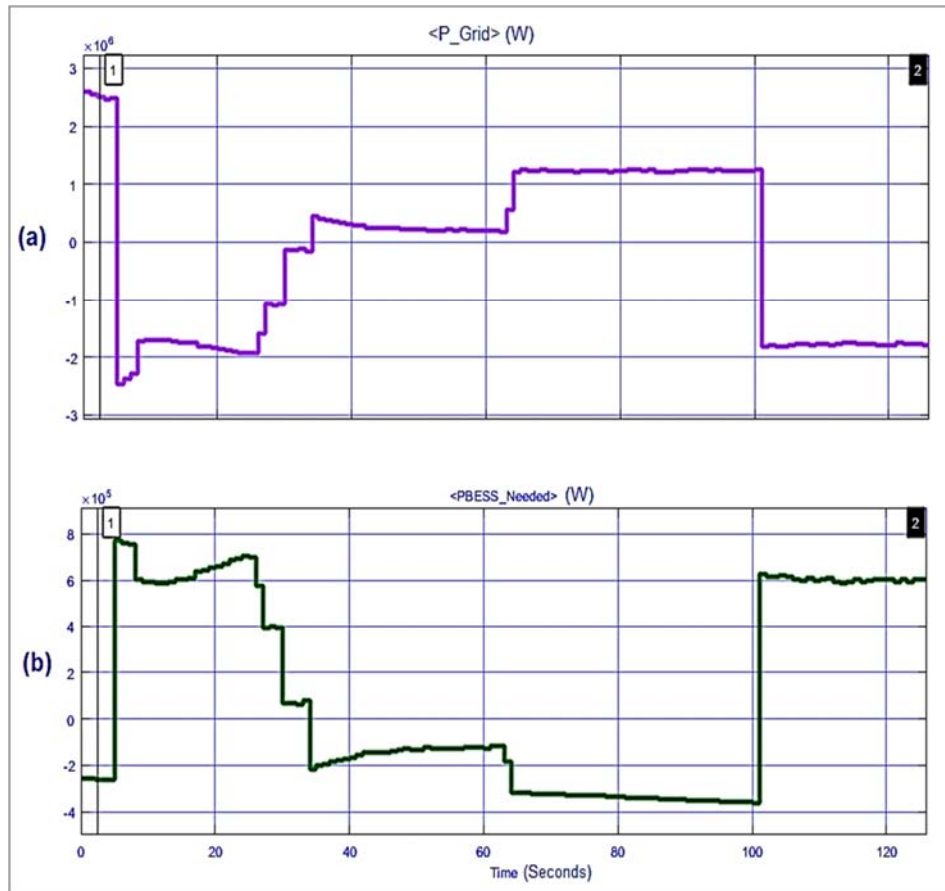


Figure 8-27: Main Grid Power needed and Battery Energy Storage System Battery needed for Case Study 3 simulated using OPAL-RT simulator

8.5.4 Summary of Results and their Impact on Railway Yard

The table 8.3 represents the summarised values and modes of the microgrid system during the various set operational conditions for the three developed and modelled case studies. It can be seen that, with the designed and modelled microgrid system for the railway yard, both operation mode (i.e. on-grid and off-grid modes) the system is working successfully.

Table 8-3: Summary of the Three Case Studies Modelled

Case Study	Operating Mode	SOC Initial Value	P_RES	Load Demand Initial Value	BES Charging/Discharging
1	Off-Grid	80%	<4MW	<P_RES/>P_RES/<P_RES	Charging/Discharging/Charging
2	Off-Grid	15%	<3MW	>P_RES	Charging
3	On-Grid	15%	<3MW	>P_RES	Charging

The table 8.3 further proves that the railway yard will always have enough power to supply the load demand as well as the BES coupled with RES will perform efficiently in assisting the renewables during load

shedding, maintenance and other faults occurring on the main grid. Figure 8.28 and Figure 8.29 deduces the amount of energy utilised from the renewables compared with the energy usage needed by the system from the utility grid at the simulated time intervals. It proves that, the energy bought from the utility grid will always remain in lower levels and ensures the positive impact in railway shunting yard by improving the cost of energy that is currently in higher values.

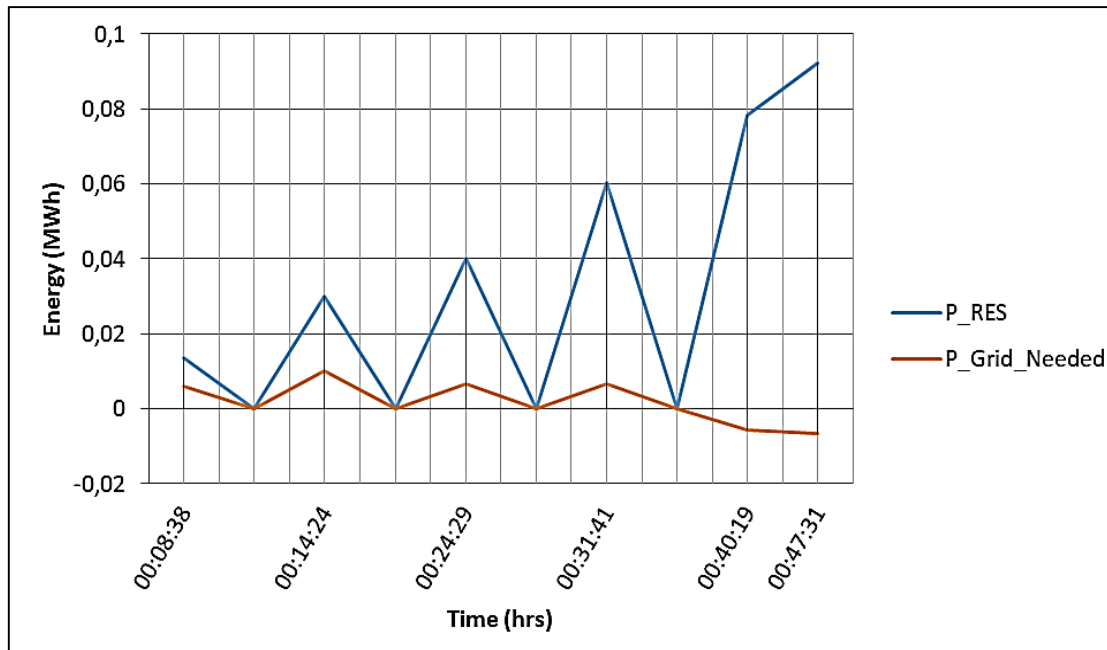


Figure 8-28: RES Energy and Needed Main Grid Energy Graphs for Case Study 2

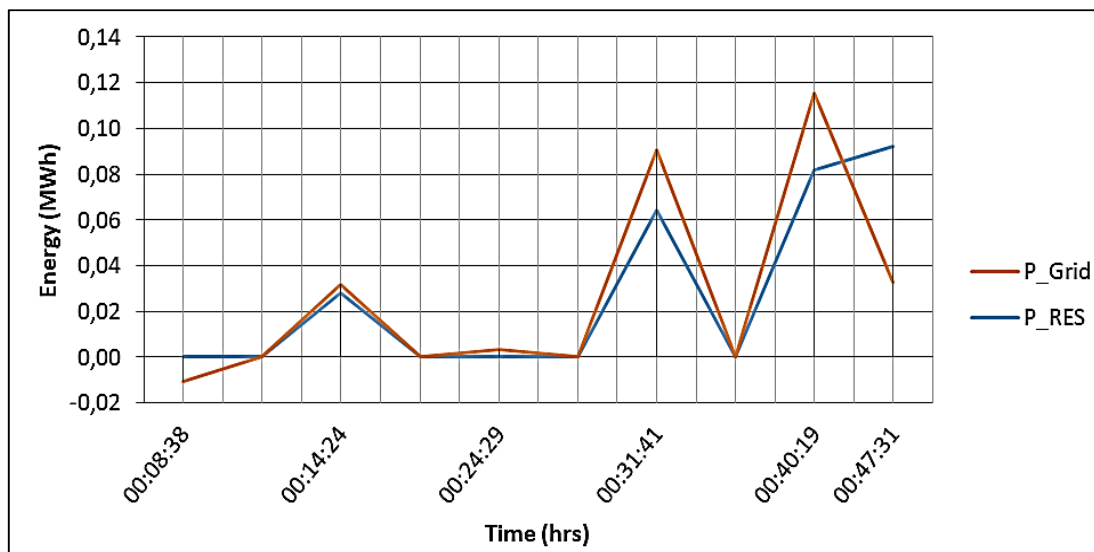


Figure 8-29: RES Energy and Needed Main Grid Energy Graphs for Case Study 3

Therefore, the microgrid system operating in grid mode proves that the unused power on the microgrid system is sold back to the main grid, thus the microgrid system ensures that the power generated by the RES is prioritized than the main grid.

8.5.4.1 Case Study 1 Summary

Figure 8.30 shows the amount of power available from the RES and BES, the load demand as well as the operational status of the BES at the time intervals T1 and T2.

- When initially there was insufficient amount of power generated by both the RES and the BES to match the load demand, the microgrid system needed to activate the grid to match the load, this however occurs during the grid-tied mode.
- Therefore, the amount of power bought from the grid will always be less and the energy costs are improved, thus that will have a positive impact on energy cost saving for the railway company.

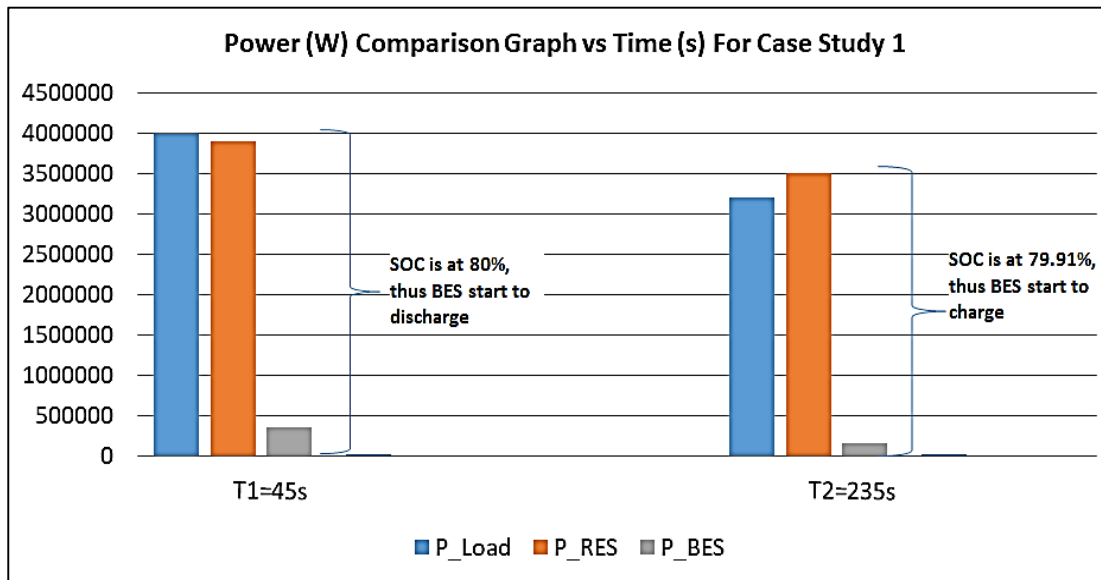


Figure 8-30: Power (W) Comparison Graph vs Time for Case Study 1

- Furthermore, in a case where the RES generates more power as needed by the load as seen on Figure 8.30 at T2, the microgrid system studied will always operate perfectly and with the energy regulations, the railway company will be able to share or sell the unused power back to main grid. Thus, improving the energy costs of the company and reliability to their customers.
- Therefore, the railway-shunting yard where the studied renewable energy microgrid system is installed, will always have enough amount of power to supply the load, thus this case study 1 proves that the microgrid system performs well without the grid connected and therefore the decline in energy cost will be successfully improved and the backup system in place.

8.5.4.2 Case Study 2 Summary

Figure 8.31, presents that the BES will remain in constant charging state during the lower rates of SOC irrespective of the amount of power available and needed by the load. This is shown using the three time

intervals T1, T2 and T3, where the levels of power produced and supplied by the RES with BES is higher or lower than the load demand.

- In this scenario, the modelled microgrid system satisfies the case where the renewables generate enough power to supply the load, the battery system activated to be in charging mode and continues to charge during the insufficient RES power generated if the SOC is still near the minimum threshold values of less than 50%.
- Thus, the life span of the battery system will be increased as well and therefore, ensuring that the railway yard will have an efficient and reliable backup supply when needed.

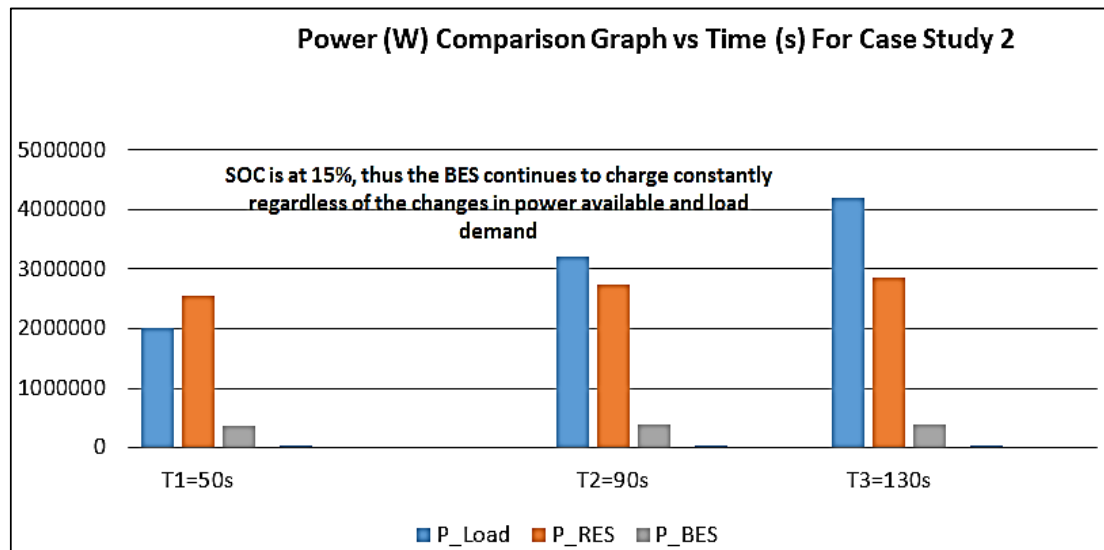


Figure 8-31: Power (W) Comparison Graph vs Time for Case Study 2

8.5.4.3 Case Study 3 Summary

Figure 8.32 illustrates the grid-tied mode system with the changing rate of charging the BES. Furthermore, the BES continues in charging state during the lower rates of SOC respectively to the amount of power produced by the renewables and load demand power. This is shown using the three time intervals T1, T2 and T3, where the levels of power produced and supplied by the RES with BES is higher or lower than the load demand.

- This case study proves that, the renewables energy-based microgrid will have a great impact in railway yard's productivity, energy costs and efficiency, thus proving that, the main grid will have less impact when connected as the renewables are the main and first priority in supplying power for the railway shunting yard.

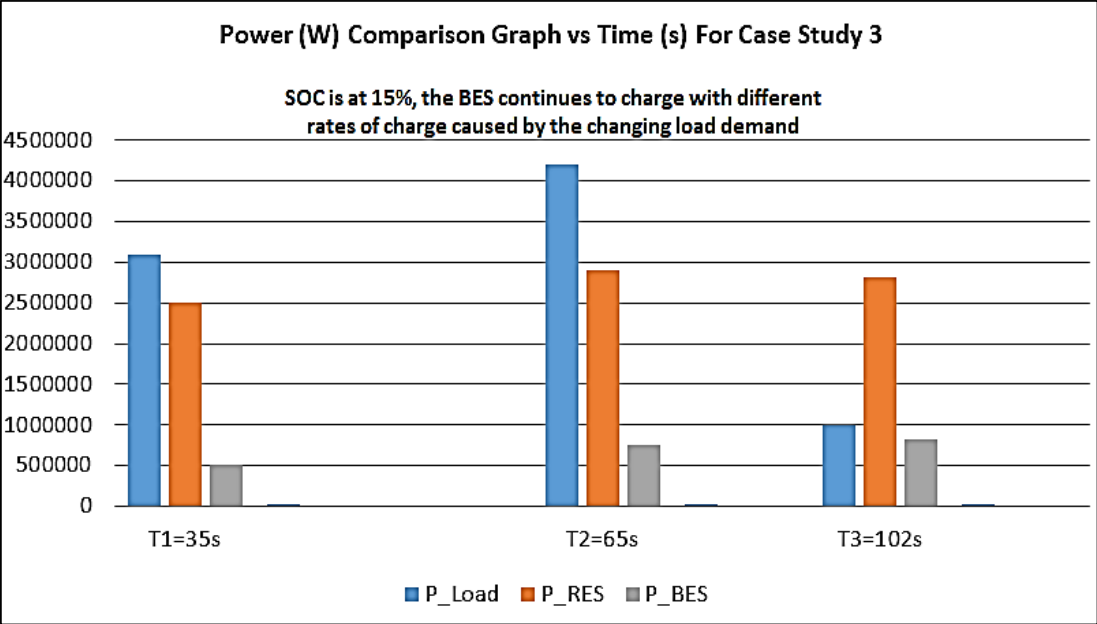


Figure 8-32: Power (W) Comparison Graph vs Time for Case Study 3

Chapter 9: Conclusion and Future work

9.1 Conclusion

The main objective of this research study was to perform a feasibility study and cost-analysis of the renewable energy microgrid system in Saldanha Bay. Therefore, this was effectively accomplished by successfully investigating the most viable and practical modelling of the DER's, ESS and the main grid interface using Homer Energy software for optimization. The results of the six different cases for the developed microgrid system interfaces were generated by Homer Energy software. Thus proving that the cheapest and efficient renewable energy-based microgrid system to be used was the one consisting of PV solar, wind energy and lithium ion battery incorporated with main grid; thus having the operating costs of R 339 362.7 per year and a net profit cost (NPC) of R11 200 000,00 of its life-span.

The second objective of this research study was to design and simulate the AC microgrid and DC microgrid/hybrid (PV solar panels and wind turbine) RE microgrid. This objective was achieved by using the data and results from Homer Energy and initially builds the solar PV model and wind turbine model, separately using MATLAB/Simulink simulation software. There were various solar PV and wind turbine technology capacities that were considered and therefore, the maximum of 1.5MW PV solar capacity was used as well as the two GE 1.5sl wind turbines using synchronous generator with the maximum power produced of 1.5MW at a maximum wind speed of 25m/s, each. The monthly average temperature and wind speed of Saldanha Bay was considered, thus the derating factor of 80% to each PV solar panel was activated as well as the hub height of 120m for the wind turbine. The power point tracking was assumed not to be installed; this was to avoid any unnecessary costs. The PV array was expected to be installed with the same inclination angle, which is equal to the site's latitude; lastly, the ground reflectance was assumed to be 20%. Thus, the specifications of both these renewable energy systems were simulated and modelled using MATLAB/Simulink simulation software separately and subsequently linked together and were able to produce the maximum of 4.5MW of power at their maximum operated levels.

The third objective of this research study was to design and simulate the energy storage system. This was attained by primarily simulating on MATLAB/Simulink the 1667Ah Lithium-ion batteries as they have the good advantages towards other types of batteries when used as storage systems. The advantages include a much more life span, less maintenance and a 90% of high rated capacity. Additionally, in order to ensure this objective of simulating the energy storage was thoroughly and successfully operated, the fuzzy logic controller (FLC) was used to effectively control the energy management system. Thus, the FLC proved an efficient control for the microgrid system, especially when multi-functions were performed on the microgrid system. The threshold of the SOC on the BESS was set to vary from 10% to 95% of its limits. Therefore, the highest value of the SOC of the battery systems set to be 95%, thus the battery discharges or stop charging when reaches its highest value.

The fourth objective studied was to link and simulate in real-time the feeder distribution with distributed energy resources and ESS models using MATLAB/Simulink and OPAL-RT simulation system. This was

achieved by coupling the designed PV solar system, wind turbine system, lithium ion batteries for energy storage as well as the utility grid forming a microgrid system. Furthermore, the simulation and modelling of this real-time microgrid system was initially performed in MATLAB/Simulink, and then RT-LAB software environment which is the real-time simulation platform used to perform the real-time modelling of the microgrid system. The simulated results on both MATLAB/Simulink and RT-LAB simulation platforms proved that the hybrid microgrid system model operates efficiently and steadily in off-grid mode and on-grid mode. Thus, ensuring the buses for both AC and DC voltages are indeed steady during the operational transition of the load conditions and distributed energy resource capacities. Therefore, the supplied power to the changing load capacities was smoothly transferred. The results obtained both in MATLAB/Simulink and RT-LAB, further shows that the prevailing power availability and load demands, the battery system can respond instantaneously and participate in the microgrid system.

The last objective of this studied renewable energy-based microgrid system was to implement, simulate and analyse the energy management system (EMS) of the renewable energy microgrid in real-time using OPAL-RT. Therefore, this was achieved by using the real-time simulator manufactured by OPAL-RT technologies that is called OP4510 simulator, which is the target PC. The required RT-LAB software version v11.3.1.314 along with MATLAB (R2015b) is installed on the host PC was also used in accomplishing this objective in order create real-time simulation environment. However, the analysis of the energy management system for this renewable energy-based microgrid system in real-time was done by creating different case studies on RT-LAB simulation platform. The following case studies were used in RT-LAB: The first case study included the off-grid mode as the operating mode. Furthermore, the SOC initially set at 80%, the generated power by the RES unable to reach its maximum values of approximately 4MW, then the varied load demand power as initially starts from lower values. The second case scenario further considered the off-grid mode wherein the varied load demand initially varied from its lower values then gradually increased and the RES generated power unable to reach its maximum values of approximately 4MW.

The SOC of the battery system was initially set to 15%. Case study 3 of microgrid system model included the utility grid. In this case study, the generated power by the RES of the microgrid system failed to generate and match the varied power needed by the load demand at its maximum generating point of approximately 2.9MW and the SOC of the battery system was at 15%. In conclusion, the aim for this research study was to design an efficient real-time microgrid system model for the freight-rail yard. However, this was effectively accomplished by coupling all the systems consisting of DER's, ESS, EMS and utility to form the renewable energy-based microgrid system. Thus, the microgrid system modelled and simulated on MATLAB/Simulink and RT-LAB proved that the power required by the rail yard loads is always equal to the power generated by renewable sources, battery energy storage system and the utility grid. Therefore, the study proved that the energy costs and production level are improved significantly by the introduction of the renewable energy microgrid system.

9.2 Future Work

The study of improving the voltage as well as load system stabilization in real-time for both DC and AC bus feeders is possible. Consequently, that could be performed by ensuring that the voltage control strategy is implemented as well as the data regarding the amount of wind speed and solar radiation are estimated and thoroughly applied in real-time. Furthermore, the selection and modelling of the most viable different types of energy storage system technologies incorporated in a microgrid system should be studied in order to get a clear view of the performance and behaviour of the system. Thus, this will ensure the effect of the response time of energy storage system when charging and discharging is monitored and improved. Lastly, the study of the impact and role that could be played by the renewable energy microgrid system in railway environment as a whole should be performed.

BIBLIOGRAPHY

- Abdilahe, A.M., Yatim, A.H.M., Mustafa, M.W., Khalaf, O.T., Shumran, A.F. and Nor, F.M., 2014. Feasibility study of renewable energy-based microgrid system in Somaliland' s urban centers. *Renewable and Sustainable Energy Reviews*, 40, pp.1048-1059.
- Adefarati, T., Bansal, R.C. and Justo, J.J., 2017. Reliability and economic evaluation of a microgrid power system. *Energy Procedia*, 142, pp.43-48.
- African Development Bank (AfDB), 2015. Rail Infrastructure in Africa: Financing Policy Options.
- Ahlgren, P. and Handberg, E., 2018. System performance analysis of an isolated microgrid with renewable energy sources and a battery and hydrogen storage system-An evaluation of different storage system configurations. CODEN: LUTEDX/TEIE.
- Akinyele, D., Belikov, J. and Levron, Y., 2018. Challenges of microgrids in remote communities: A STEEP model application. *Energies*, 11(2), p.432.
- Al-Attiyah, S. and Majumder, R., 2018. Nested Microgrids: Operation and Control Requirements.
- Alsaadi, A. and Gholami, B., 2009. An effective approach for distribution system power flow solution. *International Journal of Electrical and Computer Engineering*, 3(1), pp.1-5.
- Arcos-Aviles, D., Pascual, J., Marroyo, L., Sanchis, P. and Guinjoan, F., 2016. Fuzzy logic-based energy management system design for residential grid-connected microgrids. *IEEE Transactions on Smart Grid*, 9(2), pp.530-543.
- Arefifar, S.A., Ordonez, M. and Mohamed, Y.A.R.I., 2016. Energy management in multi-microgrid systems—Development and assessment. *IEEE Transactions on Power Systems*, 32(2), pp.910-922.
- Arriaga, M., Nasr, E. and Rutherford, H., 2017. Renewable energy microgrids in northern remote communities. *IEEE Potentials*, 36(5), pp.22-29.
- Asano, H. and Bando, S., 2008, July. Economic evaluation of microgrids. In 2008 IEEE Power and Energy Society General Meeting-Conversion and Delivery of Electrical Energy in the 21st Century (pp. 1-6). IEEE.
- Asmus, P., 2010. Microgrids, virtual power plants and our distributed energy future. *The Electricity Journal*, 23(10), pp.72-82.
- Backhaus, S.N., Swift, G.W., Chatzivasileiadis, S., Tschudi, W., Glover, S., Starke, M., Wang, J., Yue, M. and Hammerstrom, D., 2015. DC microgrids scoping study. Estimate of technical and economic benefits (No. LA-UR-15-22097). Los Alamos National Lab.(LANL), Los Alamos, NM (United States).
- Bahrami, M. and Abbaszadeh, P., 2013. An overview of renewable energies in Iran. *Renewable and Sustainable Energy Reviews*, 24, pp.198-208.
- Barklund, E., Pogaku, N., Prodanovic, M., Hernandez-Aramburo, C. and Green, T.C., 2008. Energy management in autonomous microgrid using stability-constrained droop control of inverters. *IEEE Transactions on Power Electronics*, 23(5), pp.2346-2352.

Bayrak, Z.U. and Bayrak, G., 2017. A smart energy management system design for residential power plants. *Politeknik Dergisi*, 20(4), pp.843-849.

Belu, R.G., Ghaisas, K. and Chiou, R., 2014. B. Tseng-Teaching Renewable Energy System Design and Analysis with HOMER. In 2014 ASEE Annual Conference and Exposition, Indianapolis, USA.

Bian, D., Kuzlu, M., Pipattanasomporn, M., Rahman, S. and Wu, Y., 2015. Real-time co-simulation platform using OPAL-RT and OPNET for analyzing smart grid performance. In 2015 IEEE Power & Energy Society General Meeting (pp. 1-5). IEEE.

Boysen, N., Flidner, M., Jaehn, F. and Pesch, E., 2012. Shunting yard operations: Theoretical aspects and applications. *European Journal of Operational Research*, 220(1), pp.1-14.

Bugaje, I.M., 2006. Renewable energy for sustainable development in Africa: a review. *Renewable and sustainable energy reviews*, 10(6), pp.603-612.

Spiegel-Feld, D., Cabrera, O.F., Carvallo, J.P., Garcia, D.R. and Rudyk, B., 2017. The Promise of Renewable Energy Microgrids for Rural Latin America.

Cameron, M. and Rossouw, R., 2012. 'Modelling the economic impact of electricity tariff increases on Eskom's Top Customer Segment'. In Proceedings of South African Economic Regulators Conference.

Changliang, L., Yanqun, W., Kang, B., Weiliang, L. and Chen, C., 2017. Energy management strategy research for residential microgrid considering virtual energy storage system at demand side. In 2017 13th IEEE International Conference on Electronic Measurement & Instruments (ICEMI) (pp. 273-280). IEEE.

Chen, L., Chen, H., Li, Y., Li, G., Yang, J., Liu, X., Xu, Y., Ren, L. and Tang, Y., 2018. SMES-battery energy storage system for the stabilization of a photovoltaic-based microgrid. *IEEE Transactions on Applied Superconductivity*, 28(4), pp.1-7.

Chen, Y.K., Wu, Y.C., Song, C.C. and Chen, Y.S., 2012. Design and implementation of energy management system with fuzzy control for DC microgrid systems. *IEEE Transactions on power electronics*, 28(4), pp.1563-1570.

Clark, K., Miller, N.W. and Sanchez-Gasca, J.J., 2010. Modeling of GE wind turbine-generators for grid studies. *GE energy*, 4, pp.0885-8950.

Cole, S.K. and DeYoung, R.J., 2012. Preliminary design of a solar photovoltaic array for net-zero energy buildings at NASA Langley. National Aeronautics and Space Administration, Langley Research Center.

Coleman, N.S., Hill, J., Berardino, J., Ogawa, K.L., Mallgrave, R., Sandoval, R., Qian, Y., Zhu, L., Miu, K.N. and Nwankpa, C., 2017. Hardware setup of a solar microgrid laboratory. In 2017 IEEE Power & Energy Society General Meeting (pp. 1-5). IEEE.

Cömert, Z. and Kocamaz, A.F., 2017. A novel software for comprehensive analysis of cardiocography signals "CTG-OAS". In 2017 International Artificial Intelligence and Data Processing Symposium (IDAP) (pp. 1-6). IEEE.

Costinett, D.J., 2013. Analysis and design of high efficiency, high conversion ratio, DC-DC power converters. Ph. D. dissertation.

Crabtree, G., Misewich, J., Ambrosio, R., Clay, K., DeMartini, P., James, R., Lauby, M., Mohta, V., Moura, J., Sauer, P. and Slakey, F., 2011. Integrating renewable electricity on the grid. In AIP Conference proceedings (Vol. 1401, No. 1, pp. 387-405). American Institute of Physics.

Dada, J.O., 2014. Towards understanding the benefits and challenges of Smart/Micro-Grid for electricity supply system in Nigeria. *Renewable and Sustainable Energy Reviews*, 38, pp.1003-1014.

Datta, A.J., Ghosh, A. and Rajakaruna, S., 2017. Power sharing in a hybrid microgrid with bidirectional switch. In 2017 IEEE Power & Energy Society General Meeting (pp. 1-5). IEEE.

Dawoud, S.M., Lin, X. and Okba, M.I., 2018. Hybrid renewable microgrid optimization techniques: A review. *Renewable and Sustainable Energy Reviews*, 82, pp.2039-2052.

de Souza Ribeiro, L.A., Saavedra, O.R., De Lima, S.L. and de Matos, J., 2010. Isolated micro-grids with renewable hybrid generation: The case of Lençóis island. *IEEE Transactions on sustainable energy*, 2(1), pp.1-11.

Dekeda, B. and Adonis, M., 2019. The Case for Integration of Renewables in Rail Freight Yards in South Africa. In 2019 International Conference on the Domestic Use of Energy (DUE) (pp. 156-162). IEEE.

Dekker, J., Nthontho, M., Chowdhury, S. and Chowdhury, S.P., 2012. Economic analysis of PV/diesel hybrid power systems in different climatic zones of South Africa. *International Journal of Electrical Power & Energy Systems*, 40(1), pp.104-112.

Deloitte Touche Tohmatsu Limited, 2017 . An overview of electricity consumption and pricing in South Africa An analysis of the historical trends and policies, key issues and outlook in 2017 Report prepared for Eskom Holdings SOC Ltd', p. 85. Available at: <http://www.eskom.co.za/Documents/EcoOverviewElectricitySA-2017.pdf>.

Design, C., 2010. Appendix 7 conceptual design of electrification system.

Diaz, E.R., Su, X., Savaghebi, M., Vasquez, J.C., Han, M. and Guerrero, J.M., 2015. Intelligent dc microgrid living laboratories-a chinese-danish cooperation project. In 2015 IEEE First International Conference on DC Microgrids (ICDCM) (pp. 365-370). IEEE.

Department of Energy (DoE). 2015. South Africa's energy situation - Fuel pricing in South Africa, Energy Advocacy, May(1), pp. 1–28. Available at: <http://www.energy.gov.za/files/media/Pub/Energy-Advocacy-May2015-Issue-1-newsletter.pdf>.

Dongbaare, P., Osuri, S.O. and Chowdhury, S.D., 2017. A smart energy management system for residential use. In 2017 IEEE PES PowerAfrica (pp. 612-616). IEEE.

Dragičević, T., Lu, X., Vasquez, J.C. and Guerrero, J.M., 2015. DC microgrids—Part I: A review of control strategies and stabilization techniques. *IEEE Transactions on power electronics*, 31(7), pp.4876-4891.

Du, Y., Li, F., Kou, X. and Pei, W., 2017. Coordinating multi-microgrid operation within distribution system: A cooperative game approach. In 2017 IEEE Power & Energy Society General Meeting (pp. 1-5). IEEE.

Egan, T., Gabbar, H.A., Othman, A.M. and Milman, R., 2017. Design and control of resilient interconnected microgrid for sustained railway. In 2017 IEEE International Conference on Smart Energy Grid Engineering (SEGE) (pp. 131-136). IEEE.

El Halabi, N., Garcia-Gracia, M., Comech, M.P. and Oyarbide, E., 2012. Distributed generation network design considering ground capacitive couplings. *Renewable energy*, 45, pp.119-127.

Elsayed, A.T., Mohamed, A.A. and Mohammed, O.A., 2015. DC microgrids and distribution systems: An overview. *Electric power systems research*, 119, pp.407-417.

Emleh, A., de Beer, A.S., Ferreira, H.C. and Vinck, A.H., 2015. Noise generated by modern lamps and the influence on the smart-grid communication network. In 2015 IEEE International Conference on Smart Grid Communications (SmartGridComm) (pp. 7-12). IEEE.

Enercon, 2015. Enercon Wind Turbine - Product Overview', pp. 1–19. Available at: http://www.enercon.de/fileadmin/Redakteur/MedienPortal/broschueren/pdf/en/ENERCON_Produkt_en_06_2015.pdf.

Eskom Ltd, 2015. Tariffs & Charges'. Available at: http://www.eskom.co.za/CustomerCare/TariffsAndCharges/WhatsNew/Documents/Tariff_brochure_v9_lowres.pdf.

Eskom Holdings SOC Ltd, , 2015. Task 203-Basic and Detailed Design of Medupi Rail Yard and Offloading Facility Concept Report-Executive Summary. https://www.eskom.co.za/OurCompany/SustainableDevelopments/medupi/WaterUseLicenseAppendice/s/12949-46Appendix%20D-8_Rail%20Concept%20design%20report.pdf.

Date accessed: 15/08/2018.

Esparcia, E.A., Castro, M.T., Buendia, R.E. and Ocon, J.D., 2019. Long-Discharge Flywheel Versus Battery Energy Storage for Microgrids: a Techno-Economic Comparison. *Chemical Engineering Transactions*, 76, pp.949-954.

Ezhilarasan, S., Palanivel, P. and Sambath, S., 2015. Design and development of energy management system for DG source allocation in a micro grid with energy storage system. *Indian journal of science and Technology*, 8(13), p.1.

Feldman, D. and Settle, E., 2013. Master Limited Partnerships and Real Estate Investment Trusts: Opportunities and Potential Complications for Renewable Energy (No. NREL/TP-6A20-60413). National Renewable Energy Lab.(NREL), Golden, CO (United States).

Fenglei, G., Tao, X., Hao, X., Chong, W. and Jingmeng, N., 2016. An uncertainty reduction strategy to schedule and operate microgrids with renewable energy sources. In 2016 IEEE PES Asia-Pacific Power and Energy Engineering Conference (APPEEC) (pp. 1191-1199). IEEE.

Fong, Y.C., Hu, J. and Cheng, K.W.E., 2016. Energy management strategy for parallel connected ESSs in DC microgrids with renewable energy generation. In 2016 International Symposium on Electrical Engineering (ISEE) (pp. 1-6). IEEE.

Forecast and real-time solar irradiance and weather data with global coverage and built-in accuracy reporting. 2015. Daily radiation and Clearness Index for Saldanha Bay and Annual DNI average for South Africa. <http://solargis.com/maps-and-gis-data/download/south-africa> . Date accessed: 30 June 2019

Fritz, W.L., 2012, August. Renewable energy feed in tariffs, REBID, SASGI and the smart grid. In 2012 Proceedings of the 9th Industrial and Commercial Use of Energy Conference (pp. 1-5). IEEE.

Fu, Q., Hamidi, A., Nasiri, A., Bhavaraju, V., Krstic, S.B. and Theisen, P., 2013. The Role of Energy Storage in a Microgrid Concept: Examining the opportunities and promise of microgrids. IEEE Electrification Magazine, 1(2), pp.21-29.

Gajanur, N.R., Singh, A. and Jain, A., 2016. Solar powered railway track monitoring system. In 2016 IEEE International Conference on Power and Renewable Energy (ICPRE) (pp. 190-194). IEEE.

Galai-Dol, L., De Bernardinis, A., Nassiopoulou, A., Peny, A. and Bourquin, F., 2016. On the use of train braking energy regarding the electrical consumption optimization in railway station. Transportation Research Procedia, 14, pp.655-664.

Ghosh, D. and Mandal, C., 2015. Layout Validation Using Graph Grammar and Generation of Yard Specific Safety Properties for Railway Interlocking Verification. In 2015 Asia-Pacific Software Engineering Conference (APSEC) (pp. 330-337). IEEE.

Giraldez Miner, J.I., Singh, S. and Gao, D.W., 2017. Cost Analysis of Renewable Energy-Based Microgrids (No. NREL/CP-5D00-70964). National Renewable Energy Lab.(NREL), Golden, CO (United States).

Giraldez, J., 2012. Energy Security: Microgrid Planning and Design (Presentation) (No. NREL/PR-7A30-54985). National Renewable Energy Lab.(NREL), Golden, CO (United States).

González-Gil, A., Palacin, R., Batty, P. and Powell, J.P., 2014. A systems approach to reduce urban rail energy consumption. Energy Conversion and Management, 80, pp.509-524.

Goqo, Z., Sewchurran, S. and Dorrell, D., 2017. Off-load tap-change transformer impact under high distributed PV generation. In 2017 IEEE AFRICON (pp. 1208-1213). IEEE.

Habumugisha, D., Chowdhury, S. and Chowdhury, S.P., 2013. A DC-DC interleaved forward converter to step-up DC voltage for DC Microgrid applications. In 2013 IEEE Power & Energy Society General Meeting (pp. 1-5). IEEE.

Hafez, O. and Bhattacharya, K., 2012. Optimal planning and design of a renewable energy based supply system for microgrids. Renewable Energy, 45, pp.7-15.

Holla, R.V., 2015. Energy Storage Methods-Superconducting Magnetic Energy Storage-A Review. Journal of Undergraduate Research, 5(1), pp.49-54.

Hossain, E., Perez, R. and Bayindir, R., 2016. Implementation of hybrid energy storage systems to compensate microgrid instability in the presence of constant power loads. In 2016 IEEE International Conference on Renewable Energy Research and Applications (ICRERA) (pp. 1068-1073). IEEE.

Hu, X., Chen, A., Du, C., Zhang, C. and Lin, Z., 2017. Modeling and stability analysis of hybrid AC/DC microgrid based on a hybrid model. In 2017 Chinese Automation Congress (CAC) (pp. 6516-6521). IEEE.

Iannuzzi, D., Pagano, E. and Tricoli, P., 2013. The use of energy storage systems for supporting the voltage needs of urban and suburban railway contact lines. *Energies*, 6(4), pp.1802-1820.

Ibarra, L., Rosales, A., Ponce, P., Molina, A. and Ayyanar, R., 2017. Overview of real-time simulation as a supporting effort to smart-grid attainment. *Energies*, 10(6), p.817.

Iordache, M., (2013). Optimal Strategy to Innovate and Reduce Energy Consumption in Urban Rail Systems, pp. 1–93.

Ishigaki, Y., Kimura, Y., Matsusue, I., Miyoshi, H. and Yamagishi, K., 2014. Optimal energy management system for isolated micro grids. *SEI Technical Review*, 184, pp.74-76.

Jaehn, F. and Michaelis, S., 2016. Shunting of trains in succeeding yards. *Computers & Industrial Engineering*, 102, pp.1-9.

Jensen, R., Stamp, J., Eddy, J., Henry, J., Munoz-Ramos, K. and Abdallah, T., 2015. Methodology for preliminary design of electrical microgrids. Sandia Report. SAND2015-8433.

Justo, J.J., Mwasilu, F., Lee, J. and Jung, J.W., 2013. AC-microgrids versus DC-microgrids with distributed energy resources: A review. *Renewable and sustainable energy reviews*, 24, pp.387-405.

Kachhap, S., Mohanta, D.K. and Jha, R.C., 2017. Reliability evaluation of microgrid scheduling. In 2017 International Conference on Innovations in Information, Embedded and Communication Systems (ICIIECS) (pp. 1-6). IEEE.

Kainuma, M., Shukla, P.R. and Jiang, K., 2012. Framing and modeling of a low carbon society: An overview. *Energy economics*, 34, pp.S316-S324.

Kamboj, A. and Chanana, S., 2016. Planning and operational strategy of a renewable energy microgrid considering reliability. In 2016 IEEE 1st International Conference on Power Electronics, Intelligent Control and Energy Systems (ICPEICES) (pp. 1-6). IEEE.

Karabiber, A., 2017. Power management of a hybrid energy storage system in a domestic microgrid. In 2017 10th International Conference on Electrical and Electronics Engineering (ELECO) (pp. 1404-1408). IEEE.

Kassam, A., 2010. HOMER software training guide for renewable energy base station design. GSM Association.

Katiraei, F. and Iravani, M.R., 2006. Power management strategies for a microgrid with multiple distributed generation units. *IEEE transactions on power systems*, 21(4), pp.1821-1831.

Katiraei, F., Iravani, R., Hatziargyriou, N. and Dimeas, A., 2008. Microgrids management. *IEEE power and energy magazine*, 6(3), pp.54-65.

Khan, F., Ali, M.Y., Sood, V.K., Bhuiyan, F., Insull, P. and Ahmad, F., 2017. Simulation of microgrid system with distributed generation. In 2017 IEEE Electrical Power and Energy Conference (EPEC) (pp.

1-6). IEEE.

Khan, M.W. and Wang, J., 2017. The research on multi-agent system for microgrid control and optimization. *Renewable and Sustainable Energy Reviews*, 80, pp.1399-1411.

Krismanto, A.U. and Mithulanathan, N., 2017. Identification of modal interaction and small signal stability in autonomous microgrid operation. *IET Generation, Transmission & Distribution*, 12(1), pp.247-257.

Kroposki, B., Lasseter, R., Ise, T., Morozumi, S., Papathanassiou, S. and Hatziaargyriou, N., 2008. Making microgrids work. *IEEE power and energy magazine*, 6(3), pp.40-53.

Kwon, Y., Kwasinski, A. and Kwasinski, A., 2015. Microgrids for base stations: Renewable energy prediction and battery bank management for effective state of charge control. In *2015 IEEE International Telecommunications Energy Conference (INTELEC)* (pp. 1-6). IEEE.

Lambert, T., Gilman, P. and Lilienthal, P., 2006. Micropower system modeling with HOMER. *Integration of alternative sources of energy*, 1(1), pp.379-385.

Le Ballois, S., Talakhadze, T., Vido, L. and Zarifyan, A., 2016. An experimental setup to study a hybrid drivetrain for a shunting locomotive. In *2016 Eleventh International Conference on Ecological Vehicles and Renewable Energies (EVER)* (pp. 1-7). IEEE.

Lee, E.K., Shi, W., Gadh, R. and Kim, W., 2016. Design and implementation of a microgrid energy management system. *Sustainability*, 8(11), p.1143.

Li, K. and Tseng, K.J., 2015. Energy efficiency of lithium-ion battery used as energy storage devices in micro-grid. In *IECON 2015-41st Annual Conference of the IEEE Industrial Electronics Society* (pp. 005235-005240). IEEE.

Li, S., Jain, A., Sharma, P. and Sen, S., 2016. A perception system for detecting brake levers in outdoor rail yard environments. In *2016 IEEE/RSJ International Conference on Intelligent Robots and Systems (IROS)* (pp. 2867-2873). IEEE.

Lin, E. and Cheng, C., 2009. YardSim: A rail yard simulation framework and its implementation in a major railroad in the US. In *Proceedings of the 2009 Winter Simulation Conference (WSC)* (pp. 2532-2541). IEEE.

Liu, X., Wang, P. and Loh, P.C., 2011. A hybrid AC/DC microgrid and its coordination control. *IEEE Transactions on smart grid*, 2(2), pp.278-286.

Liu, Y., Gooi, H.B. and Xin, H., 2017. Distributed energy management for the multi-microgrid system based on ADMM. In *2017 IEEE Power & Energy Society General Meeting* (pp. 1-5). IEEE.

Liu, Y.J., Chen, S.I., Chang, Y.R. and Lee, Y.D., 2017. Development of a modelling and simulation method for residential electricity consumption analysis in a community microgrid system. *Applied Sciences*, 7(7), p.733.

Lopez, N. and Espiritu, J.F., 2011. An approach to hybrid power systems integration considering different

renewable energy technologies. *Procedia Computer Science*, 6, pp.463-468.

Loukakis, E. and Karapidakis, E., 2017. Feasibility study of microgrid village with renewable energy sources. In 2017 52nd International Universities Power Engineering Conference (UPEC) (pp. 1-6). IEEE.

Lu, W., Zhao, Y., Li, W. and Du, H., 2014. Design and application of microgrid operation control system based on IEC 61850. *Journal of Modern Power Systems and Clean Energy*, 2(3), pp.256-263.

Ma Lu, S., 2018. Modelling, Control and Simulation of a Microgrid based on PV System, Battery System and VSC (Bachelor's thesis, Universitat Politècnica de Catalunya).

Ma, T., Cintuglu, M.H. and Mohammed, O.A., 2016. Control of a hybrid AC/DC microgrid involving energy storage and pulsed loads. *IEEE Transactions on Industry Applications*, 53(1), pp.567-575.

Malik, S.M., Ai, X., Sun, Y., Zhengqi, C. and Shupeng, Z., 2017. Voltage and frequency control strategies of hybrid AC/DC microgrid: a review. *IET Generation, Transmission & Distribution*, 11(2), pp.303-313.

Mansoor, M., Mariun, N., Ismail, N. and Wahab, N.I.A., 2013. A guidance chart for most probable solution directions in sustainable energy developments. *Renewable and Sustainable Energy Reviews*, 24, pp.306-313.

Markovic, D.S., Zivkovic, D., Branovic, I., Popovic, R. and Cvetkovic, D., 2013. Smart power grid and cloud computing. *Renewable and Sustainable Energy Reviews*, 24, pp.566-577.

Martin, C.M.S., Lundquist, J.K., Clifton, A., Poulos, G.S. and Schreck, S.J., 2016. Wind turbine power production and annual energy production depend on atmospheric stability and turbulence. *Wind Energy Science*, 1(2), pp.221-236.

Mazidi, P. and Bobi, M.A.S., 2017. Strategic maintenance scheduling in an islanded microgrid with distributed energy resources. *Electric Power Systems Research*, 148, pp.171-182.

M'boungui, G., Jimoh, A.A. and Ayodele, T.R., 2013. On the adaptation of South Africa experience to combine solar energy and Smart Grid in Namibia. In 2013 Africon (pp. 1-5). IEEE.

McVicar, T.R., Roderick, M.L., Donohue, R.J., Li, L.T., Van Niel, T.G., Thomas, A., Grieser, J., Jhajharia, D., Himri, Y., Mahowald, N.M. and Mescherskaya, A.V., 2012. Global review and synthesis of trends in observed terrestrial near-surface wind speeds: Implications for evaporation. *Journal of Hydrology*, 416, pp.182-205.

Mendis, N., Mahmud, M.A., Roy, T.K., Haque, M.E. and Muttaqi, K.M., 2016. Power management and control strategies for efficient operation of a solar power dominated hybrid DC microgrid for remote power applications. In 2016 IEEE Industry Applications Society Annual Meeting (pp. 1-8). IEEE.

Menete, S., Mavee, A., Ehlers, E.M. and Leung, W.S., 2017, July. Smart grid critical information infrastructure protection through multi-agency. In 2017 Computing Conference (pp. 461-468). IEEE.

Meng, L., Shafiee, Q., Trecate, G.F., Karimi, H., Fulwani, D., Lu, X. and Guerrero, J.M., 2017. Review on control of DC microgrids and multiple microgrid clusters. *IEEE Journal of Emerging and Selected Topics in Power Electronics*, 5(3), pp.928-948.

Meng, L., Zafar, J., Khadem, S.K., Collinson, A., Murchie, K.C., Coffele, F. and Burt, G.M., 2019. Fast frequency response from energy storage systems—A review of grid standards, projects and technical Issues. *IEEE Transactions on Smart Grid*, 11(2), pp.1566-1581.

Meng, W., Wang, X. and Liu, S., 2016. Distributed load sharing of an inverter-based microgrid with reduced communication. *IEEE Transactions on Smart Grid*, 9(2), pp.1354-1364.

Mengelkamp, E., Gärttner, J., Rock, K., Kessler, S., Orsini, L. and Weinhardt, C., 2018. Designing microgrid energy markets: A case study: The Brooklyn Microgrid. *Applied Energy*, 210, pp.870-880.

Momoh, J.A., 2012. *Smart grid: fundamentals of design and analysis* (Vol. 63). John Wiley & Sons.

Montuori, L. et al., 2014. Integration of renewable energy in microgrids coordinated with demand response resources: Economic evaluation of a biomass gasification plant by Homer Simulator. *Applied Energy*, 132, pp.15-22.

Morales, R., Sáez, D., Marin, L.G. and Nunez, A., 2016. Microgrid planning based on fuzzy interval models of renewable resources. In 2016 IEEE International Conference on Fuzzy Systems (FUZZ-IEEE) (pp. 336-343). IEEE.

Msigwa, C., 2019. Solar PV Based Maximum Power Point Tracking Embedded DC Voltage Regulation Incorporating Battery Storage for Micro-Grid Application. *London Journal of Research of Engineering Research*.

Mukherjee, U., Maroufmashat, A., Ranisau, J., Barbouti, M., Trainor, A., Juthani, N., El-Shayeb, H. and Fowler, M., 2017. Techno-economic, environmental, and safety assessment of hydrogen powered community microgrids; case study in Canada. *International Journal of Hydrogen Energy*, 42(20), pp.14333-14349.

Mumtaz, F. and Bayram, I.S., 2017. Planning, operation, and protection of microgrids: An overview. *Energy Procedia*, 107, pp.94-100.

Nasr, S., Iordache, M. and Petit, M., 2014. Smart micro-grid integration in DC railway systems. In IEEE PES Innovative Smart Grid Technologies, Europe (pp. 1-6). IEEE.

Nayar, C., Tang, M. and Suponthana, W., 2008. Wind/PV/diesel micro grid system implemented in remote islands in the Republic of Maldives. In 2008 IEEE international conference on sustainable energy technologies (pp. 1076-1080). IEEE.

Nazir, R., Laksono, H.D., Waldi, E.P., Ekaputra, E. and Coveria, P., 2014. Renewable energy sources optimization: a micro-grid model design. *Energy Procedia*, 52, pp.316-327.

Necci, R., Bazzi, A., Park, S.Y., Pasaogullari, U., Singh, P., Butterfield, N., Weiss, J. and Xenophontos, A., 2014. Energy efficiency and reliability solutions for rail operations and facilities (No. CT-2283-F-14-5). Connecticut. Dept. of Transportation.

Neves, D., Brito, M.C. and Silva, C.A., 2016. Impact of solar and wind forecast uncertainties on demand response of isolated microgrids. *Renewable energy*, 87, pp.1003-1015.

Nkambule, N.P. and Blignaut, J.N., 2012. The external costs of coal mining: the case of collieries supplying Kusile power station. *Journal of Energy in Southern Africa*, 23(4), pp.85-93.

Novak, H., Vašak, M., Gulin, M. and Lešić, V., 2015. Railway transport system energy flow optimization with integrated microgrid. In *Proceedings of the 12th International Conference on Modern Electrified Transport, MET 2015* (pp. 88-94).

Novak, H., Vašak, M. and Lešić, V., 2016. Hierarchical energy management of multi-train railway transport system with energy storages. In *2016 IEEE International Conference on Intelligent Rail Transportation (ICIRT)* (pp. 130-138). IEEE.

Oliveira, H.A. et al., 2017. Hybrid DC and AC power distribution network as an alternative solution for isolated microgrids. In *2017 Brazilian Power Electronics Conference (COBEP)* (pp. 1-6). IEEE.

Osmani, A., Zhang, J., Gonela, V. and Awudu, I., 2013. Electricity generation from renewables in the United States: Resource potential, current usage, technical status, challenges, strategies, policies, and future directions. *Renewable and Sustainable Energy Reviews*, 24, pp.454-472.

Otto, A. and Pesch, E., 2017. Operation of shunting yards: train-to-yard assignment problem. *Journal of Business Economics*, 87(4), pp.465-486.

Oureilidis, K.O., Bakirtzis, E.A. and Demoulias, C.S., 2016. Frequency-based control of islanded microgrid with renewable energy sources and energy storage. *Journal of Modern Power Systems and Clean Energy*, 4(1), pp.54-62.

Pillay, S., Pretorius, J.H.C. and de Canha, D., 2017. The selection of renewable energy technologies and their cost implications for a developing country: the case of South Africa. In *2017 Australasian Universities Power Engineering Conference (AUPEC)* (pp. 1-6). IEEE.

Planas, E., Gil-de-Muro, A., Andreu, J., Kortabarria, I. and de Alegría, I.M., 2013. General aspects, hierarchical controls and droop methods in microgrids: A review. *Renewable and Sustainable Energy Reviews*, 17, pp.147-159.

Planas, E., Andreu, J., Gárate, J.I., De Alegría, I.M. and Ibarra, E., 2015. AC and DC technology in microgrids: A review. *Renewable and Sustainable Energy Reviews*, 43, pp.726-749.

Qiao, W., Sharma, A., Hudgins, J.L., Jones, E.G. and Rilett, L., 2011. Wind/solar hybrid generation-based roadway microgrids. In *2011 IEEE power and energy society general meeting* (pp. 1-7). IEEE.

Rajesh, K.S., Dash, S.S., Rajagopal, R. and Sridhar, R., 2017. A review on control of ac microgrid. *Renewable and sustainable energy reviews*, 71, pp.814-819.

Rao, W.F., Zhang, B., Pan, J.F., Wu, X.Y., Yuan, J.P. and Qiu, L., 2017. Voltage control strategy of DC microgrid with direct drive wave energy generator. In *2017 7th International Conference on Power Electronics Systems and Applications-Smart Mobility, Power Transfer & Security (PESA)* (pp. 1-7). IEEE.

Rehman, S., Mahbub, A.M. and Meyer, L.M., 2015. Al-Hadhrami. Feasibility Study Of A Wind-Pv-Diesel Hybrid Power System For A Village.

- Ren, W., 2017. The feasibility of microgrids for large facilities.
- Rezaee, S., Ebrahimi, S., Amiri, N., Huang, Y. and Jatskevich, J., 2017. Accurate and fast power sharing among inverters in AC microgrids with constant power loads. In 2017 IEEE 18th Workshop on Control and Modeling for Power Electronics (COMPEL) (pp. 1-8). IEEE.
- Rokrok, E., Shafie-Khah, M. and Catalão, J.P., 2017. Comparison of two control strategies in an autonomous hybrid microgrid. In 2017 IEEE PES Innovative Smart Grid Technologies Conference Europe (ISGT-Europe) (pp. 1-6). IEEE.
- Ruban, A.A.M., Rajasekaran, G.M. and Rajeswari, N., 2015. Implementation of energy management system to PV-Wind hybrid power generation system for DC microgrid applications. *Int Res J Eng Technol*, 2(08), pp.204-10.
- Sáiz-Marín, E., Lobato, E. and Egido, I., 2017. New challenges to wind energy voltage control. Survey of recent practice and literature review. *IET Renewable Power Generation*, 12(3), pp.267-278.
- Sampaio, P.G.V. and González, M.O.A., 2017. Photovoltaic solar energy: Conceptual framework. *Renewable and Sustainable Energy Reviews*, 74, pp.590-601.
- Saranya, S.D., Sathyamoorthi, S. and Gandhiraj, R., 2015. A fuzzy logic based energy management system for a microgrid. *ARPN Journal of Engineering and Applied Sciences*, 10(6), pp.2663-2669.
- Sarkar, S.K., Badal, F.R., Das, S.K. and Miao, Y., 2017. Discrete time model predictive controller design for voltage control of an islanded microgrid. In 2017 3rd International Conference on Electrical Information and Communication Technology (EICT) (pp. 1-6). IEEE.
- Sbordone, D.A., Di Pietra, B. and Bocci, E., 2015. Energy analysis of a real grid connected lithium battery energy storage system. *Energy Procedia*, 75, pp.1881-1887.
- Schnitzer, D., Lounsbury, D.S., Carvalho, J.P., Deshmukh, R., Apt, J. and Kammen, D.M., 2014. *Microgrids for Rural Electrification: A critical review of best practices based on seven case studies*. United Nations Foundation.
- Semënov, D., Mirzaeva, G., Townsend, C.D. and Goodwin, G.C., 2017. A battery storage control scheme for AC microgrids. In 2017 20th International Conference on Electrical Machines and Systems (ICEMS) (pp. 1-6). IEEE.
- Syedmahmoudian, M., Arrisoy, H., Kavalchuk, I., Oo, A.M. and Stojcevski, A., 2015. Rationale for the use of DC microgrids: feasibility, efficiency and protection analysis. *Energy and Sustainability V: Special Contributions*, 206, p.69.
- Shafiee, Q., Dragičević, T., Vasquez, J.C. and Guerrero, J.M., 2014. Hierarchical control for multiple DC-microgrids clusters. *IEEE Transactions on Energy Conversion*, 29(4), pp.922-933.
- Li, B., Chen, T., Wang, X. and Giannakis, G.B., 2017. Real-time energy management in microgrids with reduced battery capacity requirements. *IEEE Transactions on Smart Grid*, 10(2), pp.1928-1938.
- Shiles, J., Wong, E., Rao, S., Sanden, C., Zamani, M.A., Davari, M. and Katiraei, F., 2017. Microgrid

protection: An overview of protection strategies in North American microgrid projects. In 2017 IEEE Power & Energy Society General Meeting (pp. 1-5). IEEE.

Singh, R. and Lalk, J., 2016. An investigation into the barriers to energy efficiency within medium to large manufacturing firms operating within the eThekweni municipal area. *South African Journal of Industrial Engineering*, 27(3), pp.287-302.

Singh, S.K., Padhy, B.P., Chakrabarti, S., Singh, S.N., Kolwalkar, A. and Kelapure, S.M., 2014. Development of dynamic test cases in OPAL-RT real-time power system simulator. In 2014 Eighteenth National Power Systems Conference (NPSC) (pp. 1-6). IEEE.

Slann, L.J., 2013. An innovative microgrid solution for a large housing development in South Africa. Stellenbosch University.

Smee, C.S.W., Perin, I. and Nussey, P.F., 2015. Autonomous solar supply for railway signalling. In 2015 IEEE PES Asia-Pacific Power and Energy Engineering Conference (APPEEC) (pp. 1-4). IEEE.

Smith, N. and McCann, R., 2017. Energy shaping control of a back-to-back converter for microgrid applications. In 2017 IEEE Power & Energy Society General Meeting (pp. 1-5). IEEE.

Spiryagin, M., Wu, Q., Wolfs, P., Sun, Y. and Cole, C., 2018. Comparison of locomotive energy storage systems for heavy-haul operation. *International Journal of Rail Transportation*, 6(1), pp.1-15.

Stadelmann, M. and Castro, P., 2014. Climate policy innovation in the South—Domestic and international determinants of renewable energy policies in developing and emerging countries. *Global Environmental Change*, 29, pp.413-423.

Starke, M., Tolbert, L.M. and Ozpineci, B., 2008. AC vs. DC distribution: A loss comparison. In 2008 IEEE/PES Transmission and Distribution Conference and Exposition (pp. 1-7). IEEE.

Stevens, J. and Schenkman, B. 2008. 'DC Energy Storage in the CERTS Microgrid John Stevens , Sandia National Laboratories Benjamin Schenkman , Sandia National Laboratories'.

Stock, A., Stock, P. and Sahajwalla, V., 2015. Powerful potential: Battery storage for renewable energy and electric cars. Climate Council of Australia Limited, Australia.

Su, Y., 2015. Economic and environmental impact assessment of Micro Grid', *Lecture Notes in Engineering and Computer Science*, 2, pp. 626–629.

Teo, T.T., Logenthiran, T., Woo, W.L. and Abidi, K., 2016. Fuzzy logic control of energy storage system in microgrid operation. In 2016 IEEE Innovative Smart Grid Technologies-Asia (ISGT-Asia) (pp. 65-70). IEEE.

Tephirik, N., Kanokbannakorn, W., Kerdphol, T., Mitani, Y. and Hongesombut, K., 2018. Fuzzy logic control of a battery energy storage system for stability improvement in an islanded microgrid. *Sustainability*, 10(5), p.1645.

Transnet SOC Ltd., 2016. Rail Development Plan. Chapter 3, pp49- 198.

<https://www.transnet.net/BusinessWithUs/LTPF%202017/LTPF%20Chapter%203%20Rail%20Development%20Plan.pdf>. Date accessed: 09/04/2018.

Unamuno, E. and Barrena, J.A., 2015. Hybrid ac/dc microgrids—Part I: Review and classification of

topologies. *Renewable and Sustainable Energy Reviews*, 52, pp.1251-1259.

Ustun, T.S., 2016. The importance of microgrids & renewable energy in meeting energy needs of the Brazilian Amazon. In 2016 IEEE International Conference on Power and Energy (PECon) (pp. 1-6). IEEE.

Vasant, L.G. and Pawar, V.R., 2017. Solar-wind hybrid energy system using MPPT. In 2017 International Conference on Intelligent Computing and Control Systems (ICICCS) (pp. 595-597). IEEE.

Wang, B., 2015, April. The Application and Study of MATLAB in Electrical Engineering and Its Automation. In International Conference on Advances in Mechanical Engineering and Industrial Informatics. Atlantis Press.

Wang, R., 2018. Intelligent microgrid management and EV control under uncertainties in smart grid. Springer.

Williams, N.J., Jaramillo, P. and Taneja, J., 2018. An investment risk assessment of microgrid utilities for rural electrification using the stochastic techno-economic microgrid model: A case study in Rwanda. *Energy for Sustainable Development*, 42, pp.87-96.

Xu, Z., Yang, P., Zheng, C., Zhang, Y., Peng, J. and Zeng, Z., 2018. Analysis on the organization and Development of multi-microgrids. *Renewable and Sustainable energy reviews*, 81, pp.2204-2216.

Yang, S.L. and Shen, C., 2013. A review of electric load classification in smart grid environment. *Renewable and Sustainable Energy Reviews*, 24, pp.103-110.

Yaramasu, V., Wu, B., Sen, P.C., Kouro, S. and Narimani, M., 2015. High-power wind energy conversion systems: State-of-the-art and emerging technologies. *Proceedings of the IEEE*, 103(5), pp.740-788.

Rosado, S.P. and Khadem, S.K., 2018. Development of community grid: Review of technical issues and challenges. *IEEE Transactions on Industry Applications*, 55(2), pp.1171-1179.

Zahnd, A., McKay, K.H. and Komp, R., 2006. Renewable energy village power systems for remote and impoverished Himalayan villages in Nepal.

Zeng, Z., Yang, H., Zhao, R. and Cheng, C., 2013. Topologies and control strategies of multi-functional grid-connected inverters for power quality enhancement: A comprehensive review. *Renewable and Sustainable Energy Reviews*, 24, pp.223-270.

Zhou, Y. and Ho, C.N.M., 2016. A review on microgrid architectures and control methods. In 2016 IEEE 8th International Power Electronics and Motion Control Conference (IPEMC-ECCE Asia) (pp. 3149-3156). IEEE.

Zikalala, D.P. and Chowdhury, S.P., 2015. Prospects and challenges of implementing smart grid technologies in South Africa.

Zobaa, A.F. and Bansal, R.C. eds., 2011. Handbook of renewable energy technology. World Scientific.